

UNIVERSITÉ DU QUÉBEC À MONTRÉAL

DÉVELOPPEMENT DE SUBSTRATS MACROMOLÉCULAIRES UTILISÉS  
POUR DES ÉTUDES DE MICROSCOPIE ÉLECTROCHIMIQUE À BALAYAGE

MÉMOIRE

PRÉSENTÉ

COMME EXIGENCE PARTIELLE

DE LA MAÎTRISE EN CHIMIE (OPTION BIOCHIMIE)

PAR

ISABELLE BEAULIEU

AVRIL 2009

UNIVERSITÉ DU QUÉBEC À MONTRÉAL  
Service des bibliothèques

Avertissement

La diffusion de ce mémoire se fait dans le respect des droits de son auteur, qui a signé le formulaire *Autorisation de reproduire et de diffuser un travail de recherche de cycles supérieurs* (SDU-522 – Rév.01-2006). Cette autorisation stipule que «conformément à l'article 11 du Règlement no 8 des études de cycles supérieurs, [l'auteur] concède à l'Université du Québec à Montréal une licence non exclusive d'utilisation et de publication de la totalité ou d'une partie importante de [son] travail de recherche pour des fins pédagogiques et non commerciales. Plus précisément, [l'auteur] autorise l'Université du Québec à Montréal à reproduire, diffuser, prêter, distribuer ou vendre des copies de [son] travail de recherche à des fins non commerciales sur quelque support que ce soit, y compris l'Internet. Cette licence et cette autorisation n'entraînent pas une renonciation de [la] part [de l'auteur] à [ses] droits moraux ni à [ses] droits de propriété intellectuelle. Sauf entente contraire, [l'auteur] conserve la liberté de diffuser et de commercialiser ou non ce travail dont [il] possède un exemplaire.»

## REMERCIEMENTS

L'auteure tient à remercier Prof. Janine Mauzeroll et Dr Matthias Geissler pour leur aide et leur supervision lors de ce projet. Prof. Borhane Annabi pour l'accessibilité à son matériel de recherche. Dr Dimitre Karpuzov pour les analyses XPS. Marie-Josée Crevier et Michel Marion pour leur aide en culture cellulaire ainsi qu'à toute l'équipe technique du département de chimie de l'UQÀM.

Je tiens à remercier toutes les personnes ayant contribué à l'élaboration de ce mémoire. D'abord, à mes collègues du laboratoire Mauzeroll, pour votre aide, spécialement à Danielle Dansereau pour tes précieux conseils. Janine, merci de m'avoir donné la chance de travailler avec toi, même si je ne connaissais absolument rien de l'électrochimie. À mes amis, de m'avoir changé les idées dans les moments difficiles. Il ne faut surtout pas sous-estimer les pouvoirs du divertissement (vive le Comité Organisationnel d'Événements Mondains du 3<sup>e</sup>). Finalement, à ma famille, papa, maman et Frédéric, merci de votre soutien constant, sans vous, rien de tout cela n'aurait été possible.

## TABLE DES MATIÈRES

LISTE DES FIGURES.....	v
LISTE DES TABLEAUX.....	viii
LISTE DES ABRÉVIATIONS, SIGLES ET ACRONYMES.....	ix
LISTE DES SYMBOLES.....	x
RÉSUMÉ.....	xii
INTRODUCTION.....	1
CHAPITRE I	
CHAPITRE DE LIVRE: ELECTROCHEMICAL SENSORS AND THEIR USE IN CELL STUDIES.....	6
1.1 Introduction.....	7
1.2 Basic Principles of Ultramicroelectrodes.....	9
1.3 Ultramicroelectrodes in Cell Studies.....	13
1.3.1 Disc and Fiber UMEs.....	13
1.3.2 Electrochemical Micropipets.....	16
1.4 Biological Scanning Electrochemical Microscopy.....	18
1.4.1 Basic Principles of SECM.....	18
1.4.2 Biological Scanning Electrochemical Microscopy (Bio-SECM).....	19
1.4.3 Constant-Distance Feedback Controllers.....	20
1.5 Biomaterial Design: Cell Patterns Used in Bio-SECM.....	21
1.5.1 Microfluidic Systems for Cell Patterning.....	21
1.5.2 HeLa Cell Patterns.....	25
1.5.3 Fluorescence-Based Cell Status Assay.....	26
1.6 Conclusions.....	28
1.7 References.....	47
CHAPITRE II	
ARTICLE SCIENTIFIQUE: OXYGEN PLASMA TREATMENT OF POLYSTYRENE	

AND ZEONOR SUBSTRATES FOR ADHESION OF PATTERNED CELLS.....	55
2.1 Introduction.....	58
2.2 Experimental Section.....	60
2.2.1 Preparation of Plastic Substrates.....	60
2.2.2 Surface Characterization.....	60
2.2.3 Fabrication of Microcapillary Systems.....	61
2.2.4 Patterning of Cells.....	61
2.2.5 Biocompatibility Tests.....	62
2.2.6 Optical and Fluorescence Imaging.....	62
2.2.7 Flow Measurements.....	63
2.3 Results and Discussion.....	63
2.3.1 Surface Analysis.....	63
2.3.2 Biocompatibility.....	65
2.3.3 Adhesion and Cell Growth on Plasma-Treated Surfaces.....	66
2.3.4 Cell Pattern Formation.....	67
2.4 Conclusion.....	68
2.5 References.....	81
CONCLUSION.....	84
APPENDICE A INVITATION À CONTRIBUER À L'ÉCRITURE D'UN CHAPITRE DE LIVRE.....	86
APPENDICE B PERMISSIONS D'UTILISATION ET DE MODIFICATION DE MATÉRIEL AVEC DROIT D'AUTEUR.....	88
APPENDICE C LISTE DES RÉFÉRENCES DE L'INTRODUCTION.....	92

## LISTE DES FIGURES

Figure	Page
I.1	Microscopie électrochimique à balayage pour laquelle l'électrode se déplace (A) en mode hauteur constante (SECM) et (B) en mode distance constante (Bio-SECM).....2
I.2	Cellule électrochimique contenant une lame de plastique sur laquelle des cellules sont immobilisées selon un tracé déterminé. (1) vue latérale (2) vue de haut.....3
1.1	Diffusion occurring at an electrode. A) Linear diffusion to a large planar disk electrode. B) Hemispherical diffusion to a planar disk UME.....31
1.2	A) Local amperometric detection of single-vesicle adrenaline released from an individual bovine chromaffin cell. A carbon-fiber disk ultramicroelectrode (CF-UME, 5 mm in diameter, polarized to +800 mV vs. Ag/AgCl) was directly placed above the center of a single bovine chromaffin cell at a distance of <1 μm. B) When the selected cell was stimulated with 100 mM KCl solution, exocytosis was initiated and detected by the appearance of spikes in the amperometric UME current.....32
1.3	SEM images of the ends of A) bare and B) insulated carbon fibers that are 10 μm in diameter.....33
1.4	Voltammograms of FcCH <sub>2</sub> OH oxidation at a 112-nm platinum tip obtained in bulk solution (curve 1) and inside a human breast epithelial (MCF-10A) cell (curves 2–5).....34
1.5	SEM images of the ends of A) a gold-coated pulled borosilicate micropipet and B) an insulated 70-nm-thick gold ring micropipet.....35
1.6	Removal of blocking polymer layers from a microelectrode. A) SEM image of the end of a blocked gold ring micropipet. The insulating material, a thin layer of cathodic electrophoretic paint (Cathodip™ Ft83-0250, BASF) covers both side walls and ring face of the micropipet. B) Schematic representation of the experimental setup used for blasting the polymer layer off the ring-shaped electrode surface.....36
1.7	A,B) Optical micrographs (survey and close-up view) of a pulled micropipet attached to a Giant Unilamellar Vesicle (GUV) which is composed of 1,2-dioleoyl-sn-glycero-3-phosphocholine (DOPC), ubiquinone-10 and 1-acyl-2-[(2-nitrobenz-2-oxa-1,3-diazol-4-yl)aminostearoyl]-sn-glycero-3-phosphocholine (NBD-PC). C) Input square-wave applied to the micropipet used to patch on the GUV. D) A

	patch of the micropipet onto the GUV typically results in an increase of the micropipet resistance ( $G\Omega$ ). .....	37
1.8	The electrochemical reaction of dissolved reversible redox species (O and R, respectively) at the UME/solution interface is mass transfer limited, at least for potentials far exceeding the redox potential of O. The localized hemispherical diffusion zone in front of the UME is used to detect topography and/or reactivity of a nearby surface.....	38
1.9	A) Schematic presentation of an SECM line scan over immobilized cells in constant height and constant distance mode. B) Instrumental design of a Bio-SECM. C) Detection principles of selected constant distance controllers.....	39
1.10	SECM imaging of immobilized cells. ....	40
1.11	Fabrication and use of PDMS-based microfluidic devices. A) Printing a CAD file onto a transparency foil constitutes a convenient and generally accessible way to generate a photomask. B) A master is fabricated by contact mode optical lithography. The mask is placed onto a thin film of photoresist (e.g., SU-8) formed by spin-coating on a silicon substrate. When illuminated with UV light, crosslinking of the photoresist is induced within the transparent windows of the mask, making exposed regions of the resist become insoluble in an organic medium that is used for development. C) The photoresist pattern is transferred into a layer of PDMS by replica molding. In this process, liquid pre-polymers of PDMS are poured onto the master, cured thermally, and peeled away. ....	41
1.12	Patterning of cells in microfluidic environments. A) Design of a simple $\mu$ CS for linear arrangement of cells. B) Optical micrograph of a 400- $\mu$ m-wide microchannel in contact with a Zeonor <sup>®</sup> substrate during filling with a HeLa cell suspension. C) Pattern of HeLa cells on a plastic support obtained by incubating the suspension with a Zeonor <sup>®</sup> substrate at 37 °C in a 5% CO <sub>2</sub> atmosphere saturated in water for 5 h. ....	42
1.13	Scheme of a cell undergoing apoptotic or necrotic processes. ....	43
1.14	Schematic illustration of lipid asymmetry loss in an apoptotic cell. ....	44
1.15	Simplified scheme of a double stranded DNA structure. ....	45
1.16	Fluorescence-based cell status assay. ....	46
2.1	Surface topography of Zeonor 1060R substrates as revealed by AFM measurements. ....	70
2.2	XPS survey spectra of PS and Zeonor 1060R substrates treated with O <sub>2</sub> plasma at 0, 5 and 100 W/sccm. ....	71

2.3	High resolution spectrum of the C 1s signal of Zeonor 1060R treated with O <sub>2</sub> plasma at 100 W/sccm taken after 20 days upon exposure.....	72
2.4	Necrotic and apoptotic cell death induced by Triton X-100 (0.075%) or tributyltin (2.0 μM), respectively as revealed by fluorescence microscopy.....	73
2.5	Biocompatibility of Zeonor and PS substrates as determined by fluorescence microscopy. ....	74
2.6	Patterning of cells within channels of a μCS. ....	75

## LISTE DES TABLEAUX

Tableau	Page
2.1 Wetting Properties of PS Surfaces as a Function of Plasma Power.....	76
2.2 Wetting Properties of Zeonor Surfaces as a Function of Plasma Power.....	77
2.3 Atomic Concentration of Plasma-Treated Zeonor and PS Surfaces as determined by XPS Measurements .....	78
2.4 Percentage of Cell Confluency on Zeonor Surfaces as a Function of Plasma Power.....	79
2.5 Percentage of Cell Confluency on PS Surfaces as a Function of Plasma Power.....	80

## LISTE DES ABRÉVIATIONS, SIGLES ET ACRONYMES

AC	Alternative current, Courant alternatif
AFM	Atomic force microscopy, Microscope à force atomique
ATP	Adénosine triphosphate
Bio-SECM	Biological scanning electrochemical microscopy, Microscopie électrochimique à balayage biologique
CCD	Charge coupled device, Dispositif à transfert de charges
CAD	Computer-aided design, Conception assistée par ordinateur
CF	Carbon fiber, Fibre de carbone
CV	Cycle voltammetry, Voltampérométrie cyclique
DNA	Deoxyribonucleic acid, Acide désoxyribonucléique (ADN)
DC	Direct current, Courant continu
FcCH <sub>2</sub> OH	1-(ferrocenyl)methanol ou Ferrocène méthanol
NSOM	Near-field scanning optical microscopy, Microscopie optique en champ proche
PDMS	Polydiméthylsiloxane
PS	Phosphatidylsérine
SEM	Scanning electron microscopy, Microscopie électronique à balayage
SECM	Scanning electrochemical microscopy, Microscopie électrochimique à balayage
SCCM	Standard Cubic Centimeters per Minute, Débit en centimètre cube par minute d'un gaz ramené à la pression atmosphérique
SCLM	Scanning chemiluminescence microscopy, Microscopie de chimioluminescence à balayage
STM	Scanning tunnelling microscopy, Microscopie à balayage à effet tunnel
UME	Ultramicroélectrode
UV	Ultraviolet
XPS	X-Ray photoelectron spectroscopy, Spectroscopie des photoélectrons en rayons X

## LISTE DES SYMBOLES

$c$	Concentration de l'espèce électroactive (mol/m <sup>3</sup> )
$\mu\text{CS}$	Microcapillary system, Système microcapillaire
$\partial c_o$	Variation de concentration de l'espèce O
$D$	Coefficient de diffusion de l'espèce électroactive en solution (m <sup>2</sup> /s)
$D_o$	Coefficient de diffusion de l'espèce O (m <sup>2</sup> /s)
$D$	Depth, Profondeur (m)
$\Delta E_{1/2}$	Variation du potentiel à demi-vague (V)
$F$	Constante de Faraday (96,48534 × 10 <sup>3</sup> C/mol) où C = Coulombs
$I$	Intensité du courant (A)
$I_{ss}$	Intensité du courant de l'état stationnaire (A)
$J_o$	Densité de flux de l'espèce O (mol/(s·m <sup>2</sup> ))
$n$	Nombre d'électron
$\Delta P$	Différence de pression (Pa) où Pa = Pascals
$Q$	Débit de liquide (m <sup>3</sup> /s)
$r$	Rayon de la sonde électroactive (m)
$R$	Résistance ( $\Omega$ ) ou Résistance à l'écoulement (Pa s/m <sup>3</sup> )
$RI$	Potentiel de chute ohmique (V)
$t$	Position de l'espèce O dans le temps (s)
$x$	Position de l'espèce O dans l'espace (m)
$w$	Largeur (m)
$\nabla^2$	Opérateur Laplacien

$\delta$	Épaisseur de la couche de diffusion (m)
$\pi$	Pi, Constante d'Archimède (3,141592)
$\lambda_{\text{ex}}$	Longueur d'onde d'excitation (nm)
$\lambda_{\text{em}}$	Longueur d'onde d'émission (nm)

## RÉSUMÉ

Le but de ce mémoire est de développer des substrats biologiques pour le Bio-SECM. Cette nouvelle méthode analytique est en émergence et elle est intéressante puisqu'elle permet des études électrochimiques appliquées aux systèmes biologiques, comme des cellules cancéreuses. Pour se faire, les cellules biologiques doivent être immobilisées sur des plastiques biocompatibles fonctionnalisés de façon à ce que les cellules soient disposées en ligne droite. En effet, si les cellules ont toujours la même disposition, la localisation par l'électrode est plus facile et rapide. Il s'agit donc d'un projet multidisciplinaire réunissant la biologie (culture cellulaire), la toxicologie et la chimie de surface. Afin de s'assurer de l'adhésion cellulaire, les surfaces de 2 plastiques, le Zeonor<sup>®</sup> 1060R et le polystyrène, sont modifiées par un traitement au plasma d'oxygène. Ceci permet l'ajout de groupements fonctionnels polaires contenant au moins un atome d'oxygène ce qui charge la surface et la rend hydrophile. Afin de vérifier si le traitement est efficace, des mesures d'AFM, de XPS et d'angles de contact sont effectuées. Ensuite, pour s'assurer de la biocompatibilité des surfaces, la vérification de l'état cellulaire est faite par microscopie à fluorescence en utilisant 3 fluorophores : l'Alexa fluor 488 couplé à l'Annexin V (début d'apoptose), le Hoechst 33258 (apoptose avancée) et l'iodure de propidium (nécrose). Enfin, l'adhésion de cellules alignées est faite grâce à des méthodes de lithographie, soit la photolithographie et la lithographie molle. Ces procédés permettent d'obtenir un moule de PDMS contenant des canaux microfluidiques dans lesquels les cellules sont injectées. Les principaux résultats montrent que les deux plastiques peuvent devenir hydrophiles suite au traitement au plasma puisqu'ils présentent des groupements carboxyliques et hydroxyliques à leur surface. Aussi, ils sont biocompatibles et même si la division cellulaire semble plus efficace sur le polystyrène, le Zeonor permet de former des lignes de cellules pouvant servir aux analyses électrochimiques.

Mots-clés : cellules, lithographie, biocompatibilité, fluorescence, électrochimie

## INTRODUCTION

Il existe plusieurs instruments nouvellement utilisés pour faire des analyses biologiques difficilement exécutables auparavant. D'abord, l'AFM a permis, entre autre, d'observer la force inductrice du déploiement d'une protéine.<sup>1-3</sup> Aussi, la STM peut être utilisée pour imager des molécules comme l'ADN pour observer leur structure et leur conformation.<sup>1,4</sup> La technique d'intérêt dans le présent mémoire, est la SECM. Elle consiste à approcher une électrode nano ou micrométrique à quelques microns de la surface pour mesurer les variations de courant qui dépendent de la réactivité surfacique. Cette technique a été employée pour étudier les systèmes biologiques pour les premières fois vers la fin des années 90.<sup>5-7</sup> Elle offre différentes possibilités d'analyses, telle que le suivi de l'activité respiratoire cellulaire<sup>8,9</sup>, la détection de neurotransmetteurs sécrétés par des vésicules<sup>10</sup>, l'étude de la diffusion transdermique de médicaments<sup>11</sup> et l'évaluation de la cytotoxicité par des mesures de viabilité ou par un suivi de l'expulsion de conjugués de détoxification<sup>12,13</sup>.

La SECM peut être utilisée en deux modes distincts, soit en hauteur constante ou en distance constante. Le premier mode est employé en SECM conventionnelle alors que l'électrode se déplace parallèlement au substrat sans tenir compte de sa topographie (Figure I.1A). Le désavantage de ce mode SECM est la difficulté de mesurer les variations de courant au-dessus des zones plus éloignées de l'électrode. En effet, puisque les espèces électrochimiques doivent diffuser sur une plus longue distance, elles sont diluées dans la masse de la solution avant d'être détectées par l'électrode. Il est possible de contrevenir à ce problème en distance constante (Figure I.1B) puisque le mouvement de l'électrode dépend de la topographie du substrat permettant ainsi de limiter la perte de signal.

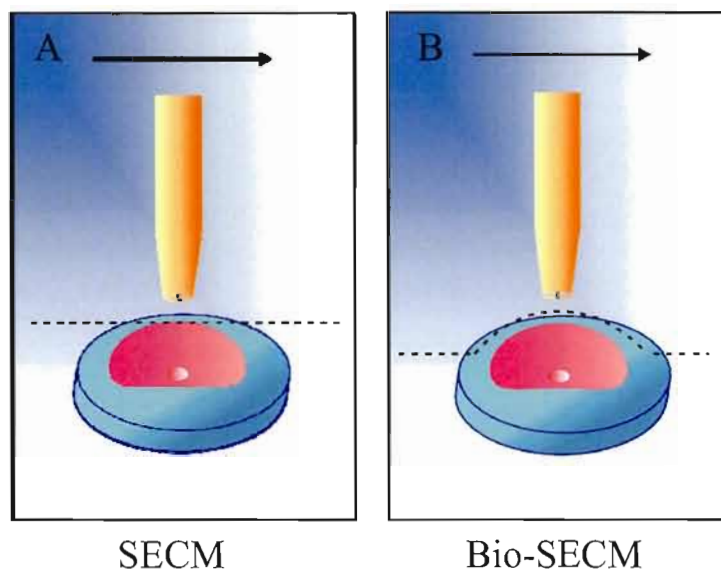


**Figure I.1.** Microscopie électrochimique à balayage pour laquelle l'électrode se déplace (A) en mode hauteur constante (SECM) et (B) en mode distance constante (Bio-SECM).

Le déplacement de l'électrode est contrôlé d'un moteur à pas qui permet la correction de la pente du substrat dans les axes x et y et un autre qui assure le mouvement dans l'axe des z. La distance constante est maintenue grâce à un mécanisme de réaction basé sur des forces de cisaillements (shear forces). Cette composante donne la possibilité de s'approcher d'une cellule biologique sans l'endommager. Ce nouveau mode d'analyse donne naissance à la Bio-SECM qui combine la SECM avec un microscope inversé à fluorescence donnant la possibilité d'observer les changements morphologiques de la cellule tout en faisant les analyses électrochimiques. Ce type de système a fait son apparition dans les années 2000<sup>10</sup> et celui du laboratoire Mauzeroll est unique puisque la distance est modulée par la phase et non par l'amplitude, ce qui donne une meilleure limite de détection à l'appareil<sup>14</sup>.

Le caractère exclusif de l'appareil demande le développement de dispositifs pour pouvoir procéder aux analyses sur les systèmes biologiques. En effet les dimensions de la cellule électrochimique, dans laquelle les analyses doivent être effectuées, ne permettent pas l'insertion d'un pétri de culture cellulaire conventionnel. Les plus petits pétris actuellement disponibles commercialement ont un diamètre de 30 mm, hors la cellule électrochimique a un

diamètre de 25 mm. C'est pourquoi, le projet demande la fabrication de disques de plastiques moulés sur mesure (Figure I.2).

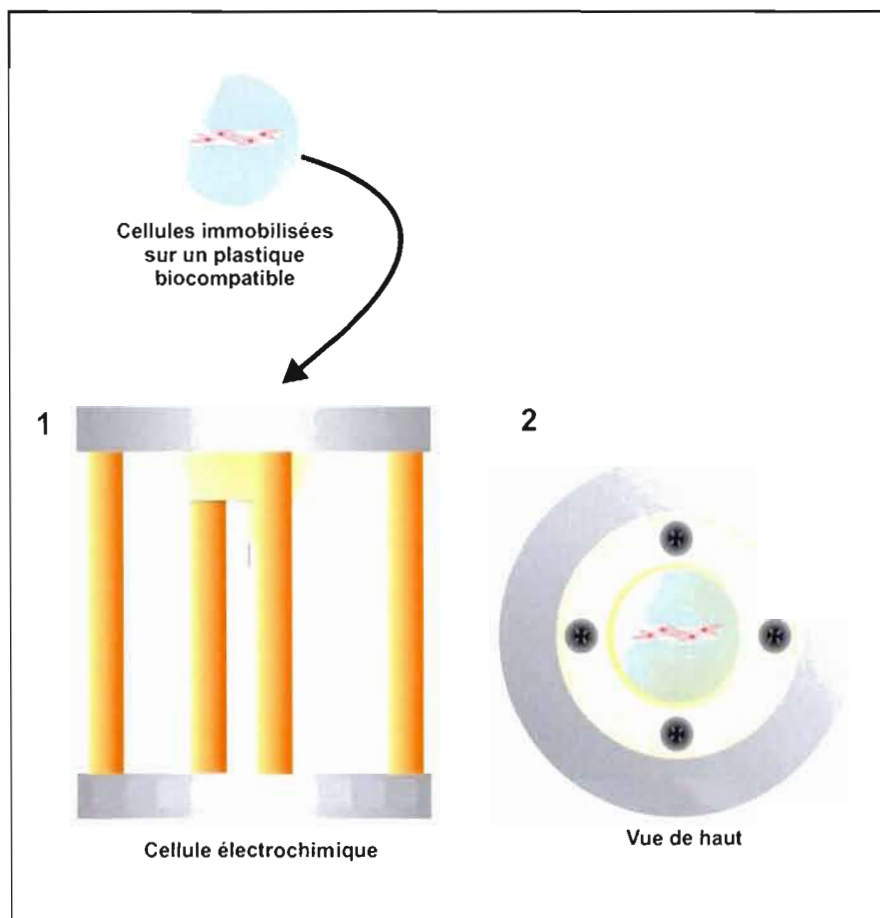


**Figure I.2.** Cellule électrochimique contenant une lame de plastique sur laquelle des cellules sont immobilisées selon un tracé déterminé. (1) vue latérale (2) vue de haut

De plus, la taille de l'électrode la rend sujette à la désactivation due à l'adhésion des molécules en solution causant ainsi la passivation de la surface de détection. Cette limitation demande l'utilisation de solutions les moins complexes que possible. Cependant, pour recréer l'environnement physiologique nécessaire à la viabilité des cellules en culture, du sérum

bovin est habituellement ajouté au milieu. Seulement, les protéines qu'il contient sont fortement adhésives et c'est pourquoi elles ne doivent pas être présentes lors des analyses électrochimiques. Puisque le temps de survie des cellules est grandement diminué dans de telles conditions, il est nécessaire d'optimiser les analyses pour réduire la durée expérimentale. Pour ce faire, les cellules doivent être immobilisées sur les disques de plastiques de sorte que leur localisation soit facilitée. Ainsi, il est nécessaire que les cellules s'adhèrent de façon linéaire sur la surface toujours au même endroit afin de pouvoir positionner rapidement l'électrode. Ceci demande l'utilisation de techniques lithographiques telles que la photolithographie et la lithographie molle<sup>15-17</sup>. Ces méthodes permettent la production de moules de PDMS contenant des canaux microfluidiques dans lesquelles les cellules peuvent être introduites.<sup>18-21</sup>

Aussi, il est essentiel de s'assurer que les surfaces utilisées sont adéquates pour l'adhésion cellulaire. Les plastiques utilisés, le Zeonor<sup>®</sup> 1060R et le polystyrène, sont alors fonctionnalisés à l'aide de l'application d'un plasma d'oxygène. Ce traitement permet d'introduire des fonctions polaires telles que des carbonyles, des carboxyles et des hydroxyles. La nouvelle hydrophilicité des plastiques aide à l'introduction de la suspension cellulaire à l'intérieur des canaux microfluidiques en ayant recours aux forces de capillarité sans l'utilisation de pompe. Les cellules entrent dans le canal suite à leur injection et une fois adhérentes à la surface, le moule peut être retiré et les cellules forment alors une ligne de la largeur du canal. Ainsi, les cellules peuvent être localisées visuellement, à l'aide du microscope et électrochimiquement grâce à l'électrode. La ligne de cellules peut être mise au centre sous l'électrode en déplaçant le microscope en x et en y, puis les variations de courant sont détectés par l'électrode en la bougeant avec les moteurs du Bio-SECM dans les axes x, y et z.

Lorsque l'on fait de la culture cellulaire, il est important de s'assurer de la biocompatibilité de la surface sur laquelle les cellules sont déposées. Il s'agit d'un autre volet important du projet impliquant la microscopie à fluorescence. En effet, des fluorophores marquant les cellules en début d'apoptose, en apoptose avancée et en nécrose sont employés pour vérifier si les cellules sont toujours dans leur état normal ou si elles sont en train de

mourir. Il s'agit de l'Alexa fluor 488 couplé à l'Annexin V (début d'apoptose)<sup>22</sup>, le Hoechst 33258 (apoptose avancée)<sup>23</sup> et l'iodure de propidium (nécrose)<sup>24</sup>.

Le présent mémoire inclut deux publications dont je suis la première auteure, le chapitre I intitulé « Chapitre de livre : *Electrochemical Sensors and their Use in Cell Studies* » et le chapitre II : « Article scientifique : *Oxygen Plasma Treatment of Polystyrene and Zeonor Substrates for Adhesion of Patterned Cells* ». Étant donné que le chapitre I comporte une grande partie théorique et une revue de littérature incluant un historique des travaux dans le domaine, le mémoire arbore une forme particulière. En effet, la théorie n'est pas répétée dans l'introduction pour éviter la redondance. Tel que stipulé dans l'Annexe I du Règlement n° 8, le chapitre comporte une partie contribuant à l'avancement de la science puisque plusieurs résultats expérimentaux y sont présentés. De plus, le chapitre II accepté dans *Langmuir* est une continuité de la première publication. Il s'agit d'un article traditionnel comprenant: résumé, introduction, section expérimentale, résultats et discussion, conclusion et références. Étant donné que les références du chapitre de livre et de l'article sont déjà présentes dans les publications, elles ne sont pas répétées dans la section référence du mémoire. Cette section incluse dans l'appendice C fait seulement état des références utilisées dans l'introduction.

## CHAPITRE I

### CHAPITRE DE LIVRE: ELECTROCHEMICAL SENSORS AND THEIR USE IN CELL STUDIES

Le chapitre de livre qui suit porte sur les sondes électrochimiques et leur utilisation dans les études cellulaires. Dans un premier temps, un survol de la littérature est présenté. Celui-ci inclut les principaux travaux de recherche qui sont à l'origine du développement du SECM ainsi que les études faites sur divers systèmes biologiques. Les avancements possibles dans le futur sont aussi énoncés. Par exemple, une meilleure compréhension du transport de molécules électroactives vers l'intérieur ou l'extérieur des cellules pourrait aider au développement de médicaments plus ciblés. Ensuite sont présentés: la théorie concernant l'électrochimie et l'étude de cellules, la fabrication des substrats biologiques et les tests de biocompatibilité par fluorescence. Finalement notre contribution technique et certains des résultats expérimentaux y sont décrits. En effet, le Bio-SECM étant unique au laboratoire Mauzeroll, les caractéristiques de l'appareil sont présentées. Ce système permet d'observer la morphologie des cellules grâce à un microscope à fluorescence au moment de faire les analyses électrochimiques à distance constante. Également, des résultats préliminaires de formation de lignes de cellules obtenues par lithographie molle y sont montrés. De plus, l'injection des cellules dans les canaux est faite sans ajout substantiel de molécules d'adhésion, contrairement à la pratique courante, seule leur présence naturelle dans le sérum étant mise à contribution. Ce chapitre sera présenté dans le livre intitulé « The Chemistry, Physics and Engineering of Responsive Materials ».

## Electrochemical Sensors and their Use in Cell Studies

Chapitre 10 dans *The Chemistry, Physics and Engineering of Responsive Materials*, Bratcher, M.S., Gaddy, G.A., Kiserow, D. et Maher, M.W. (éds); John Wiley and Sons Publishing; sous presse.

Isabelle Beaulieu,<sup>1</sup> Matthias Geissler,<sup>2</sup> Danielle Dansereau<sup>1</sup> & Janine Mauzeroll<sup>1,\*</sup>

<sup>1</sup> Chemistry Department, Université du Québec à Montréal

<sup>2</sup> Institut des matériaux industriels, Conseil national de recherches du Canada

\* To whom correspondence should be addressed: [mauzeroll.janine@uqam.ca](mailto:mauzeroll.janine@uqam.ca)

### **1.1 Introduction**

Electrochemical sensors have found widespread use in a broad range of scientific and technological areas where they are employed to monitor electrochemical processes (e.g., electron and ion transfer reactions) at interfaces, in solution, or in air. The central part of most electrochemical sensors is an ultramicroelectrode (UME) – an electrode having dimensions in the micro- or nanometer range. UMEs were first developed by Engstrom and co-workers<sup>1</sup> and subsequently integrated into scanning electrochemical microscopy (SECM) by Bard and co-workers.<sup>2</sup> In SECM, the UME serves as a mobile probe that enables electrochemical activity of a surface to be recorded with remarkable sensitivity, short response times, and high spatial resolution.<sup>3</sup> Although the origins of SECM are in electroanalytical surface science, this technique has attracted increasing attention for biological application and the study of living organisms because it can i) quantify the flux of molecules entering or leaving a cell, ii) probe locally electrochemical reactions occurring at or inside a cell, and iii) perform the same measurements on single cells, cell features, confluent cells and tissues. Moreover, SECM measurements can be combined with other biosensing techniques, making it possible to perform multiple experiments on a living object simultaneously.

The abilities of SECM have been demonstrated in a number of ways. For example, bacterial redox activity<sup>4</sup> and respiration<sup>5</sup> have both been probed. The first in vivo measurements on intact plants revealed topography and photosynthetic electron transport of a single guard cell.<sup>6</sup> The metabolism of menadione was studied by measuring the glutathione

conjugated metabolite (thiodione) efflux in hepatocytes.<sup>7</sup> The influence of calcium ions on osteoclast activity was recorded to evaluate the reliability of in vitro models compared to in vivo activity.<sup>8</sup> White and co-workers accessed molecular transport in mouse skin using SECM, which allowed for quantification of the absolute flux rate through an individual pore.<sup>9</sup> Following in vitro fertilization, the oxygen consumption of bovine embryos has been measured in a non-invasive manner, which was used to evaluate the quality of the embryos and their potential for further development.<sup>10</sup> Moreover, Ding and co-workers studied two kidney fibroblast-like cell lines with atomic force microscopy (AFM), confocal microscopy (CM) and SECM, thereby detecting reactive oxygen species (ROS) produced by living cells.<sup>11</sup> Mirkin and co-workers were the first to measure the redox activity on a single mammalian cell.<sup>12</sup> Single-cell electrochemical behavior had previously been difficult to extract from measurements performed on confluent cells. By comparing fluorescence and SECM images of the same cells, selective detection of metastatic breast cells was possible.<sup>13</sup> Matsue and co-workers pioneered the use of SECM in conjunction with fluorescence imaging by evaluating the influence of chemicals on cell viability.<sup>14</sup> Bard and co-workers have placed the SECM directly above the stage of an inverted microscope; positioning the electrode over yeast cells allowed for measuring cell viability and the efflux of a menadione-glutathione conjugate.<sup>15</sup> A similar set up was used by Schulte and co-workers to study release of adrenalin and noradrenalin from chromaffin cells and to obtain topographical measurements of a single fibroblast.<sup>16</sup> These authors are also credited for coining the term biological SECM (Bio-SECM).

Further advances in SECM study of biological samples will be strongly tied to improvements in instrumental design and the availability of nanoprobe allowing for high sensitivity measurements in combination with other analytical methods.<sup>17-20</sup> It is also linked to the employment of compatible cell substrates,<sup>21</sup> access to simple microlithographic techniques to produce cell patterns, and routine use of cytotoxicity measurements. This chapter is intended to provide a short survey of our efforts in each of these areas with respect to current trends in the field. We subdivided this chapter into a set of dedicated sections that are organized in the following manner. Section 1.2 describes the basic principles underlying electrochemical measurements with UMEs. This is followed by a brief review of electrochemical sensors for cell studies (Section 1.3). Specifically, we discuss disk and fiber

UMEs (Section 1.3.1) as well as micropipets (Section 1.3.2) which all can be employed for various types of cell transport studies. Section 1.4 deals with technical aspects of SECM, focusing on three main topics. First, we briefly outline instrumental and operational principles of this technique (Section 1.4.1). We then describe the use of SECM as an analytical tool, with particular emphasis on systems that were designed for probing living cells (Section 1.4.2). We review advances in SECM instrumentation essentially from a conceptual rather than conclusive point of view. In Section 1.4.3 we discuss the different modes of feedback control that are suitable for probing living cells. Section 1.5 is dedicated to the substrate and the biological probe itself. In Section 1.5.1 we describe the design, fabrication and functioning of relatively simple elastomeric microcapillary systems ( $\mu$ CSs) that can be used for confining cells on surfaces with spatial control. This is followed by a short summary of our recent efforts on patterning HeLa cell cultures on plastic substrates (Section 1.5.2). Section 1.5.3 is finally devoted to fluorescence-based essays revealing the status of a cell during or after electrochemical probing. Section 1.6 concludes this chapter with personal remarks on present as well as future aspects of biosensing using SECM.

## **1.2 Basic Principles of Ultramicroelectrodes**

Historically, the term UME was first applied to micrometer-sized electrochemical sensors since the proper term microelectrode has already been used for electrodes in the millimeter size regime. Today, several groups prefer consistency in terminology and the term microelectrode solely be referred to micrometer-sized sensors.<sup>22</sup> Herein, we use the term UME to define electrochemical sensors that have dimensions ranging from tens of micrometers to the nanometer scale. UMEs can be prepared from different electroactive materials (e.g., carbon, platinum, or gold) using a number of fabrication schemes. Moreover, geometry of an electrode can vary depending on the intended application, including microdisks, microrings, microbands, microcylinders (e.g., a single fiber), microspheres, and microhemispheres as the most common forms. A more detailed description of selected UMEs is provided in Section 3. A comprehensive survey of UME preparation methods is available elsewhere.<sup>23</sup>

UMEs have unique properties that make them ideal sensors for biological SECM. Their small size allows an unhampered approach to cells and provides lateral resolution for imaging single cells. In addition, they present improved faradaic-to-charging current ratios leading to increased signal-to-noise ratios.<sup>24</sup> For example, current signals as low as 30 fA can be measured depending on the electronics of a particular instrument and the size of the UME used. Also, the potential applied to a UME can be altered rapidly (up to  $10^6$  V/s) as a result of reduced charging currents. The ohmic drop of the potential,  $RI$ , is relatively small for UMEs since the measured currents are low. Finally, they rapidly reach steady-state conditions, which is a prerequisite for the use of UMEs in SECM imaging. In the case of a disk UME the expression for this steady-state current,  $I_{ss}$ , (A) is defined as

$$I_{ss} = 4nFDcr \quad (1)$$

where  $n$  is the number of electrons involved in the electrochemical process,  $F$  is the Faraday constant ( $96.48534 \times 10^3$  C/mol),  $D$  is the diffusion coefficient of the electroactive species in solution ( $\text{m}^2/\text{s}$ ),  $c$  is the concentration of the electroactive species ( $\text{mol}/\text{m}^3$ ) and  $r$  is the radius (m) of the electroactive sensor. At steady-state, the sensing zone of a UME is precisely defined and localized within a restricted solution volume at the electrode/solution interface. This implies that the response of the sensor in a homogenized electroactive solution is independent of the actual position until the UME is brought in close proximity to a surface that can interact with its sensing zone. Since the behavior of the UME is affected by mass transport of dissolved electroactive material in the vicinity of the electrode, the presence of a nearby surface can hinder or add to the flux of material detected by the sensor.

The presence of a steady-state current during a faradaic process separates UME electrochemical behavior from that of classical electrodes used in electroanalytical chemistry. There is, however, no clear dependency of dimensions, such as the radius of the electroactive disk, and UME properties. It rather is a relationship between size and shape of the electrode and the thickness of the diffusion layer that dictates what the observed electrochemical behavior shall be. In the case of a reversible charge-transfer reaction involving a dissolved electroactive substance, O, the current measured at the UME is proportional to the flux,  $J_o$ ,

(mol/(s m<sup>2</sup>)) of O at the solution/sensor electrode interface, which is described by Fick's first law as

$$-J_o(x,t) = D_o \partial c_o(x,t) / \partial x \quad (2)$$

where  $x$  and  $t$  denote positions in space and time, respectively. Fick's first law states that the flux of O is proportional to the concentration gradient,  $\partial c_o / \partial x$ , at a particular moment and location. The change in concentration of O,  $\partial c_o$ , with time is described by Fick's second law generalized for any geometry by

$$\partial c_o(x,t) / \partial t = D_o \nabla^2 c_o \quad (3)$$

where  $\nabla^2$  is a Laplacian operator characteristic of different diffusion geometries. The operator used in the case of linear diffusion to a planar electrode would be different from that of spherical diffusion observed, for example, at a gold sphere electrode.

Equations 2 and 3 reveal that the concentration profile of the reacting electroactive substance is dependent on both distance from the electrode/solution interface where the electrochemical process is occurring and time. Practically, this relationship implies that by switching the UME potential from a value where no electrochemical reaction occurs to that where O is reduced, O will be consumed, hence  $c_o$  will approach zero at the electrode/solution interface ( $x = 0$ ) and  $\partial c_o / \partial x$  will develop within a defined region of the bulk solution. The volume of solution in which diffusion of O to the electrode solution interface occurs is called the diffusion layer and is also dependent on the electrolysis time. The thickness of the diffusion layer,  $\delta$ , for planar semi-infinite diffusion is defined as

$$\delta = \sqrt{(\pi Dt)} \quad (4)$$

where  $\pi$  is the circular constant (3.141592). To observe UME behavior, the following two conditions must be fulfilled.<sup>24</sup>

- 1) The electrolysis time must be sufficient, given the dimensions of the sensor, to reach steady-state conditions.
- 2) The ratio of  $\delta r$  must be much larger than 1.

At short electrolysis time, small planar UME sensors behave like large planar electrodes. This can be experimentally observed by progressively increasing the scan rate during cyclic voltammetry (CV) at a 25  $\mu\text{m}$  disk UME. For scan rates below 10–20 mV/s, a sigmoidal CV response that reaches a steady-state current is observed. At higher scan rates, a characteristic “duck-like” shape voltammogram is obtained. With increasing time, the diffusion layer develops to its full potential in bulk solution and UME behavior is developed if condition 2) is met. The time that is necessary to reach steady-state is dependent on the surface area of the sensor. A sensor having characteristic dimensions of  $r = 1 \text{ mm}$  would require more than  $4 \times 10^4 \text{ s}$  for its current signal to be dominated by the steady-state component at 90%, while a UME with  $r = 1 \mu\text{m}$  would achieve steady-state conditions in only 0.04 s.<sup>24</sup>

There are two important contributions to the current measured at an electrochemical sensor: the flux of substance normal to the electrode plane called linear diffusion (Figure 1.1A) and the flux of substance at the edges of the sensor which is referred to as hemispherical diffusion (Figure 1.1B). The latter is responsible for the lack of uniformity in current density commonly measured across an electrode surface. For a large planar sensor, linear diffusion dominates and the contribution of the hemispherical diffusion to the overall current is minimal. This leads to  $\delta r$  much smaller than 1 and the advent of classical electrode behavior. As the size of the sensor decreases, the contribution of the hemispherical diffusion to the overall current increases and the diffusion-limited flux to the electrode becomes constant with time. Since the current is proportional to  $J_0$  as described in eq 2, a steady-state current is observed. This current is further related to  $c_0$  (eq 1) because the time derivative of eq 3 is zero.<sup>24</sup> This situation occurs when  $\delta r$  is much larger than 1.

### 1.3 Ultramicroelectrodes in Cell Studies

#### 1.3.1 Disc and Fiber UMEs

Electrochemical sensors used to study single cells and cell patterns must have appropriate dimensions, be stable over the time scale of the experiment, be sensitive and selective to the analyte and have a high signal-to-noise ratio. The materials commonly used for the preparation of these sensors include carbon, platinum and gold. For the purpose of quantitative studies or cell imaging, the preferable sensor geometry is often a disk-shaped electrode surface because its behavior is theoretically well understood and widely documented in the literature. Ideally, the electrode area should be on the order of or smaller than the surface area of the cells to be studied. The surrounding insulating material (e.g., glass, paint, or wax) should be minimized not to hinder close approach to the cells. Initially, carbon was the preferred material for cell studies because it was thought to be less susceptible to electrode fouling than platinum and gold. Recent studies using platinum UMEs in extracellular<sup>7</sup> and intracellular<sup>25</sup> experiments observed no significant fouling of the metal surface by cell constituents. Arguably, gold sensors would best be used in extracellular studies given the high affinity of sulfur-containing proteins to gold. Gold remains nevertheless an interesting material for the preparation of UMEs mainly due to ease of sensor preparation and its sensitivity to quinone-containing compounds.<sup>15</sup> The sensitivity and selectivity of the UME electrode material to an analyte interacting with or originating from a cell is hard to predict. Carbon has been used to detect the release of catecholamine neurotransmitters on individual adrenal gland cells (PC-12) and chromaffin cells.<sup>26,27</sup> These cells undergo exocytosis thereby releasing hormones and neurotransmitters from membrane-bound storage vesicles into the extracellular space. In this case, a carbon UME with a diameter of 1–2  $\mu\text{m}$  was placed directly above the center of an immobilized cell at a separation distance of  $<1 \mu\text{m}$  (Figure 1.2A). The UME response related to the detection of vesicular chemical release coming from secretory vesicles is shown in Figures 1.2B to 1.2D. Prior to recording, the formed secretory vesicles were loaded with a desired chemical transmitter. During cell signaling, the loaded vesicles dock at the plasma membrane,

rearrange and upon the presence of an external stimulus are released into the extracellular space following activation of the  $\text{Ca}^{2+}$  ion channels.

The carbon UME sensor is obtained by sealing a carbon fiber (CF) into an insulating sheath followed by careful polishing (in the case of glass) or sectioning with a scalpel (in the case of polymers such as polyethylene, propylene, or electrophoretic paint). There are several methods that can be used to produce disk-shaped CF-UMEs with diameters of 5–10  $\mu\text{m}$  (Figure 1.3).<sup>28,29</sup> Further reduction in diameter of CF-UMEs can be achieved through electrochemical,<sup>24,30,31</sup> electrical,<sup>32</sup> flame,<sup>24,33-35</sup> or ion beam<sup>36</sup> etching procedures. Modification of the carbon electrode surface with complexes or enzymes is often needed to improve the selectivity of sensors to other important cell analytes such as nitrogen oxide or glucose.<sup>34,37-39</sup> Alteration of electrode properties however requires a significant sensor response analysis prior to the electrochemical cell studies.

Bare, disk-shaped platinum UMEs are used for extra- and intracellular local measurements of oxygen gas,<sup>25</sup> cell metabolites (e.g., thiodione),<sup>7,15</sup> and reactive oxygen species.<sup>40</sup> Typically, they are produced by sealing platinum nano- or microwires with thin tapers of pulled glass capillaries and then polishing the excess glass.<sup>41-46</sup> This can be achieved by pulling an annealed platinum wire (25  $\mu\text{m}$  diameter) into glass (e.g., made of borosilicate or quartz) under vacuum using a laser pipet puller. Shape and size of the sensor are controlled through optimization of the pulling parameters. This fabrication technique is highly dependent on the delicate exposure of the Pt electrode surface by polishing. The characteristic voltammograms recorded at these sensors are fully retraceable and attain a steady-state current at sweep rates as high as 10 V/s.<sup>25</sup> Ultrasharp platinum disk UMEs of nanometer dimensions are produced in the same way (Figure 1.4, *inset*). With a tip radius being 1,000 times smaller than that of a cell, these UMEs can penetrate a cell without apparent damage to the membrane and measure membrane potentials.

When human breast epithelial cells (MCF-10A) are exposed to a solution of a hydrophobic redox substance, such as 1-(ferrocenyl)methanol ( $\text{FcCH}_2\text{OH}$ ), partition of the substance occurs between the extra- and intracellular domains. The potential of the cell membrane can be estimated by measuring the voltammograms at a platinum UME sensor outside and inside the cell (Figure 1.4A). In the case of  $\text{FcCH}_2\text{OH}$  oxidation, the difference of 36 mV between the half-wave potentials ( $\Delta E_{1/2}$ ) in curves 1 and 2 is attributed to the potential

drop across the cell membrane of the MCF-10A cells (Figure 1.4A). Reproduced with different UMEs, a mean  $\Delta E_{1/2}$  of  $46 \pm 4$  mV (for  $n = 18$  at the 95% confidence interval) was obtained. The addition of depolarizing agents (e.g., valinomycin at a concentration of 600 nM) to the solution was expected to diminish the membrane potential. In each of the seven experiments performed on MCF-10A cells in presence of valimoycin,  $\Delta E_{1/2}$  decreased markedly, and an average value of  $\Delta E_{1/2} = 16.7$  mV was observed for FcCH<sub>2</sub>OH mediator. Although there is some variability in the membrane potential values reported in the literature, measured average values for  $\Delta E_{1/2}$  are somewhat higher than most numbers obtained for mammalian cells by different techniques (e.g., 58.6 mV vs. 2.7 mV reported for MCF-7 human mammary tumor cells).<sup>47</sup> In this experiment, the platinum UME potential was measured with respect to an Ag/AgCl reference electrode positioned in the extracellular solution. Since membrane polarization can be induced by the current flow between the intracellular platinum UME and the external reference electrode, the dependence of  $\Delta E_{1/2}$  on the concentration of FcCH<sub>2</sub>OH was studied. The ohmic potential drop across the membrane,  $RI$ , (V) with  $R$ , ( $\Omega$ ) being the membrane resistance, is proportional to  $I$ , (A) flowing at the tip of the electrode inserted in the cell. The voltammograms in Figure 1.4A represent the platinum UMEs response in a bulk solution of FcCH<sub>2</sub>OH outside the cell (curve 1) and inside the same cell (curves 2–5) for different concentrations of FcCH<sub>2</sub>OH. By varying the concentration of FcCH<sub>2</sub>OH in solution, a linear dependence of the tip current corresponding to the half-wave potential,  $I(E_{1/2})$ , is obtained (Figure 1.4B). The  $\Delta E_{1/2}$  value decreased upon dilution, and the plot of  $\Delta E_{1/2}$  vs.  $I(E_{1/2})$  was also linear (Figure 1.4C). The membrane resistance extracted from the slope of the graph is on the order of 4 G $\Omega$ . Interpolation of the plot reveals a membrane potential corrected for the polarization effect of about  $-10$  mV, which is in good agreement with values reported in the literature.<sup>47</sup> Although more in-depth work needs to be done, the use of intracellular voltammetry to measure membrane potential is a relatively straightforward technique that could easily be applied to several cell cultures. It may also complement other methods for evaluating membrane potentials, including patch clamp,<sup>48</sup> the use of ion-selective probes,<sup>49</sup> and fluorescent dyes.<sup>50</sup>

### 1.3.2 Electrochemical Micropipets

Electrochemical micropipets are a relatively new type of electrochemical sensor that is being developed for biological SECM. They consist of glass micropipets coated with a thin film of gold or platinum. With subsequent insulation of the sides of the micropipets with electrophoretic paint and heat curing, it is possible to obtain an electroactive ring in the nanometer regime at the aperture of the pipet. The nanometer dimensions of the sensor combined with their ability to dispense volumes of solution in the pL range near or inside a cell make them attractive candidates for cell transport studies. The dispensing capabilities of the micropipet outweighs the geometrical preferences for a disk electrode surface presented in Section 1.3.1. In the past, micropipets have been reported in ion-selective electrode studies that monitor ion-transfer reactions.<sup>51-54</sup> Micropipets can also be filled with enzymes to probe the catalytic activity of a surface<sup>55</sup> or be used for microdispensing experiments in conjunction with scanning chemiluminescence microscopy (SCLM).<sup>56,57</sup> The deposition of a defined electroactive layer on the outside of the micropipets allows for simultaneous dispensing of solution and electrochemical detection. This feature is critical in biological SECM in order to precisely determine the initial time,  $t_0$ , of the injection process, which is important during quantitative kinetic studies of cell transport.

The preparation of electrochemical micropipets requires several steps. Borosilicate glass capillaries are first pulled using a filament or laser puller. The shape of the resulting pipet is dependent on the pulling parameters and can be optimized to yield apertures that are 1–2  $\mu\text{m}$  in diameter having a well-defined taper that is  $\sim 0.5$  cm long. The pulled end of the micropipet is then coated with a thin film of gold by thermal evaporation. Micropipets are rotated at a rate of  $\sim 30$  rpm at an angle of 20–50 degrees with respect to the surface plane to obtain a uniform gold coating and prevent accumulation of gold at the aperture. Rotation of the micropipets is maintained throughout the entire evaporation process and during cooling of the evaporation chamber to obtain a smooth and uniform deposit. Electrical connection to the gold film is made using a fine copper coil and conductive, silver-containing epoxy resin. The gold ring electrodes are produced by insulating the side walls of the coated micropipet with an anodic or cathodic electrophoretic paint.<sup>58,59</sup> This method of insulation is effective for the preparation of submicron size sensors.<sup>30,42,60-62</sup> To prevent clogging of the capillary during the

electrophoretic deposition step, the unmodified end of the micropipet is connected to a source of nitrogen gas at a pressure of  $\sim 50$  psi. The gold-coated end of the micropipet is then inserted in the middle of a platinum coil immersed in the electrophoretic solution. Depending on the choice of paint, chronopotentiostatic deposition or CV may be used to achieve the desired coating.<sup>58,59</sup> Following deposition, the pipet is rinsed and cured by thermal treatment.

Characterization of the micropipet-based electrochemical sensor is typically done by scanning electron microscopy (SEM), CV and SECM approach curves. Figure 10-5 shows different views of gold ring micropipets with and without insulation layer. The gold film is uniform and extends down to the very edge of the micropipet aperture without blocking its opening, as demonstrated by the images in Figure 1.5A. Here, the diameter of aperture is on the order of  $2\ \mu\text{m}$  while the gold film is  $50\text{--}80\ \text{nm}$  thick. The thickness of the insulation layer at the pipet aperture is only a few tens of nanometers (Figure 1.5B). Depending on the electrochemical behavior of the pipets, a second coating of paint is sometimes needed to minimize the presence of pinholes in the polymer layer. A disadvantage of using several coatings is the possibility of blocking the end of the pipet with the insulating layer (Figure 1.6A). When such a situation arises, the blocking polymer layer can be expelled using a high-voltage source (e.g., 6 kV) that generates a spark under a helium flow at the anode (–) between the two sacrificial gold wires (Figure 1.6B). It is the field effect generated at the end of the micropipet that removes the blocking polymer layer. Successful removal of the insulation layer can be visualized electrochemically through the return of the signal (Figure 1.6C).<sup>59</sup> The electrochemical behavior of the micropipets is well-defined and follows the steady-state current that would be expected from the literature for a ring electrode.<sup>63</sup> The SECM approach curves in the positive and feedback modes are also consistent with theory.<sup>58</sup> Electrochemical micropipets are desirable sensors for cell transport studies. They can mediate injections of electroactive substances into a cell or generate constant flow of a solution nearby a cell, allowing drugs or other agents to stimulate a response from the cell. Their dispensing capabilities have been reported in a proof-of-concept dispensing/feedback SECM imaging experiment.<sup>58</sup> They can also be used patch onto a giant unilamellar vesicle to perform membrane studies as illustrated in Figure 1.7.

## **1.4 Biological Scanning Electrochemical Microscopy**

### **1.4.1 Basic Principles of SECM**

In SECM, the UME is scanned over a surface using a high-resolution 3D micropositioning system. During movement of the electrode, the steady-state current is monitored continuously. Steady-state current is observed when the electrochemical reaction of a dissolved reversible redox species at the UME/solution interface is mass transfer-limited, at least for potentials far exceeding the redox potential of the species. Given the UME's unique properties,<sup>22</sup> the localized hemispherical diffusion zone of the species in front of the UME is used to detect topography and/or reactivity of a nearby surface (Figure 1.8). Surface topography is revealed by monitoring the extent by which the diffusion of species from surface features is hindered. Large features disrupt significantly diffusion to the UME and alter the localized hemispherical diffusion zone such that a decrease in UME current is observed. Surface reactivity is evaluated from localized increases in UME current that are related to the kinetics of species regenerated at the sample surface. There are other important parameters that affect SECM responses, such as UME geometry, the UME-to-surface distance and the so-called RG factor, which is the ratio of the radii of insulating material and metal wire. A detailed explanation of their contribution is available elsewhere.<sup>2</sup>

Observed UME currents in SECM experiments are affected by both topography and/or reactivity of the sample surface; hence an un-ambiguous interpretation of SECM imaging studies requires deconvolution of each contribution. In the case of an SECM approach curve, where the UME is approached normal to the sample surface, there is no need to deconvolute the SECM response, as long as the UME is much smaller than the sample surface features. In the case of SECM imaging where the UME is positioned within a few tip radii of the sample surface and scanned parallel to the surface plane, two experimental strategies – constant-height and constant-distance – are commonly employed (Figure 1.9A). In constant-height imaging, the UME is scanned over a surface in both  $x$ - and  $y$ -directions at a fixed vertical distance ( $z$ -direction). Constant-height imaging can be readily applied to smooth and planar samples where features do not exceed preset values in height, as is the case for self-assembled monolayers of alkanethiols on gold.<sup>64</sup> Although instrumentally easier

to implement, constant-height imaging is prone to tip-sample crashes when the preset height is reduced to achieve better resolution. It is therefore unlikely that constant-height mode imaging will be used significantly in SECM studies of biological samples, especially when large aspect-ratio features, such as cells, are the subject of investigation. Constant-distance SECM imaging, on the other hand, uses an additional feedback control mechanism to maintain a constant UME-to-sample distance, making it possible to deconvolute surface topography from its electrochemical activity. Some of these feedback control mechanisms are discussed in Section 1.4.3. At present, constant-distance imaging mode is widely accepted as the norm for the application of SECM to studies with immobilized cells.

#### **1.4.2 Biological Scanning Electrochemical Microscopy (Bio-SECM)**

The concept of Bio-SECM emerged after several groups combined conventional SECMs with inverted microscopes in order to build an instrument suitable to study local electrochemical reactions at immobilized cells (Figure 1.9B).<sup>7,15,16,25,65,66</sup> The inverted microscope confers several advantages to cell studies including quick identification of healthy cells based on morphological changes and repositioning of the UME close to cells, which reduces overall experimental time. Cell activity in the context of an SECM experiment is difficult to define and can imply both direct and indirect modes of electrochemical detection. Direct detection is generally applied to cell constituents (e.g. a neurotransmitter), cell metabolites (e.g. thiodione), or cell functions (e.g. respiration). Indirect detection methods may be employed when direct measurements are difficult to perform, as is the case for some cell properties (e.g. the intracellular redox potential of a cell) and reactions occurring at its surface.

The instrumental setup of our Bio-SECM manufactured by HEKA (Germany) is schematically presented in Figure 1.9B. The instrument employs an inverted microscope comprising adapted optics for cell imaging such as Hoffman Modulation Contrast to visualize cell morphology and quickly identify healthy cells prior to performing electrochemical measurements. The microscope is also equipped with a fluorescence module and a CCD camera to perform toxicology and viability measurements simultaneously during or following SECM imaging. The entire microscope system is mounted on an *x-y* translation stage to align

the optical axis of the microscope with the UME. The UME is placed above the immobilized cell substrate residing in a specially designed electrochemical cell that also accommodates reference and auxiliary electrodes. The UME is connected to a constant-distance controller that regulates the UME-to-cell distance during imaging. The setup is placed on a vibration-damping table enclosed in a Faraday cage to shield the instrument against acoustic and electrical interference during measurements and improve fluorescence-imaging conditions.

### 1.4.3 Constant-Distance Feedback Controllers

Maintaining a constant UME-to-sample distance during SECM imaging is achieved by using the feedback signal from a distance controller that continuously monitors the position of the UME, compares it with a preset value, and adjusts the UME positions when deviations occur. Figure 1.9C presents selected examples of constant distance controller schemes that proved suitable in conjunction with SECM instrumentation. They include shear-force (e.g., optical, tuning-fork, and piezoelectric plates), UME current modulation, UME impedance, and AFM-based feedback mechanisms.<sup>26</sup> Shear-force based distance controllers rely on the detection of short-range (100–200 nm) hydrodynamic forces between the sample and a vibrating UME that approaches the surface at a predefined resonance frequency. Damping of the resonance frequency by the viscous drag of liquid in between the UME and the surface provides feedback for the SECM positioning system and is used to maintain a constant UME-to-sample distance. Resonance frequency damping of the vibrating UME can be monitored optically by projecting the Fresnel diffraction pattern that is generated from the interaction of a focused laser beam and the UME body onto a split photodiode.<sup>67</sup> Another concept of feedback control, which has originally been developed for near-field scanning optical microscopy (NSOM), involves a UME that is fixed to one leg of a tuning fork and vibrated using a piezoelectric buzzer. The resulting resonance frequency of the tuning fork produces an AC voltage output that is sensitive to the presence of shear-forces between the UME and the surface that is to be investigated.<sup>65,68-71</sup> Moreover, a combination of piezoelectric plates exciting the UME at a resonance frequency and detecting the amplitude of the UME vibration can also be used.<sup>72</sup> This scheme is employed in the HEKA instrument presented in Figure 1.9B.

An alternative approach uses the electrolysis current of a dissolved species to regulate the UME position;<sup>70,73</sup> it relies on superposition of a sinusoidal wavefunction onto a constant DC potential such that a resulting AC current flow is recorded providing feedback for constant distance imaging.<sup>66,74</sup> The use of UME impedance has also been explored as a means of retaining constant distance for SECM measurements.<sup>40,75-79</sup> In this scheme, the UME impedance is modulated to high frequencies (~50 kHz) so that it can be detected independently from Faraday processes that occur at lower frequencies. Simpler to implement than shear-force methods, UME impedance can monitor cell morphology and substrate topography in a medium that is free of redox species. Impedance-based methods are however susceptible to local impedance variations during certain biological processes such as vesicular release.<sup>68</sup> Also, the resolution of impedance-based imaging is typically lower than that obtained with competing concepts, such as constant-current imaging (Figure 1.10). The use of specialized cantilevers in conjunction with AFM instrumentation proved suitable for achieving high-resolution SECM imaging.<sup>80-82</sup> Drawbacks of combined SECM-AFM strategies include relatively long acquisition times, the need to modify the surface of cantilevers, and limited robustness. The controllers described in this section all strive to master constant-distance SECM measurements performed on soft substrates, such as cells. Soft substrates are technically more challenging to probe than rigid ones (e.g., the surface of a metal film) since their interfaces are less confined. Cells are also likely to deform upon contact with the UME. Cell/UME contact may occur in the case of shear-force positioning systems that require UME-sample separation of a few hundred nanometers. The impact of this contact on frequency damping is unclear, yet it should vary significantly with the type of UME used.<sup>16</sup>

## **1.5 Biomaterial Design: Cell Patterns Used in Bio-SECM**

### **1.5.1 Microfluidic Systems for Cell Patterning**

Microfluidics generally refers to the science and technology of handling, manipulating, and processing minute amounts of liquid.<sup>83-85</sup> The central part in a microfluidic

system is a microchannel (or a set of microchannels) able to confine liquid at dimensions of between 1 and 1000  $\mu\text{m}$ . The use of microfluidic systems makes it possible to control volume, position, and transport of fluids with precision that is unprecedented by conventional operations performed at the bench-top in standard laboratory settings. These systems are particularly appealing to applications in chemistry and biology, where they can serve, for example, as miniaturized reaction vessels that enable reduction of reagents and processing times,<sup>86</sup> synthesis of particles with new shapes and forms,<sup>87</sup> or attachment of proteins and cells at selected sites on a surface.<sup>85,88</sup> The design of fluidic systems can vary depending on the intended use, and may range from simple, two-dimensional (2D) capillaries to integrated chips comprising complex circuits of fluidic structures along with functional elements such as miniaturized mixers, valves, and pumps.<sup>89</sup> In principle, such structures can be fabricated from a number of materials including both soft and rigid ones, with the former being particularly useful for research and prototyping purposes. Poly(dimethylsiloxane) (PDMS) is an elastomeric polymer that is commonly employed for soft lithography in both academic and industrial environments.<sup>90-92</sup> PDMS is well suited for biological studies due to its unique characteristics: it is flexible, chemically inert, optically transparent, durable, permeable to gases, and compatible with cells.

Microfluidic (or microcapillary) systems in PDMS are commonly prepared using rapid prototyping – a process that allows multiple copies of a desired pattern to be produced in a relatively short period of time and at low cost.<sup>92</sup> The first step in the fabrication process concerns the layout of the  $\mu\text{CS}$ . This is typically accomplished by defining the desired components (e.g., channels, inlets, outlets etc.) as transparent regions in an otherwise dark (opaque) background using a computer-aided design (CAD) program (Figure 1.11A). Features having lateral dimensions of  $>8 \mu\text{m}$  can directly be printed on a transparent polymer foil using a high-resolution photoplotter. In this way, a set of photomasks can be obtained rapidly (e.g., in less than 24 h for certain suppliers) and at a relatively low cost. For features  $<8 \mu\text{m}$  it is necessary to transfer the design into a thin layer of chromium supported on a quartz plate. The fabrication of these high-end photomasks typically involves a scanning beam of electrons to write the desired pattern into a responsive medium (e.g., a thin polymer film), which then protects selected regions of the underlying chromium layer in a subsequent etch process. Depending on the overall area to be patterned, time and cost associated with this

fabrication scheme can be considerable. The use of printed transparency foils therefore appears to be preferable for rapid prototyping, especially when test structures may be subjected to several iterations in design.

The next step is related to the formation of an original pattern in the form of topographic structures (called master) using optical lithography (Figure 1.11B). Optical lithography (also called photolithography)<sup>93</sup> uses a thin film of radiation-sensitive material (photoresist), which is applied to a silicon wafer by spin coating, and exposed to UV light of appropriate wavelength. The photomask is thereby posted between the light source and the resist film inducing illumination of the resist in a spatially controlled manner. When performed in contact mode, the mask comes in physical contact with the resist film, reproducing all features in a 1:1 ratio, as illustrated in Figure 1.11B. More sophisticated exposure tools operate with the mask being further away from the surface of the wafer, while a system of lenses projects a demagnified image of the mask onto the resist. Photoresists are organic polymers that undergo changes in structure and composition when illuminated. This renders the material either soluble (positive-tone) or insoluble (negative-tone) in a liquid medium used for development. SU-8 (an epoxy-based bis-phenol A novolac resin) is commonly employed for master fabrication due to its inherent thermal and mechanical stability,<sup>94</sup> which allows a single master to be reused many times without notable degradation.

The third step constitutes the fabrication of the  $\mu$ CS itself, which is done by replica molding of the master pattern in PDMS (Figure 1.11C). In contrast to master fabrication, this process can be performed in standard laboratory settings. It is generally preferable to coat the master with a thin film of Teflon<sup>®</sup> or a fluorinated silane before use to decrease interfacial adhesion forces so that the PDMS can be released properly after the replication process is completed. PDMS is commonly formed from an elastomer base (a vinyl-terminated siloxane) and a cross-linking reagent (a hydrogen-terminated siloxane) that are reacted in the presence of a Pt catalyst. These precursor components – being liquid at room temperature – are mixed before use, poured onto the master, and cured at elevated temperature (e.g., 40–80 °C). During the curing process, the material solidifies into a cross-linked polymer network that allows the shape of the photoresist features to be preserved with high fidelity. The ratio of the precursor components, their structure and molecular weight are all-important with respect to the elastomeric properties of the forming polymer network. Most common applications rely

on commercially available kits of Sylgard 184 (Dow Corning) for which a ratio of 10:1 (w/w) elastomer base/cross-linker is recommended. The final product has a surface hardness of 50 (Shore A) and a Young's modulus of about 2.5 MPa, generally restricting its use to the replication of structures  $>1 \mu\text{m}$ .<sup>91</sup> The features that we produced in the course of our work were, by comparison, relatively large in size with the smallest dimension being  $20 \mu\text{m}$  for both width ( $w$ ) and depth ( $d$ ) of the microchannels. Variation in  $w$  was possible over a broad range of length scales (e.g., up to  $400 \mu\text{m}$ ) without compromising the mechanical stability of microchannels.

A main advantage of PDMS (and other elastomers) over rigid materials, such as silicon or glass, is the ability to conform to other surfaces.<sup>95</sup> Using this effect, microchannels in PDMS can be enclosed conveniently by bringing the device in contact with a smooth surface, as illustrated in Figure 1.11D. In most cases, PDMS conforms spontaneously; hence no additional forces have to be applied, limiting distortion of the capillaries. The seal forming as a result of conformal contact is watertight, which is a necessary requirement for filling capillaries with a liquid. For pristine PDMS, conformal contact is normally reversible, and devices can be removed from a substrate, often without leaving notable residues on the surface. Introducing a liquid to microchannels is typically done via macroscopic access points (called inlets). Likewise, a liquid can be collected in designated areas (usually called outlets) when a desired operation has been completed. Both inlets and outlets can be generated by punching or drilling holes through the PDMS layer. For some applications, these holes can remain open in order to provide temporary access for a pipette or syringe. For others, they may serve as permanent entry points for polymer tubing that connect the channels with external reservoirs to operate under the conditions of continuous flow.

The motion of liquid inside a microchannel is given by

$$Q = \Delta P/R \tag{5}$$

where  $Q$  is the volume flow rate ( $\text{m}^3/\text{s}$ ),  $\Delta P$  is the difference in pressure across the channel (Pa), and  $R$  is the resistance to flow ( $\text{Pa s}/\text{m}^3$ ) which is dependent on fluid viscosity and overall geometry of the microchannel. Pressure-driven flow requires the use of a pumping system (e.g., a syringe pump) to be connected to one side of the channel. For example, liquid

can be pushed forward when a positive pressure is applied to the inlet. This method is however not very well suited for irreversibly sealed microchannels, as they cannot withstand very high pressures. It is equally possible to attract liquid by applying a negative pressure to the channel outlet, which is commonly preferable for systems that are bonded in a non-permanent manner. For some fluidic devices, capillary phenomena can generate a pressure drop sufficient to move a liquid in an entirely autonomous manner.<sup>96</sup> Since repeating units of dimethylsiloxane ( $-\text{O}-\text{Si}(\text{CH}_3)_2-$ ) render the surface of PDMS largely hydrophobic, exploiting capillary forces for displacing aqueous solutions may necessitate hydrophilization of fluidic structures. This can be realized through treatment of PDMS with oxygen plasma, resulting in the formation of silanol ( $\text{Si}-\text{OH}$ ) groups at the surface. Flow in linear microchannels is generally characterized by low Reynolds numbers with molecular diffusion being the dominant driving force in supply and exchange of reagents under laminar conditions.<sup>84,88</sup> Convection in liquid flow can be achieved through the implementation of passive elements such as bas-relief structures,<sup>97</sup> split-and-recombine systems,<sup>98</sup> or multivortex areas,<sup>99</sup> although it is equally possible to pursue active methods of mixing such as magnetic stirring<sup>100</sup> or acoustic actuation.<sup>101</sup>

### 1.5.2 HeLa Cell Patterns

In addition to HeLa cells, a number of mammalian cell lines have successfully been used in conjunction with soft, PDMS-based micropatterning techniques. Selected examples include human embryonic kidney (HEK), several strains of fibroblasts, hepatocytes and C2C12 mouse myoblasts.<sup>102-106</sup> Moreover, culture of bacteria and yeast cells in microfluidic environments has also been reported.<sup>107</sup> HeLa were the first immortal cell line to be maintained *in vitro* in laboratories in 1951.<sup>108-110</sup> They are robust cervical adenocarcinoma cells that can take over other cells if they are mixed in the same Petri dish.<sup>108,111-113</sup> As of today, HeLa cells are one of the most widely used cancer lines,<sup>108</sup> mainly because these cells are easy to cultivate. Moreover, they multiply at great speed with a doubling time of between 18 and 32 hours.<sup>114-116</sup>

At present, we focus on the patterning of HeLa cells on hard thermoplastic supports, which serve as a convenient and inexpensive alternative to glass. For example, Zeonor<sup>®</sup>

1060R – a polycyclic olefin copolymer<sup>117</sup> – was compatible with HeLa cells, allowing their attachment and growth in both unconfined and microfluidic environments. Patterning of cells using PDMS  $\mu$ CS can be combined with injection of proteins such as collagen or fibronectin, which promote cell adherence on glass or plastic substrates. Alternatively, cell suspensions can be directly injected into the channels when plastic supports with a proper surface chemistry are employed (Figure 1.12). Hydrophilization of the plastic surface by exposure to oxygen plasma facilitates transport of the HeLa cells into the channel, where they adhere, thereby respecting the pattern imposed by the microchannels. Using this approach, we were able to generate different cell patterns rapidly and reproducibly as shown in Figure 1.12C. Depending on the disposition of cells, single cell electrochemical measurements may be performed, evaluating for example the impact of cell confluence on cytotoxicity. We also envisage to study surface electron transfer reactions and communication events between cells arranged in linear fashion. Specially designed  $\mu$ CSs may further offer the possibility to pattern cells in a number of formats that allow for performing complex electrochemical analysis.

### 1.5.3 Fluorescence-Based Cell Status Assay

During Bio-SECM measurements, cells are exposed to conditions that may differ notably from those they experienced during culture in an incubator. For example, changes in CO<sub>2</sub> levels, temperature and media, exposure to chemicals (e.g., electroactive species, drugs etc.), and confinement in patterns can potentially affect the cell's activity and hence the recorded SECM current. It is therefore essential to assess the cell status while performing electrochemical analysis. The use of fluorescence microscopy is a rapid and convenient way to discriminate dead and living cells. The effectiveness of fluorescence-based cell monitoring, however, relies on the selection of appropriate fluorophores and their attachment to specific proteins interacting with the cell. The fluorophore combination discussed in this section is used to identify cells undergoing early and late apoptosis as well as necrosis (Figure 1.13). Clear identification of these cell-death mechanisms is important when performing Bio-SECM measurements, especially where the impact of chemically induced stress (e.g., due to exposure to a chemotherapeutic agent or a xenobiotic compound) on the

metabolic response of a cell is studied. In a majority of cases, cancer occurs when there is dysfunction in the apoptosis process. When the programmed cell death does not work properly, unwanted cells are not eliminated and start proliferating in an uncontrolled manner. As such, drug design preferentially favors the development of reagents that promote a return to normal apoptotic pathways and incur a limited toxicity level.<sup>118,119</sup>

Cells undergoing apoptosis are entering a particular morphological and biochemical dying process that is reversible. It is often said that the cell is committing suicide.<sup>120-122</sup> There are distinct morphological and biochemical differences between cells undergoing apoptosis *versus* necrosis. Apoptotic death is characterized by dehydration of the cytoplasm, leading to cell shrinkage, followed by cell invagination of the plasma membrane – a process that is called blebbing. At a later stage, apoptotic bodies are forming and the cell splits into different parts containing organelles and condensed chromatin. An important early apoptotic event involves translocation of phosphatidylserine (PS) from the inner to the outer leaflet of the membrane. The presence of externalized PS allows phagocytosis of the cell fragments without inflammation.<sup>123-126</sup> Apoptosis is a process that requires sustained levels of adenosine triphosphate (ATP), which is the source of energy for the cell.<sup>127</sup> Necrosis, on the other hand, is passive cell death that happens quickly and more violently. In contrast to apoptosis, it is irreversible and accompanied by diminution of ATP levels such that the cell cannot survive.<sup>120</sup>

In normal cells, an asymmetry exists between the two leaflets of the plasma membrane (Figure 1.14). The majority of the outer leaflet is composed of phosphatidylcholine and sphingomyelin while the inner leaflet is composed of PS and phosphatidylethanolamine. When cells enter into the apoptotic process, one of the earliest events is the loss of this asymmetry. Phospholipids, especially cytoplasm facing PS, flip to the outer leaflet<sup>121,128-131</sup> and are specifically recognized by macrophages. As a result, the cell and its fragments are phagocytosed with no significant inflammation.<sup>132,133</sup> Specific recognition of externalized PS can also be achieved by Annexin-V, a phospholipid-binding protein. In the presence of  $\text{Ca}^{2+}$ , Annexin-V has a higher affinity for negatively charged phospholipids, such as PS.<sup>121,129</sup> When fluorescently tagged (e.g., with Alexa fluor<sup>®</sup> 488,  $\lambda_{\text{ex}} = 488 \text{ nm}$ ,  $\lambda_{\text{em}} = 520 \text{ nm}$ ), Annexin-V is an ideal marker for early apoptosis (Figure 10-14). There are a number of advantages in using Alexa fluor as a dye. Generally pH-insensitive, Alexa fluor has a higher

photostability than other commonly used dyes such as fluorescein. In addition, Alexa dyes are commercially available in a variety of derivatives, providing emission maxima over a broad range of wavelengths.<sup>134</sup> This is convenient when using counter dyes since it is possible to choose a dye that does not interfere spectrally.

To detect late apoptosis, Hoechst 33258 (a bis-benzimide with  $\lambda_{\text{ex}} = 352$  nm, and  $\lambda_{\text{em}} = 461$  nm) is used as a fluorophore. Cell-permeable, this dye binds to the minor groove that is formed within the double helix of two complementary DNA strands (Figure 1.15). Its sensitivity depends on the composition of the DNA nucleotides. For example, fragments that are rich in AT have an increased binding affinity with Hoechst 33258.<sup>135-137</sup> In fact, the fluorescence intensity obtained from these regions can be twice the value that is observed for regions primarily consisting of GC. In addition, fluorescence emission is influenced by DNA conformation and the chromatin state. Apoptotic cells have condensed chromatin that yields higher fluorescence signals than normal cells. Identification of necrotic cells can be accomplished with propidium iodide ( $\lambda_{\text{ex}} = 535$  nm,  $\lambda_{\text{em}} = 617$  nm). This cell-impermeable dye only stains the nuclei of cells with perforated plasma membranes.<sup>138,139</sup>

The cell status assay evaluates the state of cells at the end of an SECM measurement (Figure 1.16). It is also employed to assess the cytotoxicity of the plastic supports used for their patterned assembly. Clearly, the use of biocompatible plastics for cell substrate design is a prerequisite for performing reliable SECM measurements. Residual monomer being present at the surface of the polymer can be cytotoxic and must be removed. We therefore cleaned plastic substrates by sonication in ethanol, methanol, and nanopure water, followed by exposure to oxygen plasma. During cleaning procedures, care must be taken not to alter the physical and mechanical properties of the plastics. Retaining high optical transparency of the plastic supports is of particular importance to ensure proper inspection with the inverted fluorescence microscope.

## **1.6 Conclusions**

SECM has become a useful tool to probe chemical or biochemical activity of a surface. It does so by recording the electrochemical response of an UME as it is moved

towards or over a sample using precise positioning and feedback systems. Electrochemical detection is specific because detected molecules undergo electron transfer reactions at well-defined potentials. UMEs provide current sensitivity in the pA regime making it possible to detect even trace amounts of analytes rapidly and with high spatial control. Unlike macroelectrodes, UMEs are largely insensitive to convection and readily reach steady-state conditions (e.g., in the range of micro- to milliseconds) following the application of a potential step. They can therefore be considered as steady-state systems when moving through the solution. These different UME properties are critical for SECM imaging applications and the determination of local concentration of redox species diffusing in, being released from or interacting with cells.

Routine fabrication of nanoprobes allowing high sensitivity measurements is a prerequisite for the study of cells using SECM.<sup>17-20</sup> The choice of UME sensor material (e.g., carbon, platinum, or gold) influences the nature of the analyte detected and the sensor preparation method employed. Proof-of-concept work has already portrayed the ability of electrochemical sensors to image and quantify transport processes at a variety of cell lines. Development of Bio-SECM as a bioanalytical tool capable of following cell metabolism also depends on advances in instrumental design, the availability of suitable biocompatible cell supports<sup>21</sup> and the routine use of cytotoxicity measurements. The implementation of constant-distance controllers in SECM instrumentation is important for decoupling the cell's topography from its electrochemical activity. Several examples of controllers have been tested to this end: shear-force (optical, tuning-fork and piezoelectric plates), UME current modulation, UME impedance and AFM-based feedback mechanisms. Yet, successful application of constant-distance controllers remains challenging when used in conjunction with soft, deformable substrates such as cells.

Soft microfabrication techniques hold promise in supporting SECM-based investigation by providing proper means of controlling cell environments at well-defined length scales. The use of plastic materials as supports for cell growth offers the possibility of tuning size, shape and topography of substrates through molding or embossing. The nature of these materials however demands for careful investigation of their compatibility with living cells. Although Zeonor<sup>®</sup> 1060R proved promising in this respect, a more detailed study of several plastic materials as cell supports is currently underway. The use of elastomeric 2D

$\mu$ CSs provided an effective route to pattern HeLa cells on Zeonor<sup>®</sup> 1060R, even though this approach is not limited to plastic surfaces. In principle, microfluidic approaches should be applicable to the development of patterns with different levels of complexity, including single cells, 2D cell wires, and 3D cell assemblies. This is particularly important when experiments aimed at monitoring effects of cell communication using Bio-SECM are to be carried out.

To assess the biocompatibility of the cell substrate and impact of manipulations during lithographic processing, a fluorescent-based cell status assay is used. Integration of an inverted fluorescent microscope with SECM also allows simultaneous or subsequent evaluation of the state of the cells following SECM measurements. When performing electrochemical measurements in the presence of cells, it is important to find a balance that allows the maintenance of sample and probe stability. Biomolecules from the cell culture medium or even cells themselves can irreversibly bind to the UME, lowering its sensitivity. An option is to modify the medium while trying to respect the physiological characteristics needed for cell survival. Changing one of the components, such as medium or temperature, always necessitates tests that ensure that the cell feature studied is not altered such that a different electrochemical behavior would be observed. Here, we see potential for further development of routine protocols, aiming at improving reliability of SECM as an analytical tool.

Bio-SECM has the potential to quantify how important biological electroactive molecules work together and are transported in and out of cells. It can positively contribute to the global approach to cellular studies called systems biology. In the future, SECM is likely to have a direct impact on design of drugs and pharmaceutical targets, especially when performed in conjunction with complementary analytical methods and techniques. Therefore, much interest remains in developing integrative microscopies capable of monitoring and studying specific metabolites and proteins with high spatial resolution for both single cell and monolayer cultures. It can be expected that such experiments will provide further insights into some of the unresolved mysteries surrounding life at the molecular and cellular level.

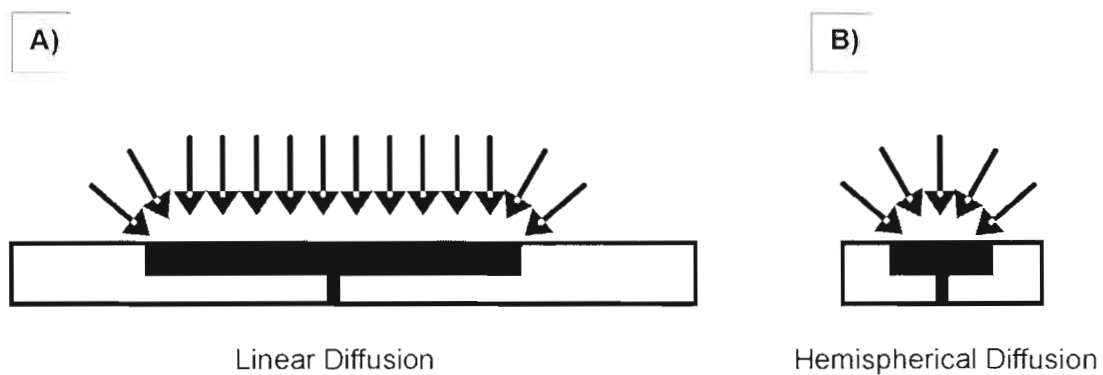


**Figure 1.1.** Diffusion occurring at an electrode. A) Linear diffusion to a large planar disk electrode. B) Hemispherical diffusion to a planar disk UME.

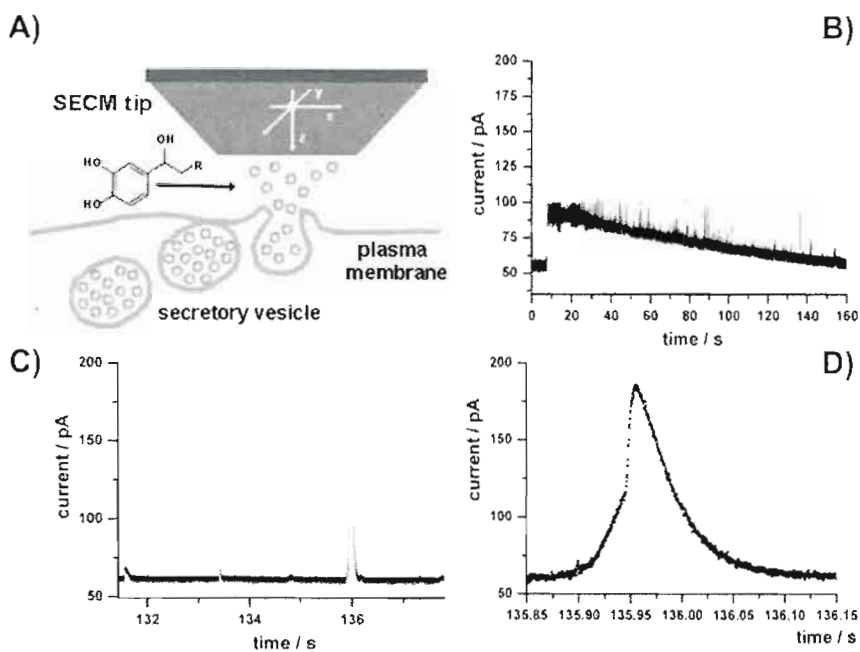


**Figure 1.2.** A) Local amperometric detection of single-vesicle adrenaline released from an individual bovine chromaffin cell. A carbon-fiber disk ultramicroelectrode (CF-UME, 5  $\mu\text{m}$  in diameter, polarized to +800 mV vs. Ag/AgCl) was directly placed above the center of a single bovine chromaffin cell at a distance of  $<1 \mu\text{m}$ . B) When the selected cell was stimulated with 100 mM KCl solution, exocytosis was initiated and detected by the appearance of spikes in the amperometric UME current. Each spike represents the chemical release from an individual secretory granule. C, D) Expanded sections of B) with higher temporal resolution. [Reproduced with permission from reference (Schulte et al. Schumann, 2007)].

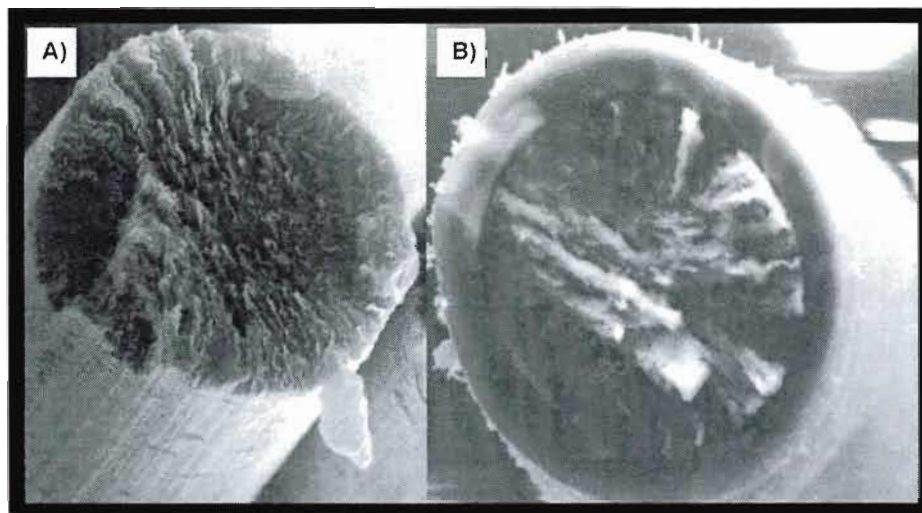


**Figure 1.3.** SEM images of the ends of A) bare and B) insulated carbon fibers that are 10  $\mu\text{m}$  in diameter. The insulating material, a thin layer of an electrodeposition paint (EDP paint), covers the side walls but not the disk-shaped face, which has been exposed by carefully sectioning the carbon fiber with a sharp scalpel blade. Resultant CF-UME is typically used for neurotransmitter and hormone release measurements on single secretory cells. [Reproduced with permission from reference (Schulte et Schuhmann, 2007)].

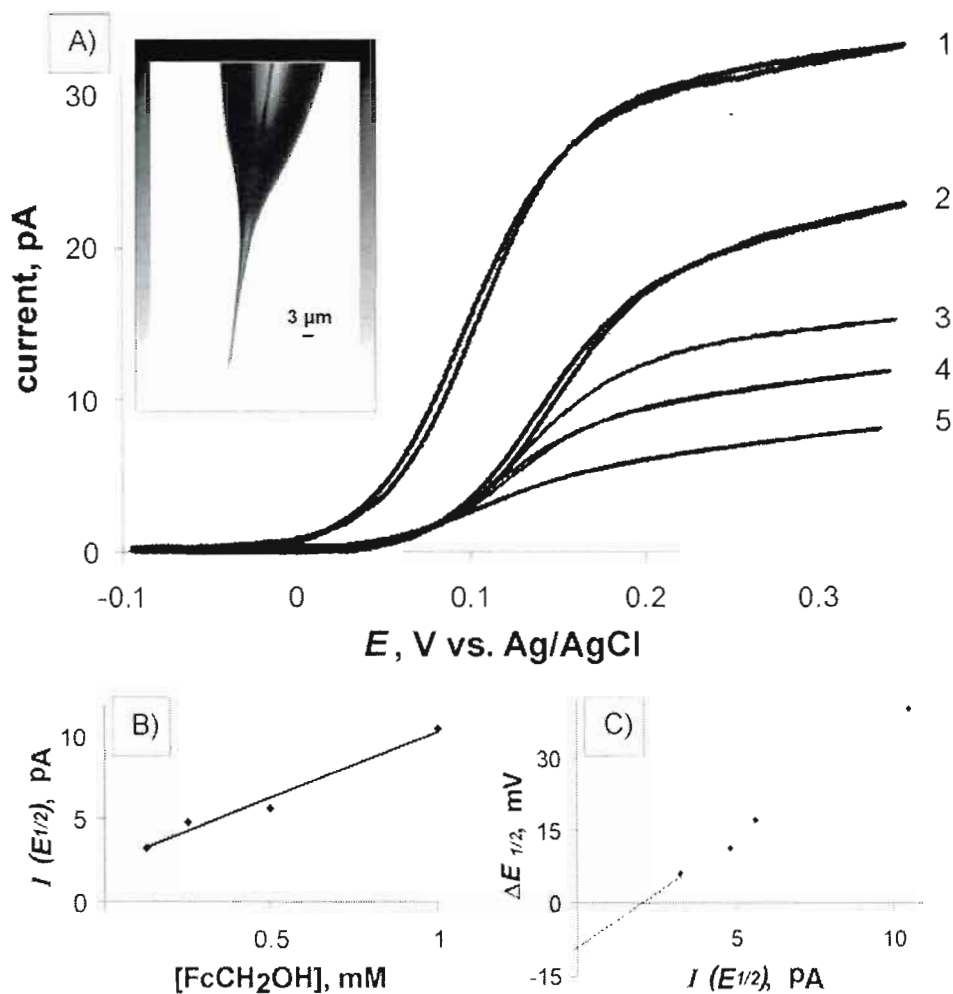


**Figure 1.4.** A) Voltammograms of FcCH<sub>2</sub>OH oxidation at a 112-nm platinum tip obtained in bulk solution (curve 1) and inside a human breast epithelial (MCF-10A) cell (curves 2–5). The following concentrations of FcCH<sub>2</sub>OH were used: 1.0 mM for curves 1 and 2, 0.5 mM for curve 3, 0.25 for curve 4, and 0.125 for curve 5. The inset shows an optical micrograph of a characteristic Pt disk laser-pulled UME. B) Dependence of the UME current at half-wave potential,  $I(E_{1/2})$ , on [FcCH<sub>2</sub>OH]. C) Dependence of the change in half-wave potential,  $\Delta E_{1/2}$ , on  $I(E_{1/2})$  [Reproduced with permission from reference (Sun *et al.*, 2008)].

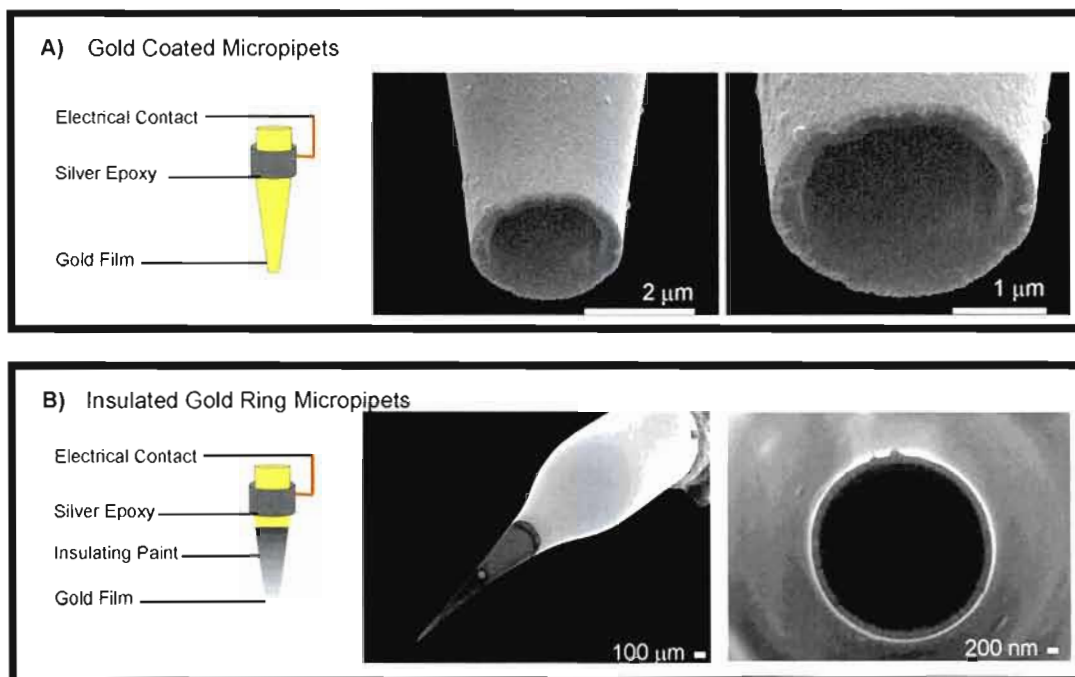


**Figure 1.5.** SEM images of the ends of A) a gold-coated pulled borosilicate micropipet and B) an insulated 70-nm-thick gold ring micropipet. The insulating material, a thin layer of cathodic electrophoretic paint (Cathodip<sup>TM</sup> Ft83-0250, BASF) selectively covers the sides but not the ring face of the micropipet. The remainder of the gold-coated film is later insulated with a varnish prior to electrochemical measurements. The resulting gold ring micropipet can dispense solutions in the pL range through its orifice. [J. Mauzeroll, S. Borensztajn & D. Marchal, unpublished results].

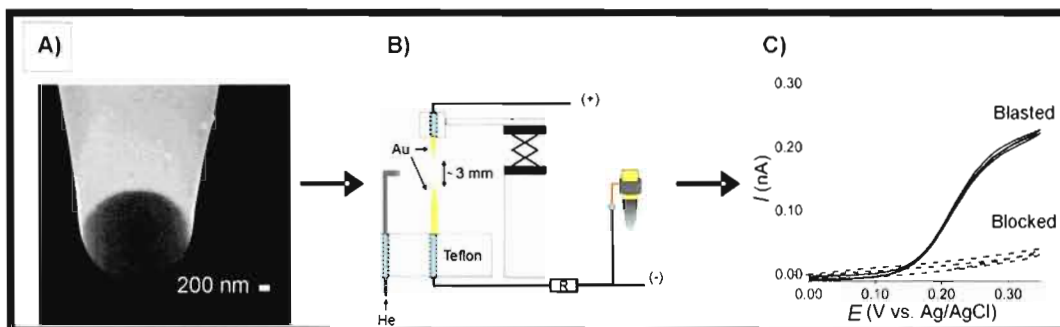


**Figure 1.6.** Removal of blocking polymer layers from a microelectrode. A) SEM image of the end of a blocked gold ring micropipet. The insulating material, a thin layer of cathodic electrophoretic paint (Cathodip™ Ft83-0250, BASF) covers both side walls and ring face of the micropipet. B) Schematic representation of the experimental setup used for blasting the polymer layer off the ring-shaped electrode surface. This process is mediated by an electric field generated at the end of the micropipet. C) Voltammograms of  $\text{FcCH}_2\text{OH}$  oxidation at blocked and blasted gold ring micropipet. [J. Mauzeroll, S. Borensztajn & D. Marchal, unpublished results].

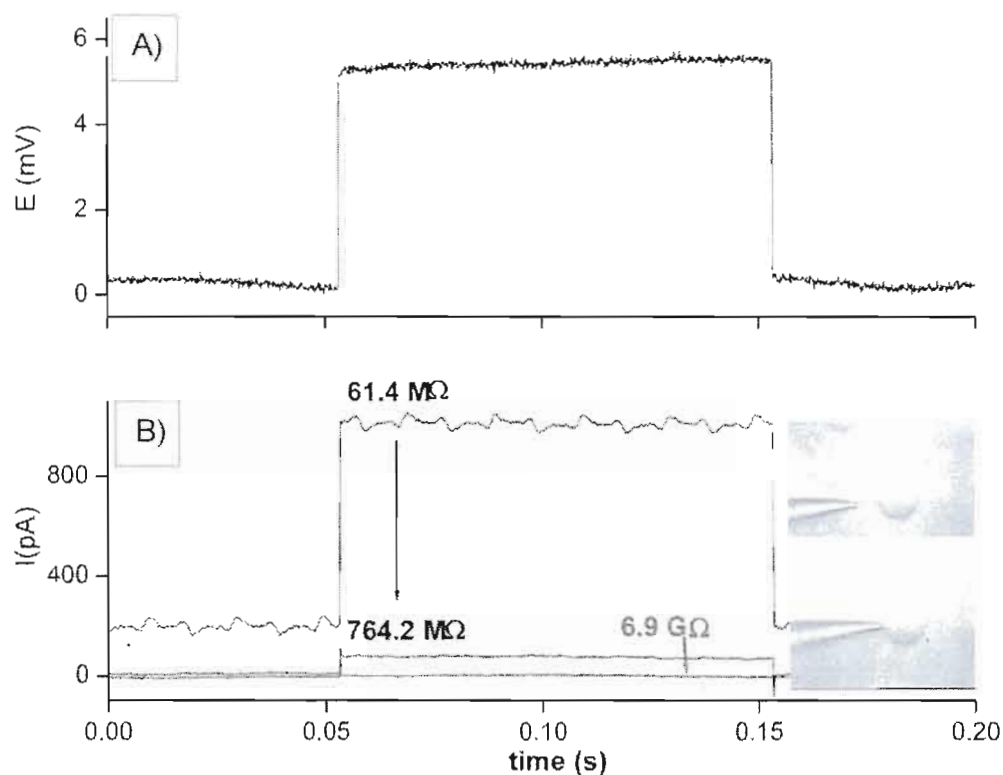


**Figure 1.7.** A,B) Optical micrographs (survey and close-up view) of a pulled micropipet attached to a Giant Unilamellar Vesicle (GUV) which is composed of 1,2-dioleoyl-sn-glycero-3-phosphocholine (DOPC), ubiquinone-10 and 1-acyl-2-[(2-nitrobenz-2-oxa-1,3-diazol-4-yl)aminostearoyl]-sn-glycero-3-phosphocholine (NBD-PC). C) Input square-wave applied to the micropipet used to patch on the GUV. D) A patch of the micropipet onto the GUV typically results in an increase of the micropipet resistance (G $\Omega$ ). Insets are optical micrographs depicting the micropipet and the GUV before and during a patch. [J. Mauzeroll & D. Marchal, unpublished results].

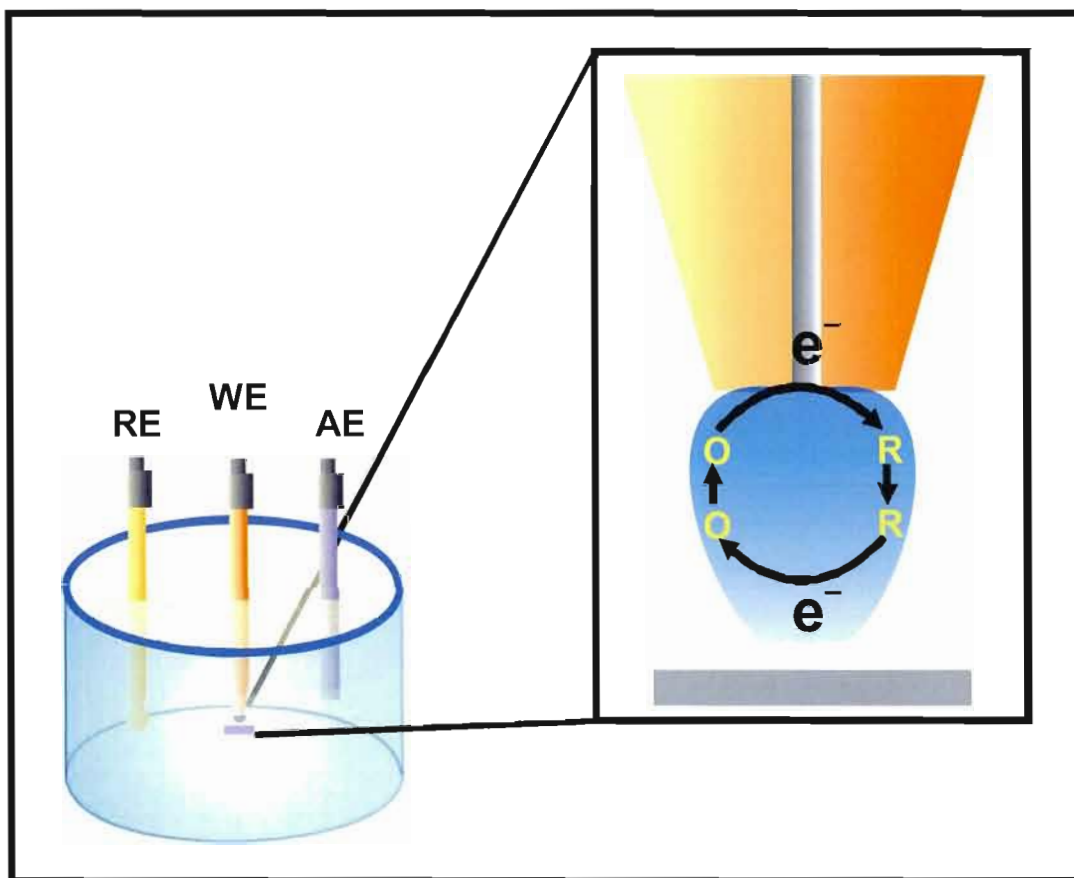


**Figure 1.8.** The electrochemical reaction of dissolved reversible redox species (O and R, respectively) at the UME/solution interface is mass transfer limited, at least for potentials far exceeding the redox potential of O. The localized hemispherical diffusion zone in front of the UME is used to detect topography and/or reactivity of a nearby surface.

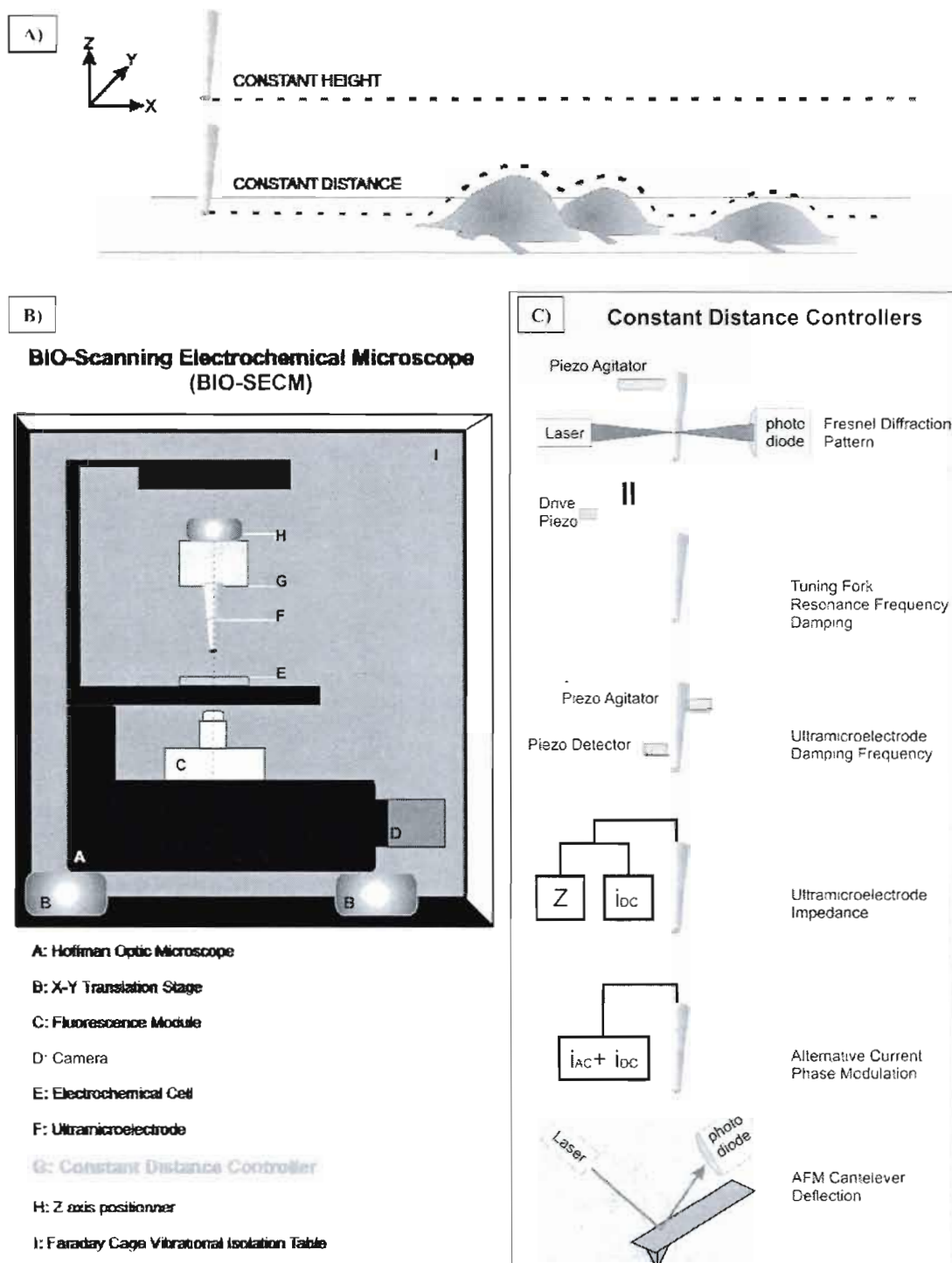


**Figure 1.9.** A) Schematic presentation of an SECM line scan over immobilized cells in constant height and constant distance mode. B) Instrumental design of a Bio-SECM. C) Detection principles of selected constant distance controllers.

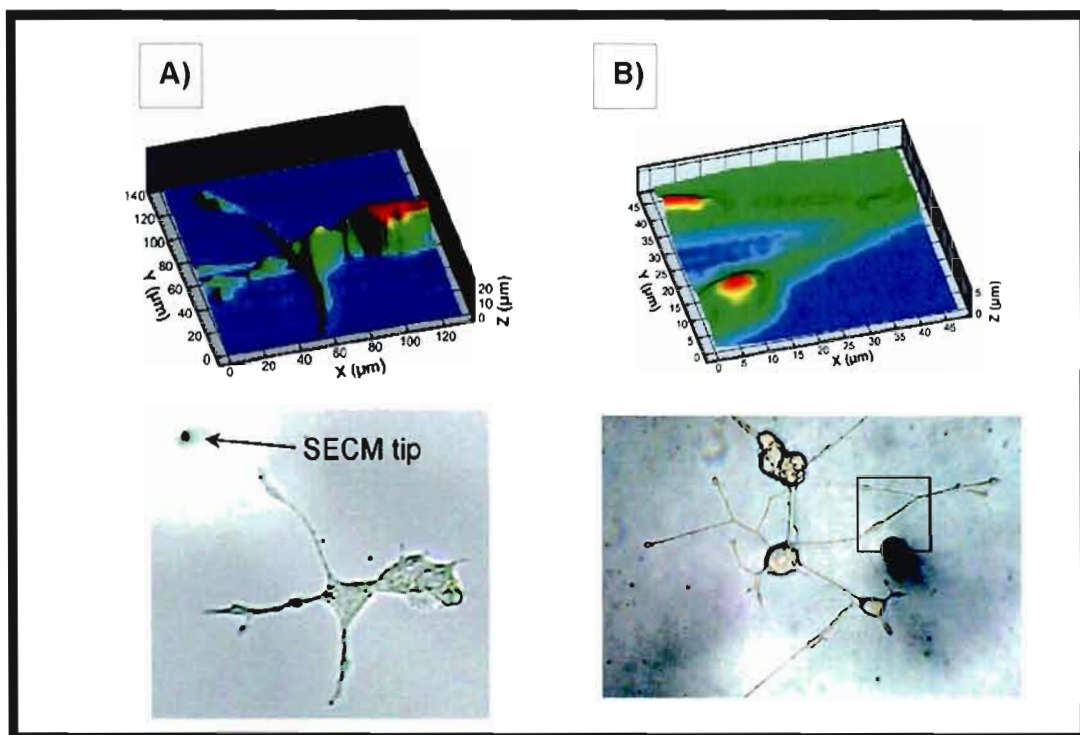


**Figure 1.10.** SECM imaging of immobilized cells. A) Topographic images acquired using constant current imaging with a 1  $\mu\text{m}$  carbon ring electrode at differentiated PC12 cells. Conditions: 1 mM  $\text{Ru}(\text{NH}_3)_6\text{Cl}_3$  in HBSS (Hank's balanced salt solution),  $E_{\text{ap}} = -0.4 \text{ V vs. } 3 \text{ M NaCl/Ag/AgCl}$  reference and Pt wire auxiliary electrodes. B) Top panel: Topographic image of differentiated PC12 cells acquired in constant UME impedance imaging mode. Bottom panel: Close-up view of a neurite bifurcation recorded in HBSS with a carbon fiber electrode (5  $\mu\text{m}$  in diameter) at  $E_{\text{ap}} = +0.75 \text{ V vs. } 3 \text{ M NaCl/Ag/AgCl}$ , a scan rate of  $7 \mu\text{m s}^{-1}$ , 90 kHz, and 10 mV p-p sine wave. [Reproduced and modified with permission from reference (Kurulugama *et al.*, 2005), copyright 2005, American Chemical Society].

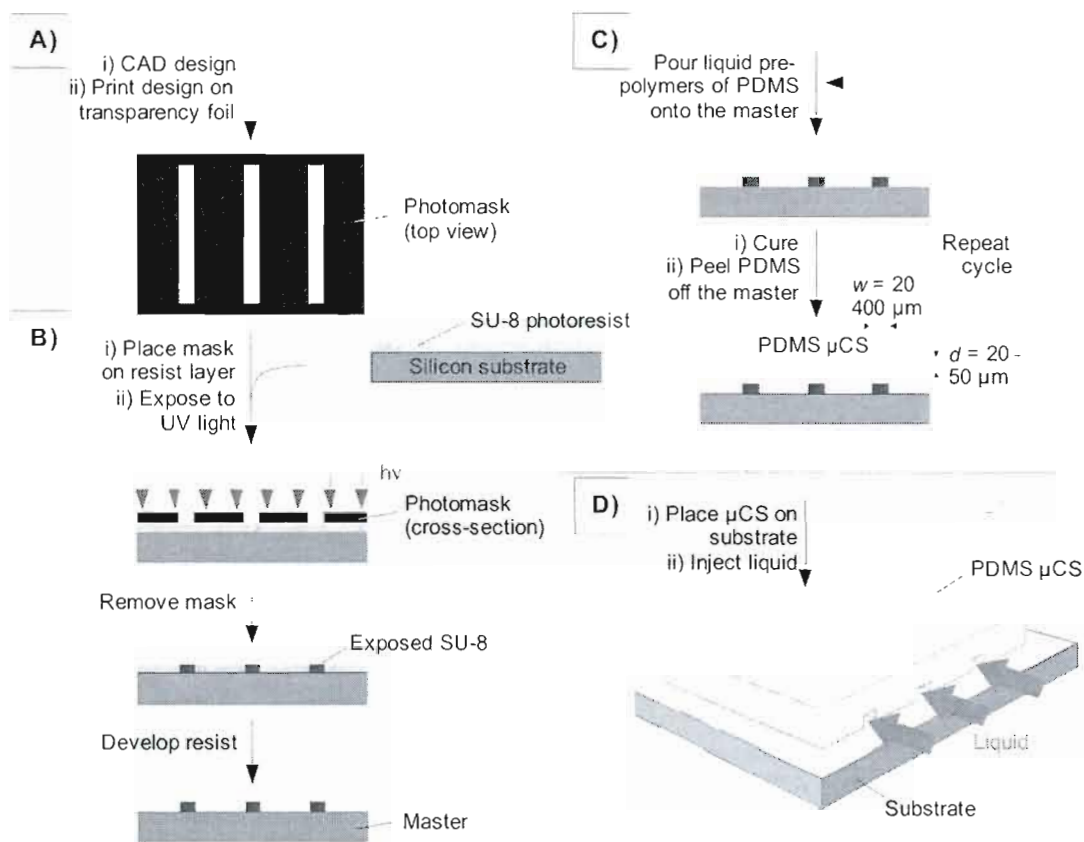


**Figure 1.11.** Fabrication and use of PDMS-based microfluidic devices. A) Printing a CAD file onto a transparency foil constitutes a convenient and generally accessible way to generate a photomask. B) A master is fabricated by contact mode optical lithography. The mask is placed onto a thin film of photoresist (e.g., SU-8) formed by spin-coating on a silicon substrate. When illuminated with UV light, crosslinking of the photoresist is induced within the transparent windows of the mask, making exposed regions of the resist become insoluble in an organic medium that is used for development. C) The photoresist pattern is transferred into a layer of PDMS by replica molding. In this process, liquid pre-polymers of PDMS are poured onto the master, cured thermally, and peeled away. The cycle can be repeated multiple times allowing numerous  $\mu\text{CS}$ s to be replicated using the same master. D) When placed on a solid substrate, conformal contact seals the surface reversibly, resulting in a set of enclosed microchannels, which can be filled with a liquid.

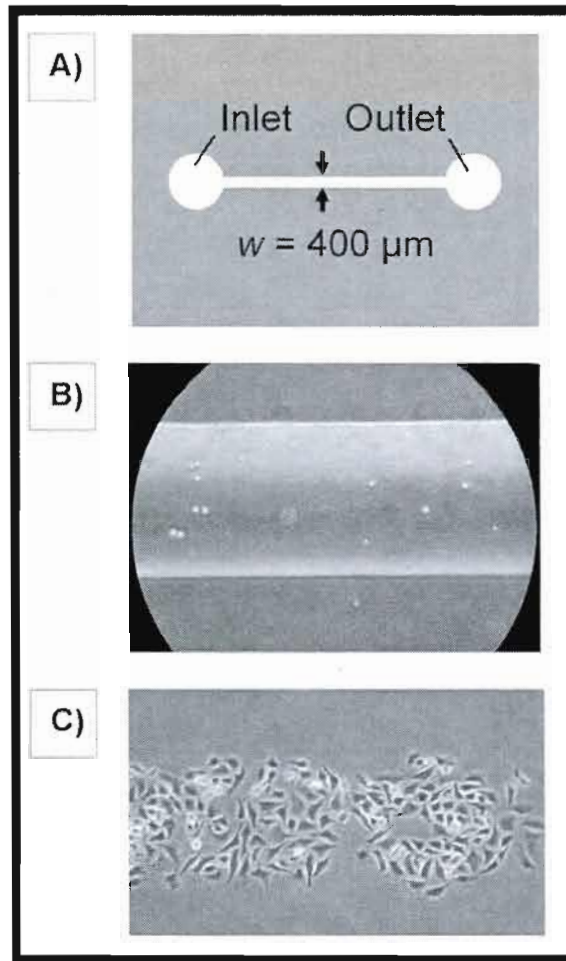


**Figure 1.12.** Patterning of cells in microfluidic environments. A) Design of a simple  $\mu\text{CS}$  for linear arrangement of cells. B) Optical micrograph of a 400- $\mu\text{m}$ -wide microchannel in contact with a Zeonor<sup>®</sup> substrate during filling with a HeLa cell suspension. C) Pattern of HeLa cells on a plastic support obtained by incubating the suspension with a Zeonor<sup>®</sup> substrate at 37 °C in a 5%  $\text{CO}_2$  atmosphere saturated in water for 5 h. Upon removal of the  $\mu\text{CS}$ , cells were submerged in Minimal Eagle Medium (MEM) prior to acquisition of the picture. Cells are confined to a stripe-like pattern imposed by the dimensions of the microchannel (e.g.,  $w = 400 \mu\text{m}$ ).

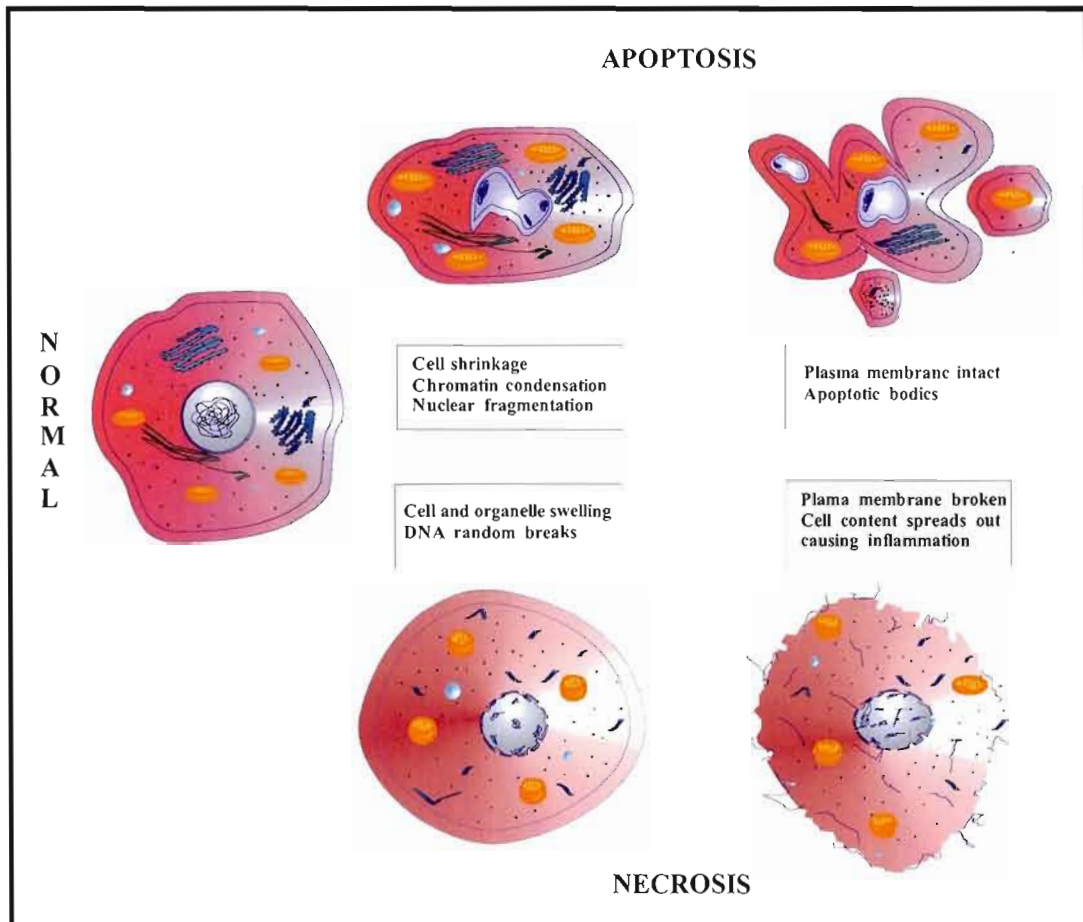


**Figure 1.13.** Scheme of a cell undergoing apoptotic or necrotic processes. An apoptotic cell first loses intracellular liquid and shrinks. The chromatin is then condensed and can be found at the periphery of the nucleus. Organelles such as endoplasmic reticulum and mitochondria keep their original size and shape. Later, apoptotic bodies grow apart but are still surrounded by a membrane. Necrosis is accompanied by an increase in cell volume as well as characteristic swelling of the mitochondria. The chromatin also condenses irregularly and, unlike apoptosis, DNA ruptures at random rather than well defined positions. At a later stage the plasma membrane loses its integrity, and the cell content is released in the extracellular environment leading to inflammation.

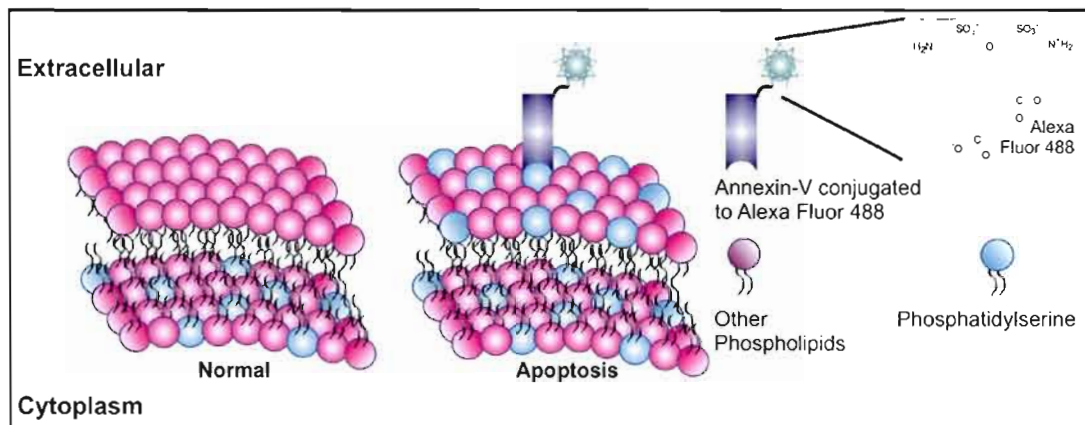


**Figure 1.14.** Schematic illustration of lipid asymmetry loss in an apoptotic cell. The transfer of PS on the outer leaflet of the plasma membrane during apoptosis is a useful feature in biology. Annexin-V is a protein that can bind specifically to externalized PS. Hence, the use of Annexin-V labeled with a fluorescent dye such as Alexa Fluor 488 makes it possible to detect apoptosis at an early stage.

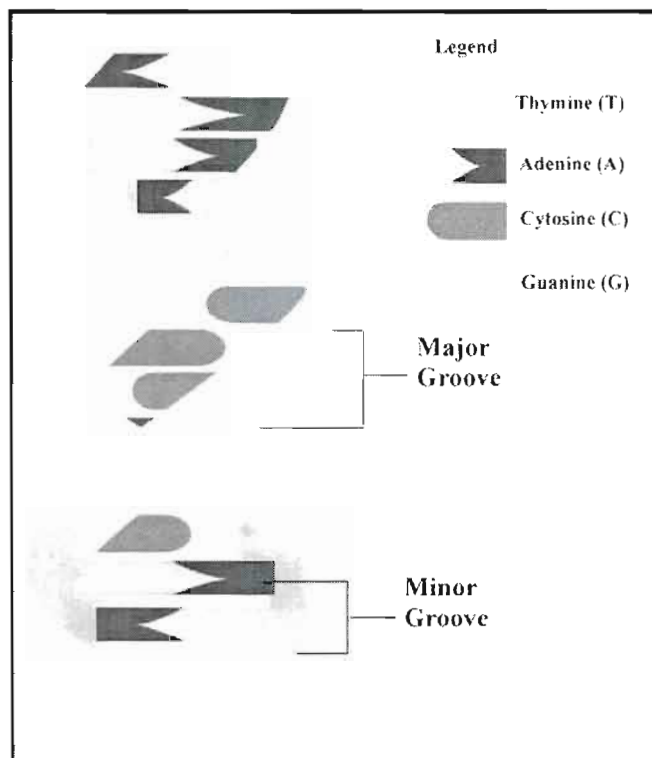


**Figure 1.15.** Simplified scheme of a double stranded DNA structure. The outer side of the helix is composed of a sugar-phosphate backbone. The two strands are connected through hydrogen bonding between complementary base pairs: Adenine (A) & Thymine (T), and Cytosine (C) & Guanine (G). Groove within the helical structure can differ in size depending on the sequence of base pairs within the two strands.

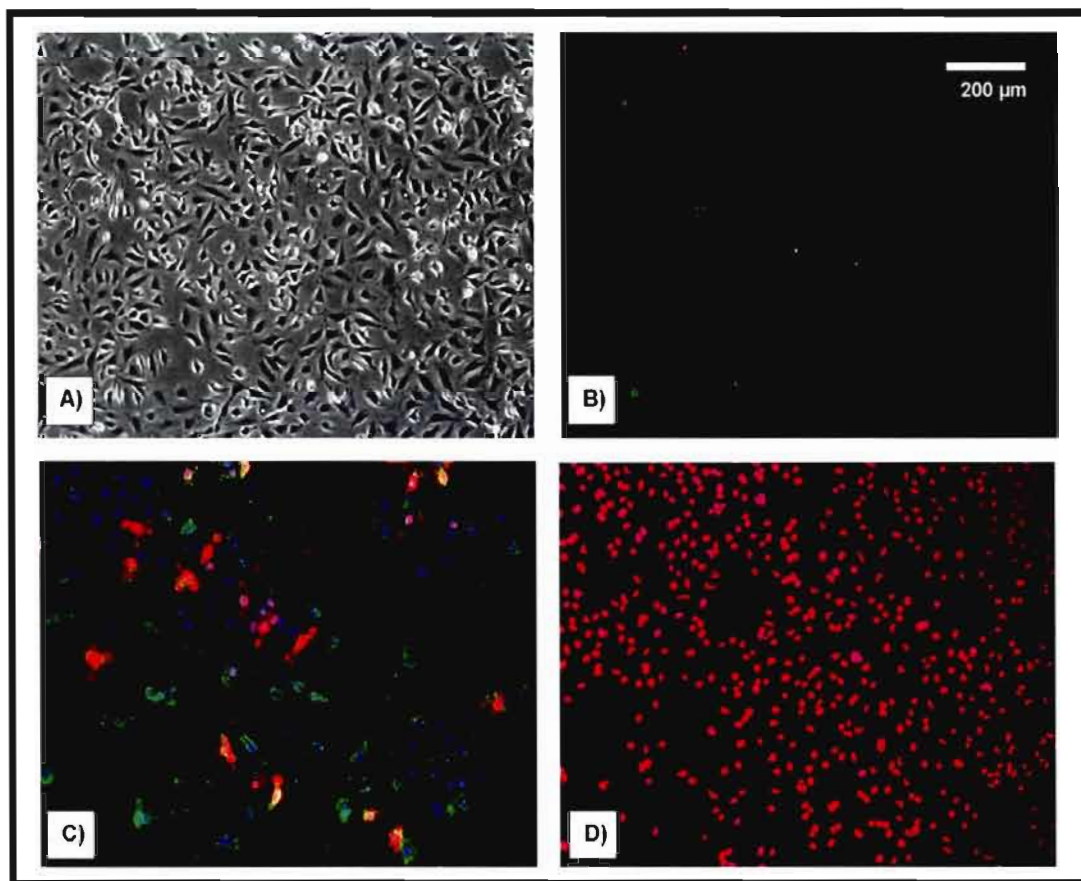


**Figure 1.16.** Fluorescence-based cell status assay. A) Optical micrograph of a control group of HeLa cells in Binding Buffer at pH = 7.4. B) Fluorescence micrograph of the same control group. Cells were first incubated with Annexin-V-Alexa Fluor 488 and Hoechst 33258 in Binding Buffer for 15 min, washed and then exposed to propidium iodide. C) Fluorescence micrograph showing cells during apoptosis which was induced by exposure to 2  $\mu$ M tributyltin (TBT) over a period of 15 min at 37  $^{\circ}$ C in Minimal Essential Medium (MEM) without serum. Cells were washed with Binding Buffer, followed by incubation with the fluorophores using the same procedure as for the control group. D) Fluorescence micrograph of cells during necrosis which resulted from exposure to 0.075 % Triton X-100 for 1 min. Cells were washed with PBS at pH = 7.4 and incubated with the fluorophores using the same procedure as for the control group but without Annexin-V-Alexa Fluor 488. Fluorescence micrographs were acquired using a Nikon Eclipse TE-2000 inverted microscope equipped with a CCD camera. Images were captured using Northern Eclipse software.

### 1.7 References

- (1) Engstrom, R. C.; Weber, M.; Wunder, D. J.; Burgess, R.; Winquist, S. *Anal. Chem.* **1986**, *58*, 844–848.
- (2) Bard, A. J.; Fan, F.-R.; Kwak, J.; Lev, O. *Anal. Chem.* **1989**, *61*, 132–138.
- (3) Engstrom, R. C.; Pharr, C. M. *Anal. Chem.* **1989**, *61*, 1099A–1104A.
- (4) Cai, C.; Liu, B.; Mirkin, M. V.; Frank, H. A.; Rusling, J. F. *Anal. Chem.* **2002**, *74*, 114–119.
- (5) Holt, K. B.; Bard, A. J. *Biochemistry (Mosc)*. **2005**, *44*, 13214–13223.
- (6) Tsionsky, M.; Cardon, Z. G.; Bard, A. J.; Jackson, R. B. *Plant Physiol.* **1997**, *113*, 895–901.
- (7) Mauzeroll, J.; Bard, A. J.; Owhadian, O.; Monks, T. J. *Proc. Natl. Acad. Sci. USA* **2004**, *101*, 17582–17587.
- (8) Berger, C. E. M.; Rathod, H.; Gillespie, J. I.; Horrocks, B. R.; Datta, H. K. *J. Bone Miner. Res.* **2001**, *16*, 2092–2102.
- (9) Scott, E. R.; Phipps, J. B.; White, H. S. *J. Invest. Dermatol.* **1995**, *104*, 142–145.
- (10) Shiku, H.; Shiraishi, T.; Ohya, H.; Matsue, T.; Abe, H.; Hoshi, H.; Kobayashi, M. *Anal. Chem.* **2001**, *73*, 3751–3758.
- (11) Zhao, X.; Petersen, N. O.; Ding, Z. *Can. J. Chem.* **2007**, *85*, 175–183.
- (12) Liu, B.; Rotenberg, S. A.; Mirkin, M. V. *Proc. Natl. Acad. Sci. USA* **2000**, *97*, 9855–9860.
- (13) Feng, W.; Rotenberg, S. A.; Mirkin, M. V. *Anal. Chem.* **2003**, *75*, 4148–4154.
- (14) Kaya, T.; Torisawa, Y. S.; Oyamatsu, D.; Nishizawa, M.; Matsue, T. *Biosens. Bioelectron.* **2003**, *18*, 1379–1383.
- (15) Mauzeroll, J.; Bard, A. J. *Proc. Natl. Acad. Sci. USA* **2004**, *101*, 7862–7867.
- (16) Bauermann, L. P.; Schuhmann, W.; Schulte, A. *PCCP* **2004**, *6*, 4003–4008.
- (17) Amemiya, S.; Guo, J.; Xiong, H.; Gross, D. *Anal. Bioanal. Chem.* **2006**, *386*, 458–471.

- (18) Bakker, E. *Anal. Chem.* **2004**, *76*, 3285–3298.
- (19) Sun, P.; Laforge, F. O.; Mirkin, M. V. *PCCP* **2007**, *9*, 802–823.
- (20) Lu, X.; Huang, W. H.; Wang, Z. L.; Cheng, J. K. *Anal. Chim. Acta* **2004**, *510*, 127–138.
- (21) Kissinger, P. T. *Biosens. Bioelectron.* **2005**, *20*, 2512–2516.
- (22) Amatore, C. In *Physical Electrochemistry: Principles, Methods, and Applications*; Rubinstein, I., Ed.; Marcel Dekker: New York, NY, 1995, p 131–208.
- (23) Zoski, C. G. *Handbook of Electrochemistry*; Elsevier Science: Amsterdam, NL, 2007.
- (24) Štulík, K.; Amatore, C.; Holub, K.; Mareček, V.; Kutnec, W. *Pure Appl. Chem.* **2000**, *72*, 1483–1492.
- (25) Sun, P.; Laforge, F. O.; Abeyweera, T. P.; Rotenberg, S. A.; Carpino, J.; Mirkin, M. V. *Proc. Natl. Acad. Sci. USA* **2008**, *105*, 443–448.
- (26) Schulte, A.; Schuhmann, W. *Angew. Chem.* **2007**, *46*, 8760–8777.
- (27) Wightman, R. M. *Science* **2006**, *311*, 1570–1574.
- (28) Chow, R. H.; Von Rueden, L.; Neher, E. *Nature* **1992**, *356*, 60–63.
- (29) Schulte, A.; Chow, R. H. *Anal. Chem.* **1996**, *68*, 3054–3058.
- (30) Chen, S.; Kucernak, A. *Electrochem. Commun.* **2002**, *4*, 80–85.
- (31) Mousa, M. S. *Appl. Surf. Sci.* **1996**, *94–95*, 129–135.
- (32) Millar, J.; Pelling, C. W. A. *J. Neurosci. Methods* **2001**, *110*, 1–8.
- (33) Wu, W. Z.; Huang, W. H.; Wang, W.; Wang, Z. L.; Cheng, J. K.; Xu, T.; Zhang, R. Y.; Chen, Y.; Liu, J. *J. Am. Chem. Soc.* **2005**, *127*, 8914–8915.
- (34) Huang, L.; Kennedy, R. T. *Trends Anal. Chem.* **2003**, *14*, 158–164.
- (35) Strein, T. G.; Ewing, A. G. *Anal. Chem.* **1992**, *64*, 1368–1373.
- (36) Zhang, X.; Zhang, W.; Zhou, X.; Ogorevc, B. *Anal. Chem.* **1996**, *68*, 3338–3343.
- (37) Yao, D. D.; Vlessidis, A. G.; Evmiridis, N. P. *Microchim. Acta* **2004**, *147*, 1–20.
- (38) Taha, Z. H. *Talanta* **2003**, *61*, 3–10.

- (39) Bedioui, F.; Villeneuve, N. *Electroanalysis* **2003**, *15*, 5–18.
- (40) Diakowski, P. M.; Ding, Z. *Electrochem. Commun.* **2007**, *9*, 2617–2621.
- (41) Wang, W.; Hu, X. *Talanta* **2006**, *68*, 1322–1328.
- (42) Slevin, C. J.; Gray, N. J.; Macpherson, J. V.; Mark A. Webb, M. A.; Unwin, P. R. *Electrochem. Commun.* **1999**, *1*, 282–288.
- (43) Katemann, B. B.; Schuhmann, W. *Electroanalysis* **2002**, *14*, 22–28.
- (44) Pendley, B. D.; Abruna, H. D. *Anal. Chem.* **1990**, *62*, 782–784.
- (45) Sun, P.; Mirkin, M. V. *Anal. Chem.* **2006**, *78*, 6526–6534.
- (46) Mauzeroll, J.; LeSuer, R. J. In *Handbook of Electrochemistry*; Zosky, C. G., Ed.; Elsevier Science: Amsterdam, NL, 2007, p 199–211.
- (47) Wonderlin, W. F.; Woodfork, K. A.; Strobl, J. S. *J. Cell. Physiol.* **1995**, *165*, 177–185.
- (48) Miedema, H.; Assmann, S. M. *J. Membr. Biol.* **1998**, *166*, 101–110.
- (49) Schlue, W.-R.; Kilb, W.; Günzel, D. *Electrochim. Acta* **1997**, *42*, 3197–3205.
- (50) Klymchenko, A. S.; Stoeckel, H.; Takeda, K.; Mély, Y. *J. Phys. Chem. B* **2006**, *110*, 13624–13632.
- (51) Liu, B.; Shao, Y.; Mirkin, M. V. *Anal. Chem.* **2000**, *72*, 510–519.
- (52) Yuan, Y.; Amemiya, S. *Anal. Chem.* **2004**, *76*, 6877–6886.
- (53) Shao, Y.; Mirkin, M. V. *Anal. Chem.* **1998**, *70*, 3155–3161.
- (54) Amemiya, S.; Bard, A. J. *Anal. Chem.* **2000**, *72*, 4940–4948.
- (55) Hengstenberg, A.; Kranz, C.; Schuhmann, W. *Chem. Eur. J.* **2000**, *6*, 1547–1554.
- (56) Kasai, S.; Zhou, H.; Matsue, T. *Chemistry Letters* **2000**, *29*, 200–201.
- (57) Hirano, Y.; Mitsumori, Y.; Oyamatsu, D.; Nishizawa, M.; Matsue, T. *Biosens. Bioelectron.* **2003**, *18*, 587–590.
- (58) Walsh, D. A.; Fernández, J. L.; Mauzeroll, J.; Bard, A. J. *Anal. Chem.* **2005**, *77*, 5182–5188.

- (59) Demaille, C. In *Handbook of Electrochemistry*; Zosky, C. G., Ed.; Elsevier Science: Amsterdam, NL, 2007, p 226–235.
- (60) Conyers, J. L.; White, H. S. *Anal. Chem.* **2000**, *72*, 4441–4446.
- (61) Güell, A. G.; Diez-Pérez, I.; Gorostiza, P.; Sanz, F. *Anal. Chem.* **2004**, *76*, 5218–5222.
- (62) Watkins, J. J.; Chen, J.; White, H. S.; Abrunã, H. D.; Maisonhaute, E.; Amatore, C. *Anal. Chem.* **2003**, *75*, 3962–3971.
- (63) Smythe, W. R. *J. Appl. Phys.* **1951**, *22*, 1499–1501
- (64) Liu, B.; Bard, A. J.; Mirkin, M. V.; Creager, S. E. *J. Am. Chem. Soc.* **2004**, *126*, 1485–1492.
- (65) Takahashi, Y.; Hirano, Y.; Yasukawa, T.; Shiku, H.; Yamada, H.; Matsue, T. *Langmuir* **2006**, *22*, 10299–10306.
- (66) Kurulugama, R. T.; Wipf, D. O.; Takacs, S. A.; Pongmayteegul, S.; Garris, P. A.; Baur, J. E. *Anal. Chem.* **2005**, *77*, 1111–1117.
- (67) Ludwig, M.; Kranz, C.; Schuhmann, W.; Gaub, H. E. *Rev. Sci. Instrum.* **1995**, *66*, 2857–2860.
- (68) Yamada, H.; Fukumoto, H.; Yokoyama, T.; Koike, T. *Anal. Chem.* **2005**, *77*, 1785–1790.
- (69) Oyamatsu, D.; Hirano, Y.; Kanaya, N.; Mase, Y.; Nishizawa, M.; Matsue, T. *Bioelectrochemistry* **2003**, *60*, 115–121.
- (70) Lee, Y.; Ding, Z.; Bard, A. J. *Anal. Chem.* **2002**, *74*, 3634–3643.
- (71) James, P. I.; Garfias-Mesias, L. F.; Moyer, P. J.; Smyrl, W. H. *J. Electrochem. Soc.* **1998**, *145*, L64–L66.
- (72) Katemann, B. B.; Schulte, A.; Schuhmann, W. *Chem. Eur. J.* **2003**, *9*, 2025–2033.
- (73) Wipf, D. O.; Bard, A. J.; Tallman, D. E. *Anal. Chem.* **1993**, *65*, 1373–1377.
- (74) Baranski, A. S.; Diakowski, P. M. *J. Solid State Electrochem.* **2004**, *8*, 683–692.
- (75) Horrocks, B. R.; Schmidtke, D.; Heller, A.; Bard, A. J. *Anal. Chem.* **1993**, *65*, 3605–3614.
- (76) Katemann, B. B.; Inchauspe, C. G.; Castro, P. A.; Schulte, A.; Calvo, E. J.; Schuhmann, W. *Electrochim. Acta* **2003**, *48*, 1115–1121.

- (77) Alpuche-Aviles, M. A.; Wipf, D. O. *Anal. Chem.* **2001**, *73*, 4873–4881.
- (78) Gabrielli, C.; Huet, F.; Keddad, M.; Rousseau, P.; Vivier, V. *J. Phys. Chem. B* **2004**, *108*, 11620–11626.
- (79) Ervin, E. N.; White, H. S.; Baker, L. A.; Martin, C. R. *Anal. Chem.* **2006**, *78*, 653–6541.
- (80) Kranz, C.; Friedbacher, G.; Mizaikoff, B.; Lugstein, A.; Smoliner, J.; Bertagnolli, E. *Anal. Chem.* **2001**, *73*, 2491–2500.
- (81) Macpherson, J. V.; Unwin, P. R. *Anal. Chem.* **2001**, *73*, 550–557.
- (82) Fasching, R. J.; Bai, S.-J.; Fabian, T.; Prinz, F. B. *Microelectron. Eng.* **2006**, *83*, 1638–1641.
- (83) Whitesides, G. M. *Nature* **2006**, *442*, 368–373.
- (84) Squires, T. M.; Quake, S. R. *Rev. Mod. Phys.* **2005**, *77*, 977–1026.
- (85) Delamarche, E.; Juncker, D.; Schmid, H. *Adv. Mater.* **2005**, *17*, 2911–2933.
- (86) Zhang, C.; Xu, J.; Ma, W.; Zheng, W. *Biotechnol. Adv.* **2006**, *24*, 243–284.
- (87) Xu, S.; Nie, Z.; Seo, M.; Lewis, P.; Kumacheva, E.; Stone, H. A.; Garstecki, P.; Weibel, D. B.; Gitlin, I.; Whitesides, G. M. *Angew. Chem. Int. Ed.* **2005**, *44*, 724–728.
- (88) Takayama, S.; McDonald, J. C.; Ostuni, E.; Liang, M. N.; Kenis, P. J. A.; Ismagilov, R. F.; Whitesides, G. M. *Proc. Natl. Acad. Sci. USA* **1999**, *96*, 5545–5548.
- (89) Thorsen, T.; Maerkl, S. J.; Quake, S. R. *Science* **2003**, *298*, 580–584.
- (90) Xia, Y.; Whitesides, G. M. *Angew. Chem. Int. Ed. Engl.* **1998**, *37*, 551–575.
- (91) Michel, B.; Bernard, A.; Bietsch, A.; Delamarche, E.; Geissler, M.; Juncker, D.; Kind, H.; Renault, J. P.; Rothuizen, H.; Schmid, H.; Schmidt-Winkel, P.; Stutz, R.; Wolf, H. *IBM. J. Res. Develop.* **2001**, *45*, 697–719.
- (92) McDonald, J. C.; Whitesides, G. M. *Acc. Chem. Res.* **2002**, *35*, 491–499.
- (93) Chiu, G. L. T.; Shaw, J. M. *IBM. J. Res. Develop.* **1997**, *41*, 3–130.
- (94) Shaw, J. M.; Gelorme, J. D.; LaBianca, N. C.; Conley, W. E.; Holmes, S. J. *IBM. J. Res. Develop.* **1997**, *41*, 81–94.

- (95) Bietsch, A.; Michel, B. *J. Appl. Phys.* **2000**, *88*, 4310–4318.
- (96) Juncker, D.; Schmid, H.; Drechsler, U.; Wolf, H.; Wolf, M.; Michel, B.; de Rooij, N.; Delamarche, E. *Anal. Chem.* **2002**, *74*, 6139–6144.
- (97) Stroock, A. D.; Dertinger, S. K. W.; Ajdari, A.; Mezić, I.; Stone, H.; Whitesides, G. M. *Science* **2002**, *295*, 647–651.
- (98) Jeon, N. L.; Dertinger, S. K. W.; Chiu, D. T.; Choi, I. S.; Stroock, A. D.; Whitesides, G. M. *Langmuir* **2000**, *16*, 8311–8316.
- (99) Sudarsan, A. P.; Ugaz, V. M. *Proc. Natl. Acad. Sci. USA* **2006**, *103*, 7228–7233.
- (100) Lu, L. H.; Ryu, K. S.; Liu, C. *J. Microelectromech. S.* **2002**, *11*, 462–469.
- (101) Liu, R. H.; Yang, J.; Pindera, M. Z.; Athavale, M.; Grodzinski, P. *Lab Chip* **2002**, *2*, 151–157.
- (102) Hsu, C. H.; Chen, C.; Folch, A. *Lab Chip* **2004**, *4*, 420–424.
- (103) Folch, A.; Ayon, A.; Hurtado, O.; Schmidt, M. A.; Toner, M. *J. Biomech. Eng.* **1999**, *121*, 28–34.
- (104) Khademhosseini, A.; Suh, K. Y.; Jon, S.; Eng, G.; Yeh, J.; Chen, G. J.; Langer, R. *Anal. Chem.* **2004**, *76*, 3675–3681.
- (105) Folch, A.; Toner, M. *Biotechnol. Progr.* **1998**, *14*, 388–392.
- (106) Gu, W.; Zhu, X.; Futai, N.; Cho, B. S.; Takayama, S. *Proc. Natl. Acad. Sci. USA* **2004**, *101*, 15861–15866.
- (107) Groisman, A.; Lobo, C.; Cho, H.; Campbell, J. K.; Dufour, Y. S.; Stevens, A. M.; Levchenko, A. *Nat. Methods* **2005**, *2*, 685–689.
- (108) Masters, J. R. *Nat. Rev. Cancer* **2002**, *2*, 315–319.
- (109) Leibel, W. *J. Bus. Ethics* **1991**, *10*, 601–604.
- (110) Jones Jr., H. W. *Am. J. Obstet. Gynecol.* **1997**, *176*, S227–S228.
- (111) Nardone, R. M. *Cell Biol. Toxicol.* **2007**, *23*, 367–371.
- (112) O'Brien, S. J. *Proc. Natl. Acad. Sci. USA* **2001**, *98*, 7656–7658.
- (113) Lacroix, M. *Int. J. Cancer* **2008**, *122*, 1–4.

- (114) Solovei, I.; Schermelleh, L.; Albiez, H.; Cremer, T. In *Cell Biology Handbook: A Laboratory Manual*; 3rd Edition ed.; Celis, J., Ed.; Elsevier Academic Press: Amsterdam 2006; Vol. 1, p 291–299.
- (115) Stangegaard, M.; Petronis, S.; Jørgensen, A. M.; Christensen, C. B. V.; Dufva, M. *Lab Chip* **2006**, *6*, 1045–1051.
- (116) De Ugarte, D. A.; Morizono, K.; Elbarbary, A.; Alfonso, Z.; Zuk, P. A.; Zhu, M.; Drago, J. L.; Ashjian, P.; Thomas, B.; Benhaim, P.; Chen, I.; Fraser, J.; Hedrick, M. H. *Cells Tissues Organs* **2003**, *174*, 101–109.
- (117) Shin, J. Y.; Park, J. Y.; Liu, C.; He, J.; Kim, S. C. *Pure Appl. Chem.* **2005**, *77*, 801–814.
- (118) Gelmon, K. A.; Eisenhauer, E. A.; Harris, A. L.; Ratain, M. J.; Workman, P. J. *Natl. Cancer Inst.* **1999**, *91*, 1281–1287.
- (119) Fesik, S. W. *Nat. Rev. Cancer* **2005**, *5*, 876–885.
- (120) Edinger, A. L.; Thompson, C. B. *Curr. Opin. Cell Biol.* **2004**, *16*, 663–669.
- (121) Van Engeland, M.; Nieland, L. J. M.; Ramaekers, F. C. S.; Schutte, B.; Reutelingsperger, C. P. M. *Cytometry* **1998**, *31*, 1–9.
- (122) Büttner, S.; Eisenberg, T.; Herker, E.; Carmona-Gutierrez, D.; Kroemer, D.; Madeo, F. *J. Cell Biol.* **2006**, *175*, 521–525.
- (123) Allen, R. T.; Hunter III, W. J.; Agrawal, D. K. *J. Pharmacol. Toxicol. Methods* **1997**, *37*, 215–228.
- (124) Lockshin, R. A.; Zakeri, Z. *Int. J. Biochem. Cell Biol.* **2004**, *36*, 2405–2419.
- (125) Hail Jr., N.; Carter, B. Z.; Konopleva, M.; Andreeff, M. *Apoptosis* **2006**, *11*, 889–904.
- (126) Guimarães, C. A.; Linden, R. *Eur. J. Biochem.* **2004**, *271*, 1638–1650.
- (127) Skulachev, V. P. *Apoptosis* **2006**, *11*, 473–485.
- (128) Devaux, P. F. *Biochemistry (Mosc.)* **1991**, *30*, 1163–1173.
- (129) Reutelingsperger, C. P. M.; Van Heerde, W. L. *Cell. Mol. Life Sci.* **1997**, *53*, 527–532.

- (130) Bevers, E. M.; Comfurius, P.; Dekkers, D. W. C.; Zwaal, R. F. A. *Biochim. Biophys. Acta* **1999**, *1439*, 317–330.
- (131) Kenis, H.; van Genderen, H.; Bennaghmouch, A.; Rinia, H. A.; Frederik, P.; Narula, J.; Hofstra, L.; Reutelingsperger, C. P. M. *J. Biol. Chem.* **2004**, *279*, 52623–52629.
- (132) Fadok, V. A.; Voelker, D. R.; Campbell, P. A.; Cohen, J. J.; Bratton, D. L.; Henson, P. M. *J. Immunol.* **1992**, *148*, 2207–2216.
- (133) Lang, F.; Gulbins, E.; Szabo, I.; Lepple-Wienhues, A.; Huber, S. M.; Duranton, C.; Lang, K. S.; Lang, P. A.; Wieder, T. *J. Mol. Recognit.* **2004**, *17*, 473–480.
- (134) Panchuk-Voloshina, N.; Haugland, R. P.; Bishop-Stewart, J.; Bhargat, M. K.; Millard, P. J.; Mao, F.; Leung, W. Y.; Haugland, R. P. *J. Histochem. Cytochem.* **1999**, *47*, 1179–1188.
- (135) Zhang, X.; Kiechle, F. L. *Biochem. Biophys. Res. Commun.* **1998**, *248*, 18–21.
- (136) Saito, M.; Kobayashi, M.; Iwabuchi, S. I.; Morita, Y.; Takamura, Y.; Tamiya, E. *J. Biochem.* **2004**, *136*, 813–823.
- (137) Gavathiotis, E.; Sharman, G. J.; Searle, M. S. *Nucleic Acids Res.* **2000**, *28*, 728–735.
- (138) Narayan, P.; Mentzer Jr., R. M.; Lasley, R. D. *Am. J. Physiol. Heart Circ. Physiol.* **2001**, *281*, H1931–H1937.
- (139) Dursun, B.; He, Z.; Somerset, H.; Oh, D. J.; Faubel, S.; Edelstein, C. L. *Am. J. Physiol. Renal. Physiol.* **2006**, *291*, F578–F587.

## CHAPITRE II

### ARTICLE SCIENTIFIQUE: OXYGEN PLASMA TREATMENT OF POLYSTYRENE AND ZEONOR SUBSTRATES FOR ADHESION OF PATTERNED CELLS

Dans le chapitre précédent, les procédés de lithographie ont été appliqués pour obtenir des cellules adhérentes selon une disposition linéaire et des tests de fluorescence ont été faits pour s'assurer que les plastiques utilisés, le Zeonor<sup>®</sup> 1060R et le polystyrène, étaient biocompatibles, donc convenable pour la culture cellulaire.

Dans le présent chapitre, nous voulons contribuer à une meilleure compréhension à ce qui influence l'adhésion des cellules sur la surface des plastiques. Ces dernières sont traitées avec un plasma d'oxygène de différents ratios puissance/flux gazeux. Ensuite des analyses de surface sont effectuées, soient: les mesures de XPS, d'angles de contact, et d'AFM pour voir les différentes fonctionnalités présentes à la surface, l'hydrophilicité nouvellement acquise et les changements de rugosité. Par la suite, le dispositif microfluidique est appliqué sur les plastiques, le déplacement du liquide par capillarité à l'intérieur des canaux est observé et l'effet du traitement sur l'écoulement est évalué. Aussi, l'impact des traitements de plasma d'oxygène sur la confluence des cellules sur la surface et l'adhésion des cellules dans les canaux est vérifié. Finalement, le test de biocompatibilité vu dans le chapitre I, est refait pour s'assurer que le traitement au plasma utilisé n'influence pas négativement la survie des cellules.

Ce chapitre permet de dévoiler les propriétés de biocompatibilité du Zeonor<sup>®</sup> 1060R qui, au meilleur de nos connaissances, est pour la première fois analysé par XPS et utilisé pour l'adhésion cellulaire. Il s'agit donc d'un nouveau matériel, inerte, peu coûteux, disponible commercialement, mis à la disposition des biologistes faisant la culture cellulaire. De plus, l'utilisation de méthodes de lithographie, simples et relativement faciles à utiliser permet de faire adhérer les cellules dans une disposition voulue. Cette façon de faire représente un avantage important pour les électrochimistes étudiant les systèmes biologiques. En effet, elle donne la possibilité de procéder plus rapidement aux analyses diminuant ainsi le risque de détérioration du matériel biologique.

## Oxygen Plasma Treatment of Polystyrene and Zeonor Substrates for Adhesion of Patterned Cells

*Isabelle Beaulieu,<sup>†</sup> Matthias Geissler,<sup>‡</sup> Teodor Veres,<sup>‡</sup> and Janine Mauzeroll<sup>†,\*</sup>*

Chemistry Department, Université du Québec à Montréal, 2101 Jeanne-Mance Street, Montreal, QC, H3C 3P8, Canada, and Industrial Materials Institute, National Research Council Canada, 75 de Mortagne Boulevard, Boucherville, QC, J4B 6Y4, Canada

\* Corresponding author. E-mail: mauzeroll.janine@uqam.ca.

<sup>†</sup> Chemistry Department, UQÀM.

<sup>‡</sup> Industrial Materials Institute.

### Abstract

Plastic substrates made of polystyrene (PS) and Zeonor 1060R were treated with oxygen plasma to introduce polar groups (e.g., carbonyl and carboxylic acid) at the surface that render these materials hydrophilic and promote patterned adhesion of HeLa cells. Resultant surfaces were characterized using contact angle goniometry, atomic force microscopy (AFM) and X-ray photoelectron spectroscopy (XPS) to monitor changes in wettability, nano-scale topography and chemical composition. Biocompatibility of the plastic surfaces was verified through fluorescence microscopy using three fluorophores, Alexa Fluor 488 conjugated to Annexin V, Hoechst 33258, and propidium iodide, indicating cells that undergo apoptosis and necrosis, respectively. Best cell growth was observed on PS treated at 5 W/sccm, for which the viability of adhering HeLa cells exceeded 90%. Patterning was accomplished using an elastomeric microcapillary system ( $\mu$ CS) made of PDMS that consisted of a set of parallel channels to align cells in linear fashion. Densely populated bands were obtained on substrates of both plastic materials when the culture medium contained  $>2 \times 10^5$  cells/mL.

**Keywords.** Oxygen plasma, plastic, cell adhesion, biocompatibility, microfluidic patterning, fluorescence microscopy, contact angle goniometry, AFM, XPS, SECM.

## 2.1. Introduction

Cells change their phenotype in response to their environment. Their metabolism, proliferation and differentiation in adhering cultures are affected by several chemical cues that make it difficult to faithfully assign *in vitro* gene expression and functional state with those that are present *in vivo*. Nevertheless, by learning to carefully control these cues, predictive cell-based assays could have a large impact on the early stages of drug discovery.<sup>1</sup> Adjustment of cell adhesion and proliferation conditions on solid supports is therefore important and has become central to a number of biotechnological areas, including single cell analysis, drug screening, and tissue engineering.<sup>2,3</sup> The work presented in this paper aims at exploring routine access to patterned cells on transparent, insulating substrates to be used in scanning electrochemical microscopy (SECM). SECM is an analytical technique that can be employed to assess cell viability,<sup>4</sup> monitor cell morphology,<sup>5</sup> and evaluate molecular transport through cell membranes with high sensitivity and resolution.<sup>6,7</sup> Continuing challenges in performing biological SECM studies include i) limiting the use of serum containing solutions during the SECM measurements to prevent tip fouling, ii) restricting the experimental time to minimize exposure of cells to less than ideal growth conditions, and iii) extending the scope of SECM measurements to cell communication studies.

In principle, cell growth can be achieved on a number of materials, yet the preferred cell culture substrates are made from plastic polymers, such as polystyrene (PS), polycarbonate and polyvinylchloride.<sup>8,9</sup> Pristine surfaces of most plastics are generally unsuitable for cell culture and therefore require modification. This can be achieved, for example, through exposure to gas plasma,<sup>10</sup> corona discharge,<sup>11</sup> or  $\gamma$ -irradiation,<sup>8</sup> followed by adsorption of molecules which stimulate cell adhesion (also called attachment factors), such as fibronectin or collagen.<sup>12</sup> The adhesive molecule can either be physisorbed from the medium<sup>13</sup> or simply added to the surface<sup>14</sup> prior to adding the cell suspension. In the present study, we use physisorption from the serum, which is preferred over external deposition of attachment factors as it reduces the number of manipulations required for cell patterning and allows for adhesion of cells within their preferred culture environment. Large deposits of single adhesion factors prior to incubation can also lead to reduced biological activity as a result of unfavourable conformational changes and restrict binding specificity to select cell bound receptors.<sup>15</sup>

Most patterning schemes rely on microfabrication techniques in conjunction with surface modification to control adhesion, shape and function of cells in a spatially-defined manner.<sup>3</sup> For example, photolithography has been used to create structural information that can differentiate cell attachment.<sup>16</sup> Whitesides and co-workers have successfully confined cells on microcontact-printed self-assembled monolayers of alkanethiolates on gold.<sup>17</sup> It is also possible to deposit cells through a stencil that limits cell interactions to the exposed areas of the surface.<sup>18</sup> Finally, a number of approaches rely on laminar flow in microcapillary systems ( $\mu$ CSs), where adhesion-promoting ligands or cells can be confined at selected sites through hydrodynamic forces,<sup>19</sup> dielectrophoresis,<sup>20</sup> or the implementation of mechanical traps.<sup>21</sup> These systems are commonly (although not exclusively) fabricated from poly(dimethylsiloxane) (PDMS) using rapid prototyping.<sup>22</sup> The use of this elastomer is favourable in part because of its ability to conform to other surfaces resulting in a water-tight seal.<sup>23</sup> Fluidic cell patterning using PDMS-based devices has also been applied to a wide range of cell types, including human umbilical vein<sup>24</sup> and bovine adrenal capillary<sup>25</sup> endothelial cells, human bladder cancer<sup>25</sup> cells, 3T3-J2 fibroblasts<sup>26</sup> and Calu-3<sup>27</sup> and LLCPK1<sup>24</sup> epithelial cells.

The development of simple and efficient patterning schemes seems to be of vital importance for future SECM investigation as it facilitates sample localization, reduces overall analysis time, and enables cell communication studies. For example, Matsue and co-workers showed that cell patterning helped evaluate cell respiration activity by SECM.<sup>28</sup> Herein, we investigate the conditions required for achieving patterned adhesion of living cells on two hard thermoplastic materials, Zeonor 1060R and PS from the serum and without additional attachment factors. Zeonor is an amorphous cyclo olefin copolymer that is produced using ring-opening metathesis of norbornene derivatives, followed by hydrogenation.<sup>29</sup> Unlike PS, this polymer is less frequently used as cell culture substrate, even though it seems convenient to this end as it is inert, non-toxic, and has optical properties well suited for transmission or fluorescence microscopy.<sup>30,31</sup> Moreover, Zeonor can be shaped using thermoforming processes (e.g., injection molding) or machined mechanically to custom-fabricate substrates of desired size and shape that can be adapted to biological SECM instrumentation. For the purpose of this study, we selected cancerous cervix epithelial (HeLa) cells which are relatively robust and hence ideally suited for adhesion and patterning experiments.<sup>32</sup> We

assessed the biocompatibility of the plastic surfaces using fluorescence microscopy in conjunction with fluorophores that stain cells undergoing apoptosis or necrosis. Fluorescence microscopy is preferable over viability tests based on flow cytometry<sup>33,34</sup> or laser scanning cytometry<sup>35</sup> since it does not require detachment of the studied cells from the surface during electrochemical analysis.

## 2.2. Experimental Section

**2.2.1. Preparation of Plastic Substrates.** Zeonor and PS slides ( $25 \times 75 \text{ mm}^2$  in area, 1 mm in thickness) were prepared by injection molding using a Boy 30A injection tool (Dr. Boy GmbH, Neustadt-Fernthal, Germany). Zeonor<sup>®</sup> 1060R (Zeon Chemicals, Louisville, KY) was molded at a temperature of 250 to 260 °C, an injection speed of 40 mm/s and a pressure of 132 bar. Molding of polystyrene (MW = 100 000, Alfa Aesar, Ward Hill, MA) was done at 195 to 205 °C, an injection speed of 30 mm/s, and a pressure of 132 bar. The mold (stainless steel, custom-fabricated) was cooled for 15 s before the slide was released. Slides were sonicated for three washing cycles of 10 min each, using methanol, ethanol and deionized (DI) water (18.2 M $\Omega$  cm), respectively, to clean the surface of monomers or residual plasticizing agents. Slides were exposed to oxygen plasma (Plasmalab80Plus, Oxford Instruments, Bristol, UK) for 4 min at a pressure of 50 mTorr, and a power/gas flow ratio of between 0.5 and 100 W/sccm.

**2.2.2. Surface Characterization.** Contact angles were measured with a contact angle goniometer (Model 200-F1) from Ramé-Hart Instrument Co. (Netcong, NJ) using DI water as the probe liquid. Images of advancing and receding drops were recorded with a CCD camera and analyzed using DROPimage Standard software. Roughness measurements on plastic surfaces were performed with a multi-mode Nanoscope IV atomic force microscope (Veeco Metrology Group, Santa Barbara, CA), operated at ambient conditions and in tapping mode using a silicon nitride cantilever (NCH Point Probe, Nanoworld, Neuchâtel, Switzerland) with a resonance frequency of 320 kHz and a spring constant of 42 N/m. For each sample, an area of  $3 \times 3 \text{ }\mu\text{m}^2$  was imaged at a rate of  $\sim 1.0 \text{ Hz}$ , and a pixel resolution of  $512 \times 512$ . XPS spectra were recorded on a Kratos Analytical AXIS ULTRA spectrometer (Manchester, UK). The instrument was equipped with a hybrid lens and a monochromatic Al *K* $\alpha$  source ( $E =$

1486.6 eV) providing a resolution of 0.4 eV. The analysis covered an area of  $700 \times 400 \mu\text{m}^2$ . Survey scans were collected between 1100 and 0 eV using an analyzer pass energy (PE) of 160 eV with 0.33 eV steps during 100 ms. High-resolution spectra were collected with a PE of 20 eV and steps of 0.1 eV during 200 ms for 8 to 40 scans. An electron flood gun was used to counterbalance charging of the insulating plastic surfaces during exposure. Elemental composition was calculated using Kratos instrument software Vision 2. Atomic concentrations were extracted from peak area calculations using a linear background with Scofield sensitivity factors and the instrument transmission functions.

**2.2.3. Fabrication of Microcapillary Systems.** Microcapillary systems were prepared from PDMS (Sylgard 184, Dow Corning, Midland, MI) by curing a mixture (10:1 w/w) of elastomer base and cross-linker on a silicon/photoresist mold at 60 °C for at least 12 h. To fabricate the mold, a silicon wafer (Silicon Quest International, Inc., Santa Clara, CA) was first baked on a hot plate at 160 °C for 15 min before a layer of SU-8 (GM1040, Gersteltec, Pully, Switzerland) was applied through spin coating. This was followed by a pre-bake at 65 and 95 °C for 5 and 15 min, respectively, using a temperature ramp of 2 °C/min. The resist layer was exposed to UV light with a wavelength of 365 nm (Hg i-line) at  $280 \mu\text{J}/\text{cm}^2$  through a quartz/Cr mask (HTA Photomask, San José, CA) using an EVG 6200 mask aligner (EV Group, Schärding, Austria). Post-exposure bake was done using the same conditions as for the pre-bake. Resist features were developed in propylene glycol monomethyl ether acetate (Sigma-Aldrich Corp., St. Louis, MO) for 2 min. The wafer was then rinsed with isopropanol (Anachemia, Montreal, QC) and dried with a stream of nitrogen gas. Resultant resist pattern was hard-baked at 130 °C for 2 h. Finally, the master was coated with a thin, anti-adhesive layer formed by exposure to 1*H*,1*H*,2*H*,2*H*-perfluorooctyl-trichlorosilane (Sigma-Aldrich) vaporized at reduced pressure. Inlets and outlets of channels were punched by hand upon release of the cured PDMS  $\mu\text{CS}$  from the mold.

**2.2.4. Patterning of Cells.** Mammalian cervix adenocarcinoma (HeLa) cells used for patterning were bought from ATCC (Manassas, VA). The cell culture medium, Minimal Essential Medium containing L-glutamine (Invitrogen, Burlington, ON), was dissolved in nanopure water purified with a Millipore Milli-Q Biocel Ultrapure water system (Fisher,

Ottawa, ON). The medium total volume contained 10% of fetal bovine serum (Invitrogen), 1% of a HYQ<sup>®</sup> MEM non-essential amino acids solution 100x (HyClone, Logan, UT) and 1% of HYQ<sup>®</sup> Penicillin-Streptomycin ( $10^4$  units/mL, HyClone). The preparation was concluded by adding 1mM of sodium pyruvate, and 2 mM of sodium bicarbonate (biotechnology grade, BioShop Canada Inc., Burlington, ON). The medium was vacuum filtered (Millipore 0.22  $\mu$ m PES membrane filters, Fisher) before adding the amino acids and the serum that were already sterile. Cells were cultured in a 75 cm<sup>2</sup> growth area flask (Sarstedt Inc., Saint-Leonard, QC) under a water-saturated atmosphere containing 5% of CO<sub>2</sub>. For patterning experiments, cells were detached from the culture flask with a solution of 0.25% w/v trypsin-0.26 mM EDTA-4Na (Sigma-Aldrich), suspended and injected in the inlet of the PDMS  $\mu$ CS. Optimal cell adhesion required a 5h resting period in the incubator prior to removal of the  $\mu$ CS.

**2.2.5. Biocompatibility Tests.** Alexa Fluor<sup>®</sup> conjugated to Annexin-V (AV-Alexa Fluor 488) ( $\lambda_{\text{ex}} = 488$  nm;  $\lambda_{\text{em}} = 520$  nm) was purchased from Invitrogen, Bisbenzimidazole Hoechst 33258 (H33258) ( $\lambda_{\text{ex}} = 352$  nm, and  $\lambda_{\text{em}} = 461$  nm) was obtained from Sigma-Aldrich, and propidium iodide (PI) ( $\lambda_{\text{ex}} = 535$  nm,  $\lambda_{\text{em}} = 617$  nm) from EMD Chemicals (Gibbstown, NJ). Each fluorescent probe tags cells during different stages of cell death. Selectivity to early apoptosis (AV-Alexa Fluor 488), late apoptosis (H33258) and necrosis (PI) was validated using tributyltin chloride (TBT, 96%, Sigma-Aldrich) and Triton X-100 surfactant (EMD Chemicals) serving as positive controls, respectively. First, cells were washed with phosphate buffered saline (PBS, pH = 7.4) prepared with PBS foil pouches (Sigma-Aldrich). Then, the first two fluorophores were added to the Petri dish containing the cells and binding buffer (HEPES, acid free, molecular biology grade, EMD Chemicals) and incubated for 15 min. After a second wash with PBS, PI was added prior to image acquisition.

**2.2.6. Optical and Fluorescence Imaging.** Optical micrographs were obtained using a TS-100 microscope (Nikon, Montreal, QC) equipped with a Go-3 QImaging (Surrey, BC) camera using Q Capture Pro software (version 5.1). Fluorescence micrographs were acquired using a Nikon Eclipse TE2000-U inverted microscope equipped with an ultraviolet excitation filter block UV-2E/C, a green excitation filter block G-2A and an endow GFP bandpass

Emission filter FGP(R)-BP (Nikon) using a Retiga 1300 CCD camera (QImaging) and Northern Eclipse software.

**2.2.7. Flow Measurements.** Two lines separated by a distance of  $\sim 1.0$  mm were traced on the lower side of the plastic slides, serving as reference marks. The  $\mu$ CS contained 3 channels each being  $31 \mu\text{m}$  in height and  $200 \mu\text{m}$  in width, which were aligned perpendicular to the underlying reference lines. Samples were placed on an Eclipse 50i microscope (Nikon) equipped with a CCD camera (Retiga 2000R Fast 1394 Mono Cooled, QImaging). Following injection of nanopure water into the inlet, the displacement of the fluid was captured on video using Nikon NIS-Element software (version 3.0). Liquid flow within capillaries was calculated from the velocity of the meniscus between the two reference lines.

## 2.3. Results and Discussion

**2.3.1. Surface Analysis.** Plasma exposure is an effective procedure to alter interfacial properties for a number of materials, most notably synthetic polymers. Depending on the composition of the ionizing gas, heteroatoms can be incorporated at the surface, thereby introducing functionality that affects wettability, surface charge and adhesion. Treatment of plastic materials with oxygen plasma generally results in the formation of hydrophilic, oxygen-containing groups<sup>36,37</sup> (e.g., carbonyl, carboxyl, ester etc.) which, in turn, increase the free energy<sup>38</sup> and promote wetting of the surface by polar solvents. As shown in Tables 1 and 2, pristine surfaces of both PS and Zeonor were hydrophobic with advancing contact angles ( $\theta_{\text{adv}}$ ) being  $>90^\circ$ .<sup>39</sup> As can be expected, surfaces of both materials became hydrophilic upon treatment with power/gas flow ratios larger than  $0.5 \text{ W/sccm}$ , resulting in advancing and receding ( $\theta_{\text{rec}}$ ) contact angles of  $<10^\circ$ . We noticed, however, that only exposure to plasma of high intensity (e.g.,  $100 \text{ W/sccm}$ ) yielded surfaces that were stable over longer periods of time (e.g., at least nine days), while contact angles generally increased for all other conditions. Hydrophobic recovery of plasma-exposed polymers is a well-known phenomenon,<sup>36</sup> which is generally attributed to migration of low-molecular weight residues along with re-arrangement of polymer chains at the surface.

We inspected plastic surfaces using AFM to determine the impact of plasma intensity on micro- and nano-scale topography (Figure 2.1). Untreated samples displayed relatively smooth surfaces with a root-mean square (RMS) roughness of  $\sim 0.5$  nm. For both materials, RMS roughness increased gradually with the power/gas flow ratio approaching values of  $\sim 25$  nm upon exposure to 100 W/sccm. This finding is a result of decomposition and abrasive removal of material from the surface during treatment.<sup>40</sup> The increase in roughness, even though remaining restricted to the lower nanometer range, may contribute to the relatively large contact angle hysteresis<sup>41</sup> that we observed when re-examining samples after a period of 9 days (see Tables 2.1 and 2.2).

The XPS spectra shown in Figure 2.2 reveal that exposure to O<sub>2</sub> plasma changes the relative peak intensities for C 1s and the O 1s signals. Pristine surfaces of both PS and Zeonor are dominated by hydrocarbon (C–H) units that give rise to strong signal intensities at 285.0 eV. The appearance of a peak at 533.6 eV in these spectra accounts for  $\sim 4$  and 5.6% of oxygen on Zeonor and PS surfaces, respectively (Table 2.3). Although it is possible that both polymer formulations include a certain degree of functionality within the network, it is likely that signals indicate the presence of oxygen-containing additives and/or molecules adsorbed at the surface while stored at ambient conditions. Upon treatment, the O 1s signal intensities increased progressively with the power/gas flow ratio, while C 1s signals decreased at the same time. The most drastic change was observed for Zeonor treated at 100 W/sccm, for which the atomic concentration of oxygen reached  $>31\%$  (Table 2.3). As a consequence, the carbon content diminished from  $>94$  to  $\sim 61\%$ . The findings for PS, on the other hand, indicate saturation of the surface for plasma intensities  $>20$  W/sccm, which is in good agreement with data reported in the literature.<sup>42,43</sup>

Deconvolution of high-resolution C 1s spectra (Figure 2.3) revealed a set of four distinct peaks (2 to 5) appearing as a result of the treatment process. The maximum of each peak was shifted towards higher energies with respect to the hydrocarbon signal at 285.0 eV (1), which is consistent with the formation of oxidized units in the polymer chains.<sup>44,45</sup> The example in Figure 2.3 illustrates the peak distribution for plasma-treated Zeonor using a standard fit algorithm. Peak (2) at 285.2 eV corresponds to carbon atoms next to an oxygen-containing group (e.g., C–CO<sub>2</sub>), while peak (3) at 286.8 eV can be attributed to carbon atoms that are directly linked to one oxygen atom (C–O) as is the case for alcohols and ethers. Peak (4) at

288 eV reveals the presence of carbonyl groups (C=O) at the surface, yet may equally relate to carbon associated with two oxygen atoms (e.g., O-C-O). Peak (5) at 289.5 eV finally corresponds to carbon in acid and ester groups (O-C=O). The distribution of these peaks was prone to variation depending on the conditions of treatment; ratios on the other hand remained relatively stable over time. For example, after 20 days of storage, peak distribution for Zeonor treated at 100 W/sccm (Figure 2.3) was (1) 26.1%; (2) 49.1%; (3) 11.2%; (4) 8.1%; and (5) 5.5%. By comparison, the corresponding spectrum for PS revealed the following set of peaks: (1) at 285.0 eV, 37.6%; (2) 285.4 eV, 38.4%; (3) 287.4 eV, 12.2%; (4) 288.4 eV, 4.5%; and (5) 289.7, 5.1%. In addition, the PS spectrum showed a shake-up energy peak at 291.8 eV<sup>36,46</sup> accounting for 2.2% of the overall signal. These findings indicate that functional groups remain intact even over longer periods of time, and hence should remain suitable for cell patterning experiments.

**2.3.2. Biocompatibility.** Compatibility of the plastic substrates was probed using fluorescence microscopy in conjunction with dyes that tag cells in different stages of their dying process. We employed three commercially available fluorophores, AV-Alexa Fluor 488, H33258 and PI, whose selectivity towards apoptotic and necrotic cell death is presented in Figure 2.4. ANOVA statistical tests using  $\alpha = 0.01$  from the Fisher-Snedecor distribution table<sup>47</sup> revealed that samples from all control experiments performed on different days could be considered as being part of the same statistical population. The negative control group represents cells untreated with a cell death inductor. Figure 2.4 shows that the majority of the cells remained untagged by the fluorophores, which corresponds to 98% of its population. Positive controls for necrosis consisted of cells exposed to 0.075% Triton X. This surfactant induces cell lysis and is often used to dissolve lipid membranes.<sup>48</sup> No variance was observed since 100% of the cells underwent necrosis, hence being tagged by PI. Upon incubation with TBT (here, 2  $\mu$ M for 15 min) apoptosis<sup>49,50</sup> was observed for a large portion of cells in the corresponding control group. The data suggests some distribution in viability because the cell population is asynchronous and cells in the S phase (e.g., during DNA synthesis) are more vulnerable than others.<sup>51</sup> In the apoptosis positive control, AV-Alexa Fluor 488 and H33258 primarily tag apoptotic cells since the average numbers of apoptotic and necrotic cells are

significantly different with  $\alpha = 0.05$  from the Student distribution table.<sup>47</sup> AV-Alexa Fluor 488 and H33258 are therefore both adequate markers for cell apoptosis.

Figure 2.5 illustrates the biocompatibility of plastic substrates, which were incubated with HeLa cells over a period of four consecutive days. The images in Figures 2.5A and 2.5B reveal a typical cell population obtained on most plasma-treated surfaces. The absence of any notable fluorescence from cells is indicative of their proper metabolic functioning. As shown in Figure 2.5C, no cell growth was observed on pristine surfaces of Zeonor 1060R. Upon exposure to oxygen plasma, cells adhered on this plastic with normal cells exceeding 90% for any of the conditions used in this study. Figure 2.5D illustrates that it was possible to attach cells on pristine PS surfaces with ~60% viability of the population. In contrast to Zeonor, pristine PS is weakly charged which likely favors cell adhesion.<sup>52</sup> Results for plasma-treated PS surfaces were largely comparable to those obtained for Zeonor. The relatively high percentage (e.g., 27%) of apoptotic cells in the case of samples treated at 0.5 W/sccm indicates that proper treatment of the surface is critical to the metabolic state of adhering cells.

**2.3.3. Adhesion and Cell Growth on Plasma-Treated Surfaces.** The serum used in this study contained fibronectin as a growth factor and adhesion promoter. Fibronectin is a protein that can associate with the collagen present in the extracellular matrix of a cell, which is considered to be a key event in the cell adhesion process.<sup>43,52</sup> We recorded the percentage of confluency in intervals of 24 h to verify progression of cell growth and proliferation on each substrate over a total period of four days (see Tables 2.4 and 2.5). Except for pristine Zeonor (Table 2.4), cells populated the surface of all samples and confluency increased gradually over time. The highest confluency on Zeonor was 50%, corresponding to the substrate exposed at 0.5 W/sccm. For other conditions of treatment, confluencies varied between 23 and 37%. For PS (Table 2.5), few cells grew on the untreated surface and little cell division (e.g., 7%) occurred during the period of observation. Substrates treated at 0.5 and 5 W/sccm showed the best rates of cell division (e.g., 80 and 60%, respectively), while confluency was on the order of 30% for all other samples. These trends are consistent with work performed by Larsson and co-workers on air plasma treated substrates.<sup>42</sup> According to previous studies, good cell growth is obtained on less hydrophilic surfaces (e.g.,  $\theta_{adv} > 25^\circ$ ). The relatively low

contact angles we obtained as a result of intense plasma treatment (see Tables 2.1 and 2.2) may partly explain the relatively poor confluency results for the corresponding samples. On the other hand, wettability does not seem to be the only criterion, since Zeonor samples often presented higher contact angles than PS with reduced cell confluency. Therefore, not only the surface itself but also the bulk properties of the polymer (e.g., its composition and morphology) may influence cell culture. The cell culturing capabilities of the treated plastics are, however, not a prerequisite for cell patterning. In the context of SECM analysis, pattern formation often implies the use of a larger concentration of cells and confluency percentage is therefore not as important as if the plastics were modified solely for cell culture.

**2.3.4. Cell Pattern Formation.** The set-up illustrated in Figure 2.6A accounts for an experimentally unsophisticated yet convenient fashion of confining cell assemblies to selected regions of a substrate. The  $\mu$ CS used for this study consisted of parallel channels, each connected to macroscopic access points (inlets and outlets, respectively) located at their extremities. The  $\mu$ CS is placed channel-side down onto a plastic substrate; conformal contact seals the surface and the embedded microcapillaries can be filled with liquid using capillary action, although the design is generally compatible with external pumping systems being connected to either inlets or outlets of the  $\mu$ CS. We validated the feasibility of this approach by estimating the velocity that can be reached by capillary force for water-based solutions on the plastic substrates without any treatment of the PDMS channels. Upon injection, displacement of water within the channels was observed in all cases except for plastics in their pristine forms, as can be expected from their respective advancing contact angles which exceed  $90^\circ$  in both cases. For the samples exposed at 0.5 W/sccm, the probe liquid entered slowly and the meniscus had an average velocity of  $<10 \mu\text{m/s}$  (see Experimental Section for details). For plastic substrates subjected to more intense plasma treatment, the velocity was substantially higher (e.g.  $>100 \mu\text{m/s}$ ) owing to their hydrophilic surfaces.

Capillary action was used to guide a suspension of cells in culture medium along the trajectories provided by the  $\mu$ CS, resulting in the formation of treads of immobilized cells on the plastic surface (Figure 2.6). We employed a culture medium that contained between 1 and  $2.5 \times 10^5$  cells/mL in conjunction with an untreated  $\mu$ CS to ensure proper sealing of the surface and to limit cell attachment at the channel walls. Interestingly, for the concentrations

$<2 \times 10^5$  cells/mL, almost no cells adhered on the plastic substrates. At high velocity, the cell suspension followed the fluid meniscus to the microchannel outlet, which provided limited interaction with the surface. For concentrations  $>2 \times 10^5$  cells/mL, we noticed that the reduced mobility of cells favored their interaction with the plastic slide once the flow is stopped and the cells are settled. It was therefore possible to attach cells on Zeonor (e.g., treated at 100 W/sccm) over the entire length of 400- $\mu$ m-wide microchannels (e.g.,  $\sim$ 5 mm). We were able to obtain similar results for PS using comparable conditions of treatment (e.g., 40 and 100 W/sccm) and incubation (Figure 2.6B). We limited incubation time within the confined environment of microchannels to retain acceptable conditions for growth and proliferation, which primarily concerns the availability of oxygen and nutrition in the solution. Interestingly, the patterned assembly remained intact for extended periods of time (e.g., several days) once the  $\mu$ CS was removed from the substrate.

#### 2.4. Conclusion

This study demonstrates that HeLa cells adhere on PS and Zeonor 1060R surfaces that have been hydrophilized using oxygen plasma at different power/gas flow ratios. Surface analysis proved useful to gain insight into chemical and morphological changes associated with this treatment process. Contrary to cell patterning strategies that rely on high concentrations of adhesion factors, cell attachment was promoted in part by the introduction of oxygen functionalities at the plastic surface. Patterning of cells on the functionalized substrates was achieved through the use of PDMS-based  $\mu$ CSs, although template-based patterning approaches may equally be useful to this end. While patterns generated on Zeonor surfaces showed well-separated cells along the trajectories that may be well-suited for single cell measurements, assemblies on PS were more confluent and would be ideal to perform cell communication studies using SECM. The concentration of cells injected in the channels appeared to be an important parameter to the formation of cell patterns; here, optimized concentrations were on the order of  $2 \times 10^5$  cells/mL. In producing cell patterns, care must be taken to limit PDMS debris and dust from entering the channel since they may cause adverse effects on the integrity of resultant patterns. Different cell delivery strategies along with variation in the design of the fluidic structures are presently being explored to further enhance

reliability of the patterning process. We believe that surface modification process presented in this study should also be compatible with a number of other cell lines, although experimental validation is yet to be achieved.

**Acknowledgment.** This work was supported by the National Science and Engineering Research Council of Canada and the Canadian Foundation for Innovation. We thank Dr. D. Karpuzov (Alberta Center for Surface Engineering and Science (ACSES) at the University of Alberta) for XPS analysis, and our colleagues D. Dansereau (UQÀM), T. Veres (IMI/NRC), H. Roberge (IMI/NRC), K.-M. Lau (IMI/NRC) and Prof. B. Annabi (UQÀM) for useful discussion and technical assistance.

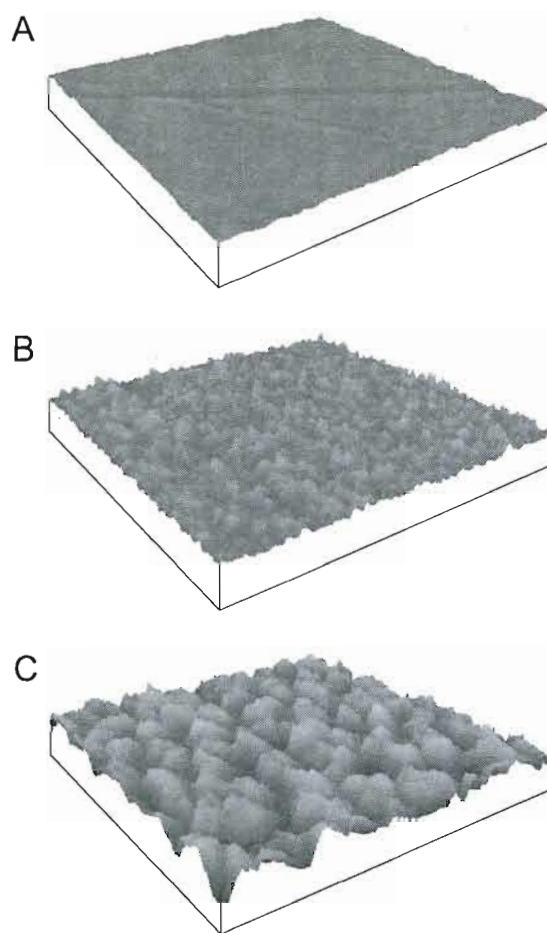


**Figure 2.1.** Surface topography of Zeonor 1060R substrates as revealed by AFM measurements. Images were taken from surfaces (A) in pristine state, and after exposure to oxygen plasma at (B) 5 and (C) 100 W/sccm. The scanned areas are  $3 \times 3 \mu\text{m}^2$  for all examples; height scales are 50, 300, and 900 nm for images in (A), (B), and (C), respectively.

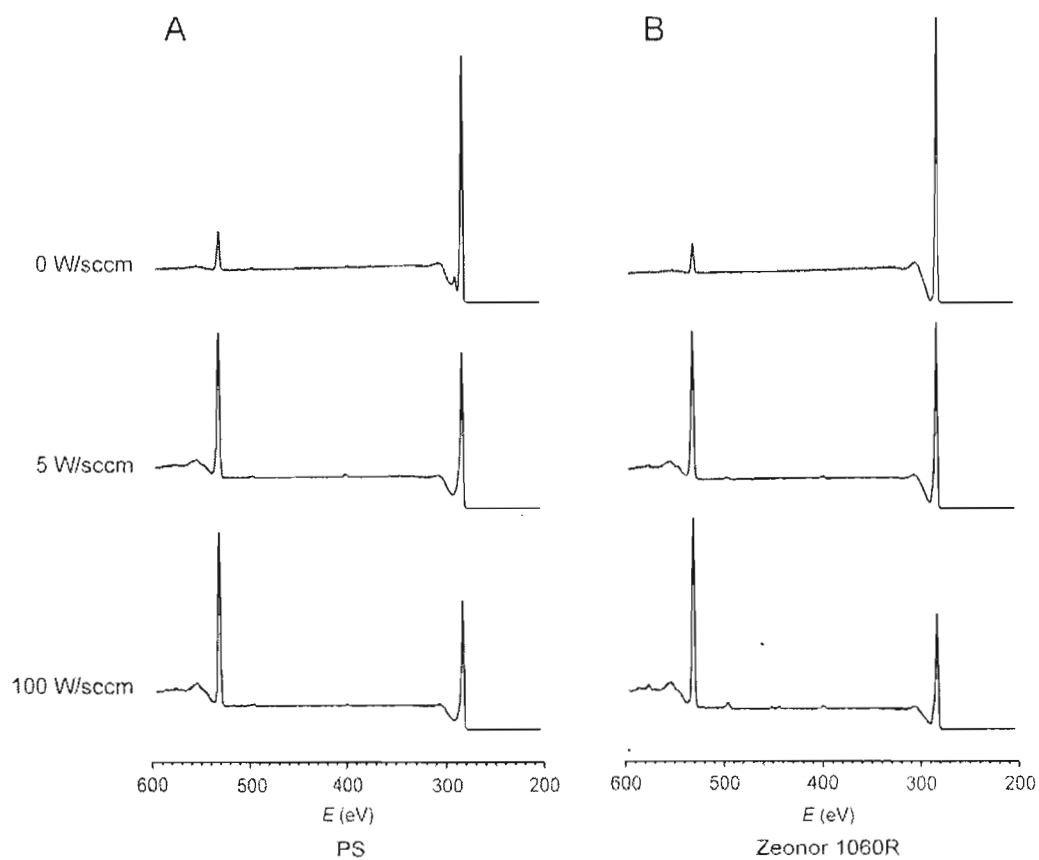


**Figure 2.2.** XPS survey spectra of PS and Zeonor 1060R substrates treated with O<sub>2</sub> plasma at 0, 5 and 100 W/sccm. Peaks of C 1s and O 1s are located at ~285 and ~533.6 eV, respectively.

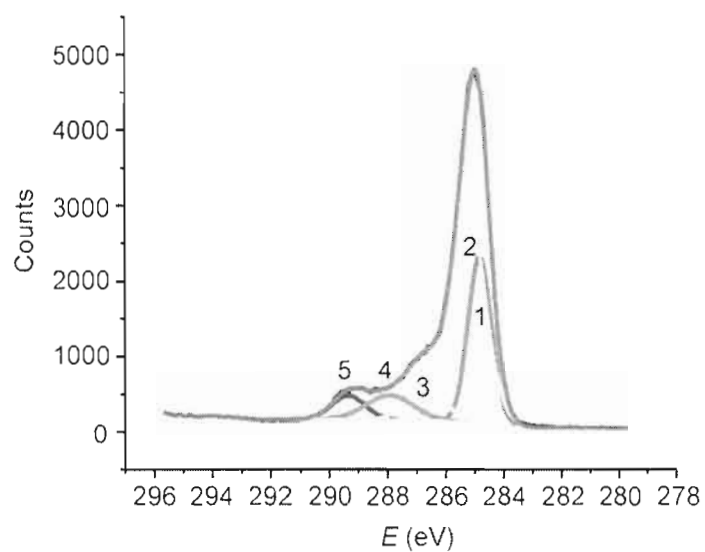


**Figure 2.3.** High resolution spectrum of the C 1s signal of Zeonor 1060R treated with O<sub>2</sub> plasma at 100 W/sccm taken after 20 days upon exposure. Fit curves correspond to (1) C-H (26.1%), (2) C-CO<sub>2</sub> (49.1%), (3) C-O (11.2%), (4) O-C-O or C=O (8.1%), and (5) O-C=O (5.5%). See text for details.

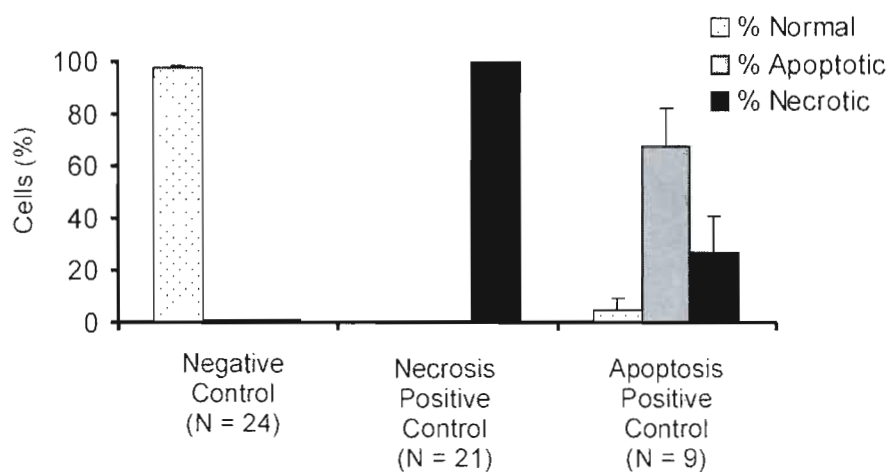


**Figure 2.4.** Necrotic and apoptotic cell death induced by Triton X-100 (0.075%) or tributyltin (2.0  $\mu$ M), respectively as revealed by fluorescence microscopy. HeLa cells were incubated with AV-Alexa Fluor 488 and H33258 in binding buffer for 15 min. Cells were washed with the buffer and PI was added prior to data acquisition.

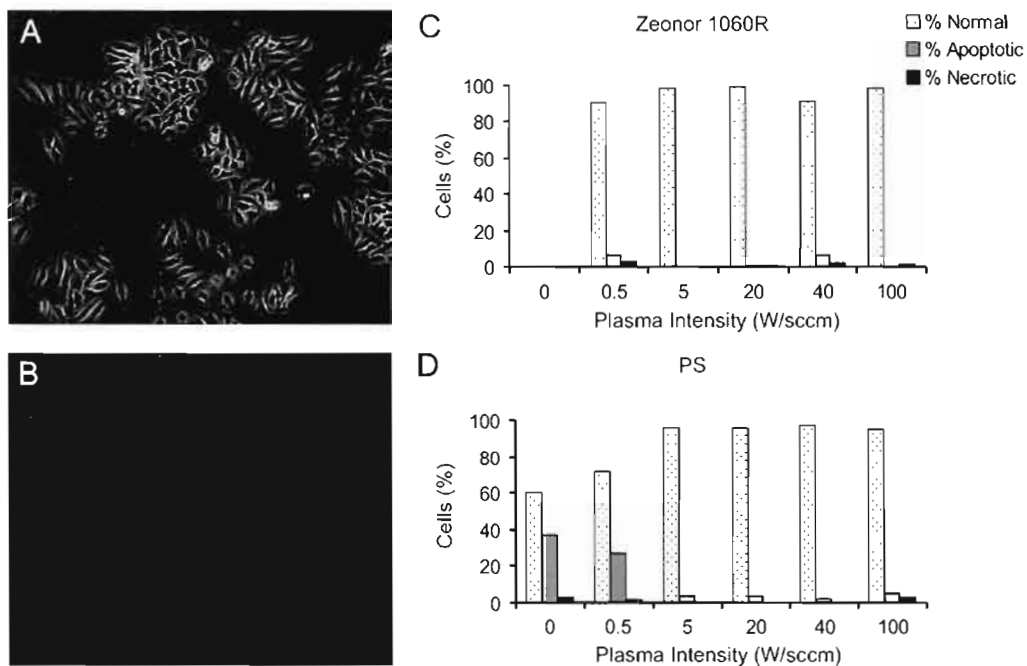


**Figure 2.5.** Biocompatibility of Zeonor and PS substrates as determined by fluorescence microscopy. (A) Optical micrograph of HeLa cells in binding buffer at pH = 7.4 adhering to a Zeonor substrate treated with oxygen plasma at 5 W/sccm. Cells were incubated for 24 h. (B) Fluorescence micrograph of the same cells upon subsequent exposure to all three cell death indicators. AV-Alexa Fluor 488 and H33258 were provided first; cells were washed with PBS after a period of 15 min, followed by addition of PI to the binding buffer. The absence of fluorescence signal indicates high viability of the population. (C, D) Quantification of cell viability on Zeonor and PS for different conditions of plasma treatment.

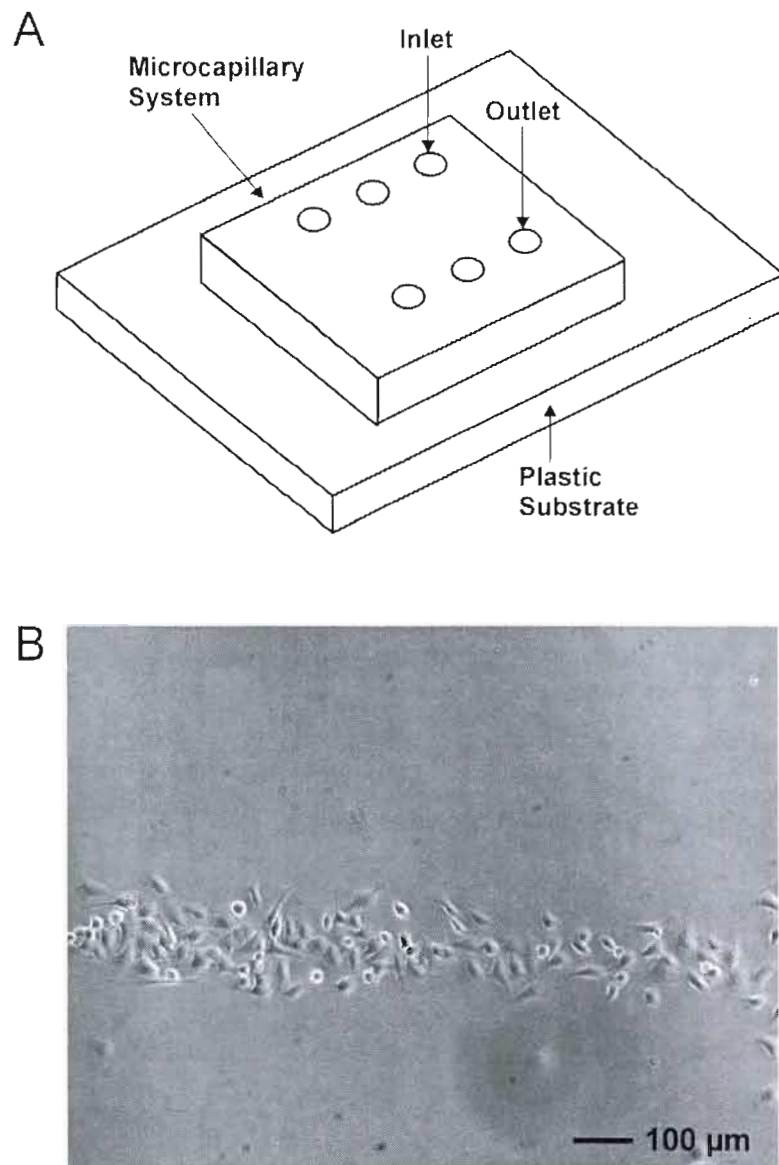


**Figure 2.6.** Patterning of cells within channels of a  $\mu$ CS. (A) Schematic of the PDMS device used for experiments. The height of channel was 27 to 31  $\mu\text{m}$ , while their widths varied between 100 and 400  $\mu\text{m}$ . (B) Optical micrograph of HeLa cells patterned on a PS surface treated with oxygen plasma at 40 W/sccm.



**Table 2.2.** Wetting Properties of Zeonor Surfaces as a Function of Plasma Power

plasma power (W/sccm)	<1 h		24 h		9 days	
	$\theta_{adv}$ (°)	$\theta_{rec}$ (°)	$\theta_{adv}$ (°)	$\theta_{rec}$ (°)	$\theta_{adv}$ (°)	$\theta_{rec}$ (°)
0	97 ± 3	72 ± 6	94 ± 3	75 ± 3	100 ± 1	74 ± 1
0.5	26 ± 3	<10	35 ± 2	12 ± 1	63 ± 2	23 ± 1
5	<10	<10	22 ± 7	<10	50 ± 4	<10
20	<10	<10	<10	<10	40 ± 4	<10
40	<10	<10	<10	<10	36 ± 3	<10
100	<10	<10	<10	<10	27 ± 3	<10

**Table 2.3.** Atomic Concentration of Plasma-Treated Zeonor and PS Surfaces as determined by XPS Measurements

plasma power (W/sccm)	Zeonor 1060R				PS			
	O (%)	N (%)	C (%)	others <sup>a</sup> (%)	O (%)	N (%)	C (%)	others <sup>a</sup> (%)
0	3.98	0.18	94.5	1.32	5.64	0.53	86.7	7.17
0.5	14.2	0.74	83.7	1.45	17.6	1.05	79.9	1.49
5	21.0	0.91	74.5	3.67	22.9	0.83	72.9	3.39
20	25.7	0.47	68.8	4.15	26.4	0.46	68.5	5.38
40	28.8	0.85	64.8	4.68	27.9	0.76	65.5	3.85
100	31.4	0.04	60.8	5.97	28.3	0.47	65.3	5.24

<sup>a</sup> Includes elements such as Na, Si, B and Al at varying percentages.

**Table 2.4.** Percentage of Cell Confluency on Zeonor Surfaces as a Function of Plasma Power

plasma power (W/sccm)	24 h	48 h	72 h	96 h
	confluency (%)	confluency (%)	confluency (%)	confluency (%)
0	0	0	0	0
0.5	8	25	37	50
5	8	17	22	23
20	8	12	23	29
40	6	12	25	35
100	6	15	30	37

**Table 2.5.** Percentage of Cell Confluency on PS Surfaces as a Function of Plasma Power

plasma power (W/sccm)	24 h	48 h	72 h	96 h
	confluency (%)	confluency (%)	confluency (%)	confluency (%)
0	5	8	9	7
0.5	5	37	63	80
5	<10	25	38	60
20	≥10	25	27	36
40	>10	18	22	25
100	20	20	25	30

## 2.5 References

- (1) Bhadriraju, K.; Chen, C. S. *Drug Discovery Today* **2002**, *7*, 612–620.
- (2) El-Ali, J.; Sorger, P. K.; Jensen, K. F. *Nature* **2006**, *442*, 403–411.
- (3) Khademhosseini, A.; Langer, R.; Borenstein, J.; Vacanti, J. P. *Proc. Natl. Acad. Sci. USA* **2006**, *103*, 2480–2487.
- (4) Kaya, T.; Torisawa, Y.-S.; Oyamatsu, D.; Nishizawa, M.; Matsue, T. *Biosens. Bioelectron.* **2003**, *18*, 1379–1383.
- (5) Zhao, X.; Petersen, N. O.; Ding, Z. *Can. J. Chem.* **2007**, *85*, 1–183.
- (6) Mauzeroll, J.; Bard, A. J.; Owhadian, O.; Monks, T. J. *Proc. Natl. Acad. Sci. USA* **2004**, *101*, 17582–17587.
- (7) Sun, P.; Laforge, F. O.; Abeyweera, T. P.; Rotenberg, S. A.; Carpino, J.; Mirkin, M. V. *Proc. Natl. Acad. Sci. USA* **2008**, *105*, 443–448.
- (8) Freshney, R. I. *Culture of Animal Cells. A Manual of Basic Technique*; 5<sup>th</sup> ed.; John Wiley & Sons: Hoboken, NJ, 2005, pp 105–113.
- (9) Harrison, M. A.; Rae, I. F. *General Techniques of Cell Culture*; Cambridge University Press: New York, NY, 1997, pp 69–88.
- (10) *Plasma Surface Modification of Polymers: Relevance to Adhesion* Strobel, M.; Lyons, C. S.; Mittal, K. L, Eds VSP: Utrecht, The Netherlands, 1994.
- (11) Onyiriuka, E. C.; Hersch, L. S.; Hertl, W. J. *Coll. Interface Sci.* **1991**, *144*, 98–102.
- (12) Folch, A.; Toner, M. *Annu. Rev. Biomed. Eng.* **2000**, *2*, 227–256.
- (13) Kaji, H.; Tsukidate, K.; Hashimoto, M.; Matsue, T.; Nishizawa, M. *Langmuir* **2005**, *21*, 6966–6969.
- (14) Folch, A.; Toner, M. *Biotechnol. Prog.* **1998**, *14*, 388–392.
- (15) Benhabbour, S. R.; Sheardown, H.; Adronov, A. *Biomaterials* **2008**, *29*, 4177–4186.
- (16) Revzin, A.; Tompkins, R. G.; Toner, M. *Langmuir* **2003**, *19*, 9855–9862.
- (17) Mrksich, M.; Dike, L. E.; Tien, J.; Ingber, D. E.; Whitesides, G. M. *Exp. Cell Res.* **1997**, *235*, 305–313.
- (18) Park, T. H.; Shuler, M. L. *Biotechnol. Prog.* **2003**, *19*, 243–253.

- (19) Takayama, S.; McDonald, J. C.; Ostuni, E.; Liang, M. N.; Kenis, P. J. A.; Ismagilov, R. F.; Whitesides, G. M. *Proc. Natl. Acad. Sci. USA* **1999**, *96*, 5545–5548.
- (20) Voldman, J.; Gray, M. L.; Toner, M.; Schmidt, M. A. *Anal. Chem.* **2002**, *74*, 3984–3990.
- (21) Wang, Z.; Kim, M.-C.; Marquez, M.; Thorsen, T. *Lab Chip* **2007**, *7*, 740–745.
- (22) McDonald, J. C.; Whitesides, G. M. *Acc. Chem. Res.* **2002**, *35*, 491–499.
- (23) Michel, B.; Bernard, A.; Bietsch, A.; Delamarche, E.; Geissler, M.; Juncker, D.; Kind, H.; Renault, J.-P.; Rothuizen, H.; Schmid, H.; Schmidt-Winkel, P.; Stutz, R.; Wolf, H. *IBM J. Res. Dev.* **2001**, *45*, 697–719.
- (24) de Silva, M. N.; Desai, R.; Odde, D. J. *Biomed. Microdevices* **2004**, *6*, 219–222.
- (25) Chiu, D. T.; Jeon, N. L.; Huang, S.; Kane, R. S.; Wargo, C. J.; Choi, I. S.; Ingber, D. E.; Whitesides, G. M. *Proc. Natl. Acad. Sci. USA* **2000**, *97*, 2408–2413.
- (26) Folch, A.; Ayon, A.; Hurtado, O.; Schmidt, M. A.; Toner, M. *J. Biomech. Eng.* **1999**, *121*, 28–34.
- (27) Mi, Y.; Chan, Y.; Trau, D.; Huang, P.; Chen, E. *Polymer* **2006**, *47*, 5124–5130.
- (28) Nishizawa, M.; Takoh, K.; Matsue, T. *Langmuir* **2002**, *18*, 3645–3649.
- (29) Shin, J. Y.; Park, J. Y.; Liu, C.; He, J.; Kim, S. C. *Pure Appl. Chem.* **2005**, *77*, 801–814.
- (30) Beattie, J. K. *Lab Chip* **2006**, *6*, 1409–1411.
- (31) Mela, P.; van den Berg, A.; Fintschenko, Y.; Cummings, E. B.; Simmons, B. A.; Kirby, B. J. *Electrophoresis* **2005**, *26*, 1792–1799.
- (32) Beaulieu, I.; Geissler, M.; Dansereau, D.; Mauzeroll, J. In *The Chemistry, Physics, and Engineering of Responsive Materials*; Bratcher, M. S., Gaddy, G. A., Kiserow, D., Maher, M. W., Eds.; John Wiley & Sons: Hoboken, NJ, in press.
- (33) Cotter, T. G.; Al-Rubeai, M. *Trends Biotechnol.* **1995**, *13*, 150–155.
- (34) Koopman, G.; Reutelingsperger, C. P.; Kuijten, G. A.; Keehnen, R. M.; Pals, S. T.; van Oers, M. H. *Blood* **1994**, *84*, 1415–1420.
- (35) Taatjes, D.; Sobel, B.; Budd, R. *Histochem. Cell Biol.* **2008**, *129*, 33–43.

- (36) Morra, M.; Occhiello, E.; Garbassi, F. *Angew. Makromol. Chem.* **1991**, *189*, 125–136.
- (37) Yasuda, H. *J. Macromol. Sci., Part A* **1976**, *10*, 383–420.
- (38) Liston, E. M.; Martinu, L.; Wertheimer, M. R. In *Plasma Surface Modification of Polymers: Relevance to Adhesion* Strobel, M., Lyons, C. S., Mittal, K. L., Eds.; VSP: Utrecht, The Netherlands, 1994, pp 3–39.
- (39) Yasuda, T.; Okuno, T.; Yasuda, H. *Langmuir* **1994**, *10*, 2435–2439.
- (40) Denes, F.; Young, R. A.; Sarmadi, M. *J. Photopolym. Sci. Technol.* **1997**, *10*, 91–112.
- (41) Kwok, D. Y.; Neumann, A. W. *Adv. Colloid Interface Sci.* **1999**, *81*, 167–249.
- (42) Johansson, B. L.; Larsson, A.; Ocklind, A.; Öhrlund, A. *J. Appl. Polym. Sci.* **2002**, *86*, 2618–2625.
- (43) Larsson, A.; Ocklind, A. In *Polymer Surface Modification: Relevance to Adhesion*; Mittal, K. L., Ed.; VSP: Utrecht, The Netherlands, 2000; Vol. 2, pp 121–135.
- (44) Sakai, Y.; Norimatsu, H.; Saito, Y.; Inomata, H.; Mizuno, T. *Thin Solid Films* **2001**, *392*, 294–298.
- (45) Diaz-Quijada, G. A.; Peytavi, R.; Nantel, A.; Roy, E.; Bergeron, M. G.; Dumoulin, M. M.; Veres, T. *Lab Chip* **2007**, *7*, 856–862.
- (46) Shard, A. G.; Badyal, J. P. S. *J. Phys. Chem.* **1991**, *95*, 9436–9438.
- (47) Scherrer, B. *Biostatistique*; 1st ed.; Gaëtan Morin Éditeur: Boucherville, QC, 1984.
- (48) Preté, P. S. C.; Malheiros, S. V. P.; Meirelles, N. C.; De Paula, E. *Biophys. Chem.* **2002**, *97*, 1–5.
- (49) Zhu, X.; Xing, M.; Lou, J.; Wang, X.; Fu, W.; Xu, L. *Toxicology* **2007**, *230*, 45–52.
- (50) Jurkiewicz, M.; Averill-Bates, D. A.; Marion, M.; Denizeau, F. *Biochim. Biophys. Acta, Mol. Cell Res.* **2004**, *1693*, 15–27.
- (51) Kaufmann, W. K.; Paules, R. S. *FASEB J.* **1996**, *10*, 238–247.
- (52) Saltzman, M. W. In *Principles of Tissue Engineering*; Lanza, R. P., Langer, R., Vacanti, J., Eds.; Academic Press: San Diego, CA, 2000, pp 221–235.

## CONCLUSION

L'étude électrochimique de systèmes biologiques par Bio-SECM présente des défis intéressants. D'abord, il faut reproduire le plus fidèlement possible le milieu physiologique auquel les cellules sont adaptées tout en éliminant les molécules pouvant se coller à l'électrode et nuire à la détection. De plus, le fait que l'appareil utilisé est particulier au laboratoire Mauzeroll, implique le besoin d'utiliser un dispositif fait sur mesure pour être introduit dans la cellule électrochimique. L'objectif premier de ce projet est donc de développer des substrats de plastiques permettant l'adhésion de cellules biologiques. De plus, l'analyse de matériel vivant demande que le processus expérimental soit fait dans un délai relativement court pour s'assurer de la qualité de l'échantillon. Le positionnement de l'électrode au-dessus de la cellule à étudier doit donc se faire rapidement pour éviter la mort cellulaire en cours d'analyse. Pour ce faire des procédés de lithographie sont utilisés dans le but d'obtenir des lignes de cellules reproductibles. Les cellules sont adhérees sur des disques de plastiques, le Zeonor<sup>®</sup> 1060R et le polystyrène, biocompatibles. Pour promouvoir l'adhésion cellulaire à la surface des plastiques, un traitement au plasma d'oxygène est employé et des groupements fonctionnels oxygénés sont alors introduits à la surface augmentant ainsi son hydrophilicité. Ce traitement augmente bel et bien les propriétés d'adhésion des substrats utilisés. De plus, ils sont appropriés pour la culture cellulaire puisque 90% des cellules sont vivantes lors des tests de viabilité, tel que déterminé par microscopie à fluorescence.

Lors de l'utilisation de lithographie molle pour former les lignes de cellules, certains problèmes ont été rencontrés. Par exemple, la formation des réservoirs, à chaque extrémité des canaux, faite à l'aide d'un poinçon cause l'apparition de certains débris qui peuvent obstruer le passage du liquide. Diverses stratégies d'injections des cellules sont envisagées pour limiter l'influence de ces débris et ainsi améliorer la répétabilité de l'adhésion linéaire. Entre autre, plutôt que de se fier seulement aux forces capillaires pour déplacer la suspension

cellulaire dans les microcanaux, des pompes péristaltiques peuvent être utilisées et assurer un flot constant.

L'adhésion cellulaire selon un arrangement bien défini, permet la localisation accélérée des cellules à étudier. De plus, des résultats préliminaires laissent envisager qu'il est bel et bien possible d'imager les cellules adhérentes de cette façon, avant qu'elles ne meurent. Éventuellement des mesures de respiration cellulaire seront faites en exploitant la réaction de réduction de l'oxygène. De telles études peuvent être utilisées pour évaluer la viabilité des cellules suite à leur exposition à des agents toxiques. En effet, lorsque les cellules meurent, elles ne consomment plus d'oxygène et celle-ci est donc réduite à l'électrode. Ainsi, le courant mesuré au-dessus de cellule morte est plus important que lorsque les cellules respirent. De plus, les améliorations possibles portées au procédé d'adhésion lithographique, laisse présager que des mesures de communication cellulaire pourront être faites en détectant le transfert d'électrons d'une cellule à l'autre. Ce type d'expériences pourrait être intéressant pour l'étude du phénomène de résistance aux médicaments de chimiothérapie. En effet, une cellule n'ayant jamais été mis en contact avec de tels médicaments peut devenir résistante au même titre que d'autres cellules de son milieu qui ont été exposées. Les mesures électrochimiques sur des cellules alignées pourraient permettre de mieux comprendre le processus de résistance et d'augmenter les chances de pallier au problème.

APPENDICE A

INVITATION À CONTRIBUER À L'ÉCRITURE D'UN CHAPITRE DE LIVRE

A.1 Lettre de l'éditeur G. A. Gaddy.....87



*Concurrent Technologies Corporation*

Tel: 410-821-4202 Fax: 410-821-4204 Email: [info@ctc.com](mailto:info@ctc.com)  
Address: 8530 Corridor Road, Savage, MD 20763

Gregory A. Gaddy, Ph.D.  
Concurrent Technologies Corporation  
8530 Corridor Road  
Savage, MD 20763  
(410) 821-4202  
[gaddyg@ctc.com](mailto:gaddyg@ctc.com)

09 October 2007

Re: The Chemistry, Physics, and Engineering of Responsive Materials contribution invitation

Janine Mauzeroll  
Département de Chimie  
Université du Québec à Montréal  
Case postale 8888, Succ. Centre-ville  
Montréal (Québec), Canada  
H3C 3P8  
(514) 987-3000 ext. 0895  
[mauzeroll.janine@uqam.ca](mailto:mauzeroll.janine@uqam.ca)

Dear Dr. Mauzeroll:

On behalf of the Editorial Staff for The Chemistry, Physics, and Engineering of Responsive Materials, John Wiley Publishers, I would like to invite you to contribute a chapter for inclusion in the Sensors Section of the book. This section is edited by CDR Robert Calhoun, USN, Ph.D. of the US Naval Academy.

We look forward to working with you and your team in the following months toward the completion of the book. Your contribution will assist in making this project a true compilation of distinguished contributors of research and development of responsive materials from academia, industry and government agencies.

Very Respectfully,  
G. A. Gaddy

---

Albany, GA • Annapolis Junction, MD • Bremerton, WA • Charleston, SC • Columbia, SC • Crystal City, VA • Dayton, OH  
Fayetteville, NC • Fort Leonard Wood, MO • Greenville, SC • Harrisburg, PA • Jacksonville, FL • Johnstown, PA • Largo, FL  
Ottawa, ON, Canada • Panama City Beach, FL • Pensacola, FL • Pittsburgh, PA • Washington, DC

[www.ctc.com](http://www.ctc.com)

## APPENDICE B

### PERMISSIONS D'UTILISATION ET DE MODIFICATION DE MATÉRIEL AVEC DROIT D'AUTEUR

B.1	Permission donnée par <i>Angewandte Chemie</i> .....	89
B.2	Permission donnée par <i>Proceedings of the National Academy of Sciences USA</i> .....	90
B.3	Permission donnée par <i>Analytical Chemistry Society</i> .....	91

PERMISSION DONNÉE PAR *ANGEWANDTE CHEMIE*

Thu, Apr 3, 2008 9:53 AM

**Subject: Antwort: Form: Permission request**  
**Date:** Wednesday, April 2, 2008 2:25 AM  
**From:** VCH-RIGHTS-and-LICENCES <RIGHTS-and-LICENCES@wiley-vch.de>  
**To:** <mauzeroll.janine@uqam.ca>  
**Conversation:** Antwort: Form: Permission request

Dear Customer,

Thank you for your email.

We hereby grant permission for the requested use expected that due credit is given to the original source.

If material appears within our work with credit to another source, authorisation from that source must be obtained.

Credit must include the following components:

- Books: Author(s)/ Editor(s) Name(s): Title of the Book. Page(s). Publication year. Copyright Wiley-VCH Verlag GmbH & Co. KGaA. Reproduced with permission.

- Journals: Author(s) Name(s): Title of the Article. Name of the Journal. Publication year. Volume. Page(s). Copyright Wiley-VCH Verlag GmbH & Co. KGaA. Reproduced with permission.

With kind regards

Bettina Loycke  
\*\*\*\*\*  
Bettina Loycke  
Copyright & Licensing Manager  
Wiley-VCH Verlag GmbH & Co. KGaA  
Boschstr. 12  
69469 Weinheim  
Germany

PERMISSION DONNÉE PAR *PROCEEDINGS OF THE NATIONAL ACADEMY OF  
SCIENCES USA*

Dear Dr. Mauzeroll,

Permission is granted for your use of the figures as described in your message below. Please cite the full journal references and "Copyright (Copyright year) National Academy of Sciences, U.S.A."

Best regards,  
Chris Lashomb for  
Diane Sullenberger  
Executive Editor  
PNAS

-----Original Message-----

From: Janine Mauzeroll  
[mailto:[mauzeroll.janine@uqam.ca](mailto:mauzeroll.janine@uqam.ca)]  
Sent: Friday, April 18, 2008 11:34 AM  
To: Lashomb, Chris  
Subject: FW: PNAS permissions

----- Forwarded Message

From: Janine Mauzeroll  
<[mauzeroll.janine@uqam.ca](mailto:mauzeroll.janine@uqam.ca)>  
Date: Fri, 18 Apr 2008 10:46:03 -0400  
To: <[clasomb@nas.edu](mailto:clasomb@nas.edu)>  
Subject: PNAS permissions

Permission Request

1. Janine Mauzeroll; UQAM; Associate Professor  
2. Chemistry Department/Département de chimie  
UQAM  
Case postale 8888, Succ. Centre-ville  
Montréal (Québec), Canada

H3C 3P8  
Tel: (514) 987-3000 ext. 0895  
FAX: (514) 987-4054  
[Mauzeroll.janine@uqam.ca](mailto:Mauzeroll.janine@uqam.ca)  
3. PNAS vol 105; no 2; January 15, 2008  
4. Title: Nanoelectrochemistry of Mammalian Cells  
5. Authors: Peng Sun, François O. Laforge, Thushara P. Abeyweera, Susan A. Rotenberg, James Carpino and Micheal V. Mirkin  
6. Page numbers of items: 444; 446  
7. Reprint items: Figure 1E & 4 and their respective figure captions

Janine Mauzeroll

Associate Professor/ Professeure agrégée  
NSERC-UFA/CRNSG-APU  
Chemistry Department/Département de chimie  
UQAM  
Case postale 8888, Succ. Centre-ville  
Montréal (Québec), Canada  
H3C 3P8  
Tel: (514) 987-3000 ext. 0895  
FAX: (514) 987-4054

PERMISSION DONNÉE PAR ANALYTICAL CHEMISTRY SOCIETY

04/01/2008 15:40 FAX 2027768112

MAR 19 2008 14:01 FR DEP. CHIMIE

514 987 4054 TO 1169870895912027 P.01/01

001/001

RECEIVED

PERMISSION REQUEST FORM

MAR 19 2008

Date: March 19, 2008

FROM: Copyright Office  
Publications Division  
American Chemical Society  
1155 Sixteenth Street, N.W.  
Washington, DC 20036

FAX: 202-776-8112

TO:  
FROM: Prof. Janine Mauzeroll  
Chemistry Department, UQAM  
Case postale 8888, Centre-ville  
Montréal (Qc), Canada H3C 3P8  
Your Phone No. 514-987-3000 ext. 0895  
Your Fax No. 514-987-4054

ACS COPYRIGHT OFFICE

I am preparing a paper entitled:

Book Section: Sensor Materials  
to appear in a (circle one)  magazine, journal, proceedings, other \_\_\_\_\_  
entitled: The Chemistry, Physics, and Engineering of Responsive Materials

to be published by: John Wiley and Sons Publishing

I would appreciate your permission to use the following ACS material in print and other formats with the understanding that the required ACS copyright credit line will appear with each item and that this permission is for only the requested work listed above:

From ACS journals or magazines (for ACS magazines, also include issue no.):

ACS Publication Title	Issue Date	Vol.	No.	Page(s)	Material to be used*
Anal. Chem.	February 15, 2005	77	4	Fig 1C p.1113 & Fig 3B p.1115	and respective figure captions

From ACS books: include ACS book title, series name and number, year, page(s), book editor's name(s), chapter author's name(s), and material to be used, such as Figs. 2 & 3, full text, etc.\*

\_\_\_\_\_  
\_\_\_\_\_  
\_\_\_\_\_

\* If you use more than three figures/tables from any article and/or chapter, the author's permission will also be required.  
Questions? Please call Arleen Courtney at (202) 872-4368 or use the FAX number above.

This space is reserved for ACS Copyright Office Use

PERMISSION TO REPRINT IS GRANTED BY THE AMERICAN CHEMICAL SOCIETY

ACS CREDIT LINE REQUIRED. Please follow this sample:  
Reprinted with permission from (reference citation). Copyright (year) American Chemical Society.

"REPRINTED IN PART..."

APPROVED BY: C. Arleen Courtney 4/1/08  
ACS Copyright Office

If box is checked, author permission is also required. See original article for address.

12/3/99

APR 01 2008 16:52

2027768112

\*\* TOTAL PAGE .01 \*\*

PAGE .01

## APPENDICE C

### LISTE DES RÉFÉRENCES DE L'INTRODUCTION

C.1	Pages de la liste des références de l'introduction.....	93
-----	---------------------------------------------------------	----

## RÉFÉRENCES

- (1) Craighead, H. *Nature* **2006**, *442*, 387–393.
- (2) Carrion-Vazquez, M.; Oberhauser, A. F.; Fowler, S. B.; Marszalek, P. E.; Broedel, S. E.; Clarke, J.; Fernandez, J. M. *Proc. Natl. Acad. Sci. USA* **1999**, *96*, 3694–3699.
- (3) Lal, R.; John, S. A. *Am. J. Physiol. Cell Physiol.* **1994**, *266*, C1–C21.
- (4) Heim, M.; Steigerwald, R.; Guckenberger, R. *J. Struct. Biol.* **1997**, *119*, 212–221.
- (5) Liu, B.; Rotenberg, S. A.; Mirkin, M. V. *Proc. Natl. Acad. Sci. USA* **2000**, *97*, 9855–9860.
- (6) Scott, E. R.; Phipps, J. B.; White, H. S. *J. Invest. Dermatol.* **1995**, *104*, 142–145.
- (7) Tsionsky, M.; Cardon, Z. G.; Bard, A. J.; Jackson, R. B. *Plant Physiol.* **1997**, *113*, 895–901.
- (8) Takii, Y.; Takoh, K.; Nishizawa, M.; Matsue, T. *Electrochim. Acta* **2003**, *48*, 3381–3385.
- (9) Kaya, T.; Torisawa, Y.-s.; Oyamatsu, D.; Nishizawa, M.; Matsue, T. *Biosens. Bioelectron.* **2003**, *18*, 1379–1383.
- (10) Bauermann, L. P.; Schuhmann, W.; Schulte, A. *PCCP* **2004**, *6*, 4003–4008.
- (11) Wightman, R. M. *Science* **2006**, *311*, 1570–1574.
- (12) Mauzeroll, J.; Bard, A. J.; Owhadian, O.; Monks, T. J. *Proc. Natl. Acad. Sci. USA* **2004**, *101*, 17582–17587.
- (13) Amemiya, S.; Bard, A. J.; Fan, F.-R. F.; Mirkin, M. V.; Unwin, P. R. *Annu. Rev. Anal. Chem.* **2008**, *1*, 95–131.
- (14) Cougnon, C.; Bauer-Espinosa, K.; Fabre, D. S.; Mauzeroll, J. *Anal. Chem.* **2009**, *in press*.
- (15) Khademhosseini, A.; Suh, K. Y.; Jon, S.; Eng, G.; Yeh, J.; Chen, G.-J.; Langer, R. *Anal. Chem.* **2004**, *76*, 3675–3681.

- (16) Park, T. H.; Schuler, M. L. *Biotechnol. Progr.* **2003**, *19*, 243–253.
- (17) Whitesides, G. M.; Ostuni, E.; Takayama, S.; Jiang, X.; Ingber, D. E. *Annu. Rev. Biomed. Eng.* **2001**, *3*, 335–373.
- (18) Xia, Y.; Whitesides, G. M. *Angew. Chem. Int. Ed.* **1998**, *37*, 551–575.
- (19) Michel, B.; Bernard, A.; Bietsch, A.; Delamarche, E.; Geissler, M.; Juncker, D.; Kind, H.; Renault, J. P.; Rothuizen, H.; Schmid, H.; Schmidt-Winkel, P.; Stutz, R.; Wolf, H. *IBM. J. Res. Develop.* **2001**, *45*, 697–719.
- (20) McDonald, J. C.; Whitesides, G. M. *Acc. Chem. Res.* **2002**, *35*, 491–499.
- (21) Folch, A.; Toner, M. *Biotechnol. Progr.* **1998**, *14*, 388–392.
- (22) Van Engeland, M.; Nieland, L. J. M.; Ramaekers, F. C. S.; Schutte, B.; Reutelingsperger, C. P. M. *Cytometry* **1998**, *31*, 1–9.
- (23) Saito, M.; Kobayashi, M.; Iwabuchi, S. I.; Morita, Y.; Takamura, Y.; Tamiya, E. *J. Biochem.* **2004**, *136*, 813–823.
- (24) Dursun, B.; He, Z.; Somerset, H.; Oh, D. J.; Faubel, S.; Edelstein, C. L. *Am. J. Physiol. Renal Physiol.* **2006**, *291*, F578–F587.